LEVEL II (1)

(6

ORBITAL ESTIMATION USING

TWO-BODY CLASSICAL ORBITAL ELEMENTS

AS MEASUREMENT UPDATES,

THESIS,

14 AFIT/GA/AA/79D-3   (10) Daryl G. Boden
                             Capt   USAF

1980

(11) 2 79   (12) 124

Approved for public release; distribution unlimited

012 5

ORBITAL ESTIMATION USING

TWO-BODY CLASSICAL ORBITAL ELEMENTS

AS MEASUREMENT UPDATES

THESIS

Presented to the Faculty of the School of Engineering

of the Air Force Institute of Technology

Air University

in Partial Fulfillment of the

Requirements for the Degree of

Master of Science

by

Daryl G. Boden, B.S.

Capt   USAF

Graduate Astronautical Engineering

December 1979

Preface

I would like to thank my advisor, Captain William Wiesel, AFIT/ENY, for his help with this thesis. His advice and insight into the orbital estimation problems greatly aided in my completion of this report.

Daryl G. Boden

Table of Contents

Table of Contents (Cont'd)

List of Figures

List of Tables

List of Symbols

A	Satellite Radar Cross-Section
B	Ballistic Coefficient
C_D	Coefficient of Drag
DU	Distance Unit
C_{nm}	Geopotential Coefficients
F10	Solar Flux Coefficient
G	Bayes Filter Gain
H	Altitude
H	Observation Matrix
H*	Observation Matrix Times State Transition Matrix
J_n	Geopotential Coefficients
K	Kalman Filter Gain
M	Mean Anomaly
N	Number of Filter Runs
P	Covariance Matrix
P_n^m	Associated Legendre Polynomial
Q	Noise Matrix
R	Direction Cosine Matrix
S_n^m	Geopotential Coefficients
T	Direction Cosine Matrix
TU	Time Unit
U	Gravitational Potential
a	Semi-major Axis
a_x, a_y, a_z	Perturbation Acceleration in Geocentric Fram

Symbol

e	Eccentricity
$\bar{e}_j$	Mean Error of Estimate of jth Element
f	Earth's Flattening
$\underline{f}$	Non-Linear State Equations
g_u, g_e, g_n	Components of Geopotential Acceleration in Local Horizon Coordinate Frame
i	Inclination
m	Satellite Mass
n	Mean Motion
n_k	Kozai Mean Motion
$\underline{r}$	Residual Vector
r	Satellite's Radius from Center of Earth
r_e	Earth's Equatorial Radius
t	Time
$\underline{v}$	Measurement Noise Vector
v_a	Velocity of Satellite wrt Atmosphere
v_x, v_y, v_z	Satellite's Velocity in Geocentric Equatorial Frame
xyz	Satellite's Position Vector in Geocentric Equatorial Frame
$\underline{x}$	Filter State Vector
$\underline{z}$	Measurement Vector
Φ	State Transition Matrix
Ω	Right Ascension of Ascending Node
$\delta\underline{x}$	Change in Filter State Vector
δ	Declination

List of Symbols (Cont'd)

Symbol	Description
ϵ	Convergence Criteria
λ	Longitude
μ	Geopotential Constant
ρ	Atmospheric Density
σ_j^2	Mean Squared Error of jth Element
σ_j	Root Mean Squared Error of jth Element
ω	Earth's Rotational Velocity
ω	Argument of Perigee

Abstract

Currently, the Space Defense Center (SDC) uses the position and velocity data of a satellite track to update the orbital elements of the satellite. An alternate approach would be to process the radar data at the tracking site and transmit two-body orbital elements to SDC as measurement updates. This would significantly reduce the data load at SDC. The truth model used in this study to evaluate filter performance and provide measurement updates to the filters includes the first four zonal harmonics and the first sectoral harmonic of the geopotential and the air drag. The estimator models include two-body dynamics and J_2 perturbations. In addition, the derivative of the semi-major axis is used to estimate the effects dueto air drag. Perfect dynamics with measurement noise are assumed for the filter models. Three filters are evaluated; Least Squares, Bayes, and Kalman. The performance of the three filters is similar. The Bayes and Kalman Filters are nearly the same and indistinguishable in this study. All three filters performed adequately with the following exceptions. The filters diverge when singularities are present in the classical orbital elements. All three filters underestimate the covariance of the estimates. Finally, the filters track noise in the estimate of the derivative of the semi-major axis, degrading the prediction capabilities of the filters.

ORBITAL ESTIMATION USING TWO-BODY CLASSICAL

ORBITAL ELEMENTS AS MEASUREMENT UPDATES

I. Introduction

The Space Defense Center (SDC) located in the NORAD Cheyenne
Mountain Complex (NCMC) is responsible for maintaining current orbital
element sets for all earth orbiting satellites. Currently, there are
more than 4500 satellites orbiting the earth. SDC accomplishes its
mission by receiving and processing data from various spacetrack
sensors located throughout the world. The data is processed at SDC and
the satellite's orbital elements are estimated at SDC. The orbital
elements are then used to predict the satellite's position for future
acquisition and tracking.

Currently, SDC estimates the orbital elements of a satellite using
the satellite's position and velocity data received from the spacetrack
sensors. Either a least squares, batch filter or a Bayesian, recursive
filter, is used in the estimation program. An average satellite orbits
the earth between twelve and sixteen times per day. Depending upon the
satellite's ground track and SDC tracking requirements, a satellite may
be tracked 10-15 times daily. Each track may contain fifteen separate
measurements of position and velocity, or ninety individual pieces of
data per track. This could result in as many as 1000 measurements per
satellite per day being transmitted from the sensors to SDC. Also,
this data must be stored at SDC for a set period of time to be
available for estimating the satellite's orbit using a batch filter.

As the number of earth satellites increases and new, improved space-track sensors provide more and better data, the communications lines to SDC and the data storage facilities at SDC are becoming overloaded.

The purpose of this thesis is to investigate the possibility of reducing the amount of data transmitted to SDC per satellite track and the amount of data stored at SDC. The proposal is to have the individual tracking sites process the position and velocity on each track and generate two-body orbital elements using on-site computers. The site will then transmit the two-body orbital elements, six pieces of data per track, to SDC. SDC will then process the orbital elements as measurement updates to an estimator which would include pertubations to the two-body orbit in the estimate.

The approach taken in this thesis is divided into three parts. First, a truth model will be developed to simulate an actual satellite orbit and to provide data for the estimators. Next, three separate estimators will be designed to estimate the satellite's orbital elements. Finally, a performance analysis of the three estimators will be conducted. All estimators will be designed to accept classical orbital elements as measurements. Various satellite orbits will be investigated to evaluate effects due to atmospheric drag, high and low eccentricity, low inclination, and a lack of tracking data due to unusual orbital geometry.

During this study the following assumptions are made:

1. The satellite is non-thrusting and unable to maneuver.

2. The satellite has a constant drag coefficient, constant mass, and constant surface area.

3. The geocentric equatorial coordinate frame is considered to

2

be an inertial reference frame.

4. The earth's gravitational field is adequately modeled using zonal harmonics through J_4 and the first sectoral terms, C_{22} and S_{22}.

5. The satellite dynamics are known perfectly.

6. The noise in the sensor tracking data is zero-mean, white, Gaussian noise.

7. The atmospheric density above at an altitude greater than 800km is assumed to be zero.

This thesis is presented in the following chapters. Chapter II describes the truth model, including satellite dynamics, coordinate frame used, and the method of obtaining measurements for use in the estimators. The third chapter presents the basic estimator model and describes the least squares, Bayes, and Kalman filters used. Chapter IV describes the various satellite orbital cases used for filter evaluation. The fifth chapter presents the estimation results and filter performance evaluation. The sixth chapter contains conclusions of this study and recommendations for future work.

II. Truth Model

The truth model fulfills two important functions in this study.
First, it simulates an actual satellite orbit. The orbit is simulated
by numerically integrating the equations of motion for the satellite
using Cowell's method. In order to do this the coordinate frame and
system differential equations must be specified. Before integration,
the initial conditions for the differential equations must also be
specified. The equations of motion contain the two-body accelerations
plus perturbative accelerations due to the earth's geopotential and
atmospheric drag. After integrating the equations of motion, the
satellite's position and velocity are output from the truth model.
Zero-mean, white, gaussian noise is then added to the position and
velocity data, simulating actual radar tracks. Finally, the position
and velocity data are converted to the classical orbital elements for
use as measurement updates to the estimators. A description of the
orbital simulation and measurement updates will be completed in the
following paragraphs.

Coordinate Frame

Before integrating the equations of motion for a satellite, a
suitable inertial reference frame must be defined. Additional reference
frames, some non-inertial, may be defined to aid in computation.
Three coordinate frames are used in this study; geocentric-equatorial,
perifocal, and local horizon coordinate frames.

For earth orbiting satellites, the geocentric equatorial frame can
be assumed to be an inertial reference frame. As shown in Figure 1,

4

the center of this frame is the center of the earth and the principle
plane is the earth's equatorial plane. The positive X-axis points in
the direction of the vernal equinox and the positive Z-axis points in
the direction of the north pole. Finally, the Y-axis completes the
right-handed XYZ coordinate frame. It can be seen in Figure 1 that
the XYZ system is not rotating with the earth, but is fixed with
respect to the stars. This system is used primarily for expressing
and integrating the equations of motion.

The perifocal coordinate frame is shown in Figure 2. The funda-
mental plane for this system is defined by the plane of the satellite's
orbit. The principle axis, X_p, points toward the perigee of the orbit.
The Y_p axis is rotated 90° in the direction of orbital motion in the
orbital plane. The Z_p axis completes the right-handed $X_pY_pZ_p$ system.
The perifocal system is used for transforming from classical orbital
elements to satellite position and velocity.

The final coordinate frame is the local horizon coordinate frame.
The center of this frame is at the intersection of the satellite's
position vector from the center of the earth and the surface of the
earth. The directions of this system are up along the radius vector,
East, and North. This frame is convenient for expressing the earth's
geopotential.

In the course of this study, it will be necessary to transform
from one coordinate frame to another. The direction cosine matrices
necessary for the various transformations are shown in Appendix A.

States - State Equations

The system states used in the truth model are the satellite
position and velocity in the geocentric-equatorial reference frame.
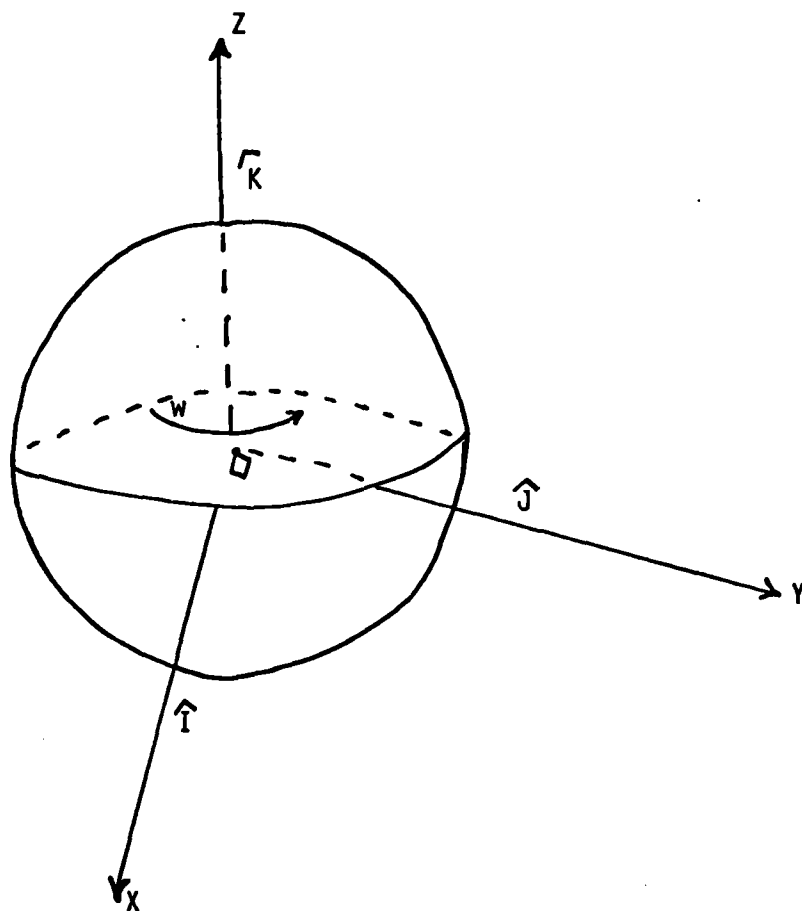
vernal equinox direction

Figure 1. Geocentric Equitorial Frame
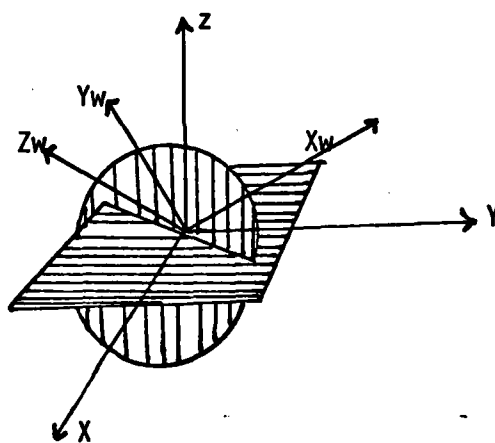
Figure 2. Perifocal Coordinate Frame

6

The state equations are shown in equation (1),

$$
\begin{bmatrix} \dot{X} \\ \dot{Y} \\ \dot{Z} \\ \dot{V}_x \\ \dot{V}_y \\ \dot{V}_z \end{bmatrix} = \begin{bmatrix} v_x \\ v_y \\ v_z \\ -\frac{\mu x}{r3} + a_x \\ -\frac{\mu y}{r3} + a_y \\ -\frac{\mu z}{r3} + a_z \end{bmatrix} \tag{1}
$$

where a_x, a_y, and a_z are accelerations due to perturbative forces. These forces will be discussed in later sections.

The units used in these equations are geocentric, canonical units. In this system the distance unit, DU, is the earth's mean equatorial radius, equation (2).

$$1 \text{ DU} = 6378.145 \text{ Km} \tag{2}$$

The time unit, TU, is chosen so that μ is equal to one.

$$1 \text{ TU} = 13.44686457 \text{ min} \tag{3}$$

Initial Conditions

Initial conditions are required for the satellite's position and velocity in order to integrate the equations of motion. These conditions are obtained by specifying a particular orbit at a particular time. The orbital elements are transformed to a position and velocity vector in the perifocal coordinate frame. The position and velocity vector are then transformed to the geocentric-equatorial coordinate frame, providing initial conditions for the state equations given in equation (1). The technique for obtaining the position and velocity from classical orbital elements is shown in Appendix B.

7

Earth's Geopotential

The gravitational potential of the earth at a point at a distance r from the center of the earth is,

$$U = \frac{\mu}{r} \left\{ 1 + \sum_{n=2}^{\infty} \left(\frac{r_e}{r}\right)^n \sum_{m=2}^{\infty} P_m^n (\sin \delta) \left[C_{nm} \cos m\lambda + S_{nm} \sin m\lambda \right] \right. \quad (4)$$

where,

μ is the earth's gravitational constant

r_e is the earth's mean equatorial radius

P_m^n is the associated legndre function of degree n and order m

C_{nm} & S_{nm} are numerical coefficients

δ is the geocentric latitude of the point

λ is the geocentric longitude of the point

For m = 0, the S_{nm} coefficients are not needed and the C_{nm} coefficients are replaced by

$$J_n = -C_{no} \quad\quad\quad (5)$$

These harmonics are independent of longitude and are called zonal harmonics. The zonal harmonic, J_1, is set equal to zero by choosing a coordinate frame with the origin at the earth's center of mass. For this study, only the terms through J_4 were retained. The terms for m = n are called sectoral harmonics. Only the first sectoral harmonic, m = n = 2, is used in this study. The remaining terms, called tesseral harmonics, are not included in this study.

The first term in equation (4) is the major term in the equations of motion for a satellite and represents the two-body motion of the satellite. This term is represented in equation (1) by the first

acceleration terms. The remaining terms in the geopotential are included in the perturbation term.

The terms of the acceleration due to the earth's geopotential are most easily expressed in the local horizon coordinate frame [Ref 9, 88-92]. In this frame

$$-\frac{\mu \underline{r}}{r^3} + \underline{a} = g_u \, \hat{u} + g_e \, \hat{e} + g_n \, \hat{n} \tag{6}$$

where

$$g_u = \frac{\partial U}{\partial r}$$

$$= -\frac{\mu}{r^2}\left\{1 + \sum_{n=2}^{\infty} (n+1) \frac{r_e}{r}^n \sum_{m=0}^{n} P_n^m (\sin\delta)[C_{nm} \cos m + S_{nm} \sin m\lambda]\right\} \tag{7}$$

$$g_e = \frac{1}{r \cos\delta} \frac{\partial U}{\partial \lambda}$$

$$= \frac{-\mu}{r^2 \cos\delta} \sum_{n=2}^{\infty} \frac{r_e}{r}^n \sum_{m=0}^{n} m \; P_n^m (\sin\delta)[C_{nm} \sin m\lambda - S_{nm} \cos m\lambda] \tag{8}$$

$$g_n = \frac{1}{r} \frac{\partial U}{\partial \delta}$$

$$= \frac{\mu}{r^2} \sum_{n=2}^{\infty} \frac{r_e}{r}^n \sum_{m=0}^{n} \cos\delta \frac{\partial}{\partial \delta} (P_n^m (\sin\delta)) [C_{nm} \cos m\lambda + S_{nm} \sin m\lambda] \tag{9}$$

The acceleration terms are then transformed to the geocentric-equatorial frame for integration. The zonal and sectoral harmonics and the associated legendre polynomials required for this study are presented in Appendix C.

Atmospheric Drag

The acceleration on a satellite caused by atmospheric drag is

$$\underline{a} = -\frac{1}{2} B \rho v_a \; v_{\underline{a}} \tag{10}$$

where,

$B = C_D \frac{A}{m}$ is the satellite's ballistic coefficient

C_D = is the drag coefficient of the satellite

A   is the satellite's cross-sectional area perpendicular to the velocity

m   is the satellite's mass

ρ is the atmospheric density at the altitude of the satellite

v_a is the velocity of the satellite relative to the atmosphere.

The satellite's ballistic coefficient is assumed to be constant for this study and is input into the system with the initial orbital elements.

The velocity of the satellite relative to the atmosphere is

$$\underline{v}_a = \begin{bmatrix} \dot{x} + \omega y \\ \dot{y} - \omega x \\ \dot{z} \end{bmatrix} \tag{11}$$

where

x, y, and z are the satellite's geocentric-equatorial coordinates

ω = .0588336001 $\frac{rad}{Tu}$ is the earth's angular rotation.

The atmospheric density, ρ, must be calculated from a model atmosphere. The model atmosphere in this study was developed by Jacchia in 1960 [Ref 7]. The model accounts for altitude above a non-spherical earth and diurnal variations in the density. The density is given by

$$\rho = \rho_0 \frac{F_{10}}{100} \left\{ 1 + 0.19 \left[\exp(0.0055H) - 1.0 \right] \left[\frac{1 + \cos \psi}{2} \right]^3 \right\} \frac{Kg}{m^3} \tag{12}$$

where

$$\text{Log}_{10} \, \rho_0 = -16.021 - 0.001985H + 6.363 \exp(-0.0026H) \tag{13}$$

$$H = 6378.145 \left[r-1 + f \, u_z^2 + \frac{3}{2} f^2 \, u_z^2 \, (1-u_z^2) \right] \tag{14}$$

is the height of the satellite above the earth.

r   is the satellite's radius

$f = 1/298.3$ is the earth's flattening

$u_z = \sin \delta$

δ is the satellite's geocentric declination

F_{10} is the solar flux at 10.7 cm

$\cos\psi = u_x \cos (D-50°) + u_y \sin (D-50°)$

$D = (\text{Day of year}) \times 360°/365.25 \text{ days}$

$u_x = \hat{u} \cdot \hat{i}$ ⎞ $\hat{u}$ is a perifocal frame unit vector, $\hat{i}$ and $\hat{j}$ are

$u_y = \hat{u} \cdot \hat{j}$ ⎠ geocentric equatorial unit vectors.

For this study it is assumed that $\rho = 0$ for altitudes greater than 800km.

Measurements

After the equations of motion are integrated, orbital elements must be calculated for updates to the estimators. The satellite's geocentric-equatorial position and velocity are output from the numerical integration. Zero-mean, white, gaussian noise is then added to the data to simulate errors in the radar data. The standard deviation is 500m in the position and 10m/sec in the velocity. The position and velocity data, including noise is then converted to classical orbital elements. These elements are:

a - semi-major axis

e - eccentricity

11

i - inclination

ω - argument of perigee

Ω - right ascension of ascending node

M - mean anomaly

t - time of track

The method of transforming from a position and velocity vector to classical orbital elements is shown in Appendix D.

III. Estimation

In orbit determination, the system model is a non-linear set of equations. The parameters in the model are well known and the assumption of perfect dynamics is adequate for the estimation problem. Also the observation relations are in general non-linear. The observations are corrupted by zero-mean, white noise.

Three separate estimators are used to estimate the orbital parameters. The filters are a least squares filter, a Kalman filter, and an inverse covariance Bayes filter.

The model dynamics, observation relationship, and the three filters are discussed in the following sections.

Dynamics

The dynamics in this section are the same as the dynamics discussed in Chapter II; however, a simpler model is proposed to reduce computational time and expense. The model proposed in this section is essentially the same as the model currently used at SDC in their standard model [Ref 14].

The system models of the estimators are designed to model the two-body dynamics plus J_2 effects and air drag. Only the secular terms in J_2 are considered. The secular effects due to J_2 appear in the derivatives of argument of perigee, right ascension, and mean anomaly. The presence of atmospheric drag reduces the semi-major axis a and eccentricity e. Due to the difficulty in modeling the atmosphere, and therefore the air drag, the derivatives of a and e are included in the system states and the atmospheric effect is estimated. The system states used

13

in the estimators are (see List of Symbols):

$$\underline{x}^T = [a, e, i, \omega, \Omega, M, \dot{a}, \dot{e}] \qquad (15)$$

An approximate solution to the non-linear system is given by

$$\underline{x}(t) = \underline{f} (\underline{x} (t_0), t) \qquad (16)$$

or,

$$a(t) = a_0 + \dot{a}(t-t_0) \qquad (17)$$

$$e(t) = e_0 + \dot{e}(t-t_0) \qquad (18)$$

$$i(t) = i_0 \qquad (19)$$

$$\omega(t) = \omega_0 + \dot{\omega}(t-t_0) \qquad (20)$$

$$\Omega(t) = \Omega_0 + \dot{\Omega}(t-t_0) \qquad (21)$$

$$M(t) = M_0 + n_k(t-t_0) + \frac{1}{2} \dot{n}(t-t_0)^2 \qquad (22)$$

$$\dot{a} = \dot{a}_0 \qquad (23)$$

$$\dot{e} = \dot{e}_0 \qquad (24)$$

where

$$\dot{\omega} = \frac{-3nJ_2r_e^2}{2a^2(1-e^2)^2} \left(\frac{5}{2} \sin^2 i - 2\right) \qquad (25)$$

$$\dot{\Omega} = \frac{-3nJ_2r_e^2}{2a^2(1-e^2)^2} \cos i \qquad (26)$$

$$\dot{n} = \frac{3}{2} a^{-5/2} \dot{a} \qquad (27)$$

$$n_k = n + \dot{\varepsilon} \qquad (28)$$

is the Kozai mean motion

$$\dot{\varepsilon} = \frac{-3J_2r_e^2n}{2a^2(1-e^2)^{3/2}} \left(\frac{3}{2} \sin^2 i - 1\right) \qquad (29)$$

14

A linearization of equations (17) through (24) yields the state transition matrix, ϕ, an 8 X 8 matrix. ϕ is given by

$$\phi = \overline{\nabla} \cdot \underline{f} \qquad (30)$$

The elements of ϕ are given in Appendix E.

Observation Relationships

The measurement updates to a filter are given in general by

$$\underline{z} = \underline{h}\,(\underline{x}(t_0),\, t) + \underline{v} \qquad (31)$$

where $\underline{h}$ must be determined through geometric relationships between the measurements and the states. For example, if the satellite's position and velocity vectors are used as measurement updates, then a set of equations similar to those in Appendix B would be required. Also coordinate transformations from the station centered to perifocal reference frames would be required. This is currently the method used at SDC. In this study the measurements are the classical orbital elements. These measurements are a linear combination of the states.

$$\underline{z} = H\,\underline{x} + \underline{v} \qquad (32)$$

where

$$H = \begin{bmatrix} 1 & 0 & 0 & 0 & 0 & 0 & 0 & 0 \\ 0 & 1 & 0 & 0 & 0 & 0 & 0 & 0 \\ 0 & 0 & 1 & 0 & 0 & 0 & 0 & 0 \\ 0 & 0 & 0 & 1 & 0 & 0 & 0 & 0 \\ 0 & 0 & 0 & 0 & 1 & 0 & 0 & 0 \\ 0 & 0 & 0 & 0 & 0 & 1 & 0 & 0 \end{bmatrix} \qquad (33)$$

$\underline{v}$ is a zero-mean, white noise.

The associated covariance matrix for the noise v, is Q. It is assumed for this study that the noise components are uncorrelated, so that the off-diagonal components of Q are zero.

In order to determine the diagonal elements of Q, it is assumed that the initial tracking data had standard deviations of 500m in the position vector and 10m/sec in the velocity vector. This noise was added to the position and velocity vector and the orbital elements were calculated. This process was repeated ten times and then an average error for each orbital element was calculated. The results show that a single value for the diagonal elements of Q is adequate. The value used in this study is 10^8.

Least Squares Filter

The least squares filter used in this study is a batch filter. Thus, every time an update is required the data must be batch processed to update the state estimate. In this study, the state vector is updated after every ten measurements, using the previous estimate as the reference trajectory. The basic algorithm used in this study is given in the following steps [Ref 13, 62-63].

1. Input measurements, z_i at times t_i, measurement noise Q_i, and reference orbit $\underline{x}_r(t_0)$. z_i will be a 6 X 10 matrix for the six elements measured at ten different times. As stated, Q is a diagonal matrix with a single, constant value at each diagonal element. Also, the reference trajectory $\underline{x}_r(t_0)$ is the previous state estimate evaluated at time t_0.

2. Propagate the state vector $\underline{x}_r$ to each time t_i and calculate $\underline{x}(t_i)$ and the state transition matrix $\phi(t_i, t_0)$.

3. Assemble, Q and H.

$$Q = \begin{bmatrix} Q_1 & & & & \\ & Q_2 & & & \\ & & \ddots & & \\ & & & \ddots & \\ & & & & Q_{10} \end{bmatrix} \qquad (34)$$

$$H^* = \begin{bmatrix} H_1 \; \Phi(t_1, t_0) \\ H_2 \; \Phi(t_2, t_0) \\ \vdots \\ H_{10} \; \Phi(t_{10}, t_0) \end{bmatrix} \qquad (35)$$

4. Calculate the covariance matrix, P.

$$P = (H^{*T} \; Q^{-1} \; H^*)^{-1} \qquad (36)$$

5. Calculate the residuals $\underline{r}(t_i)$ and assemble into a vector.

$$\underline{r}(t_i) = \underline{z}(t_i) - H(t_i) \; \underline{x}(t_i) \qquad (37)$$

$$\underline{r} = \begin{bmatrix} \underline{r}(t_1) \\ \underline{r}(t_2) \\ \vdots \\ \underline{r}(t_{10}) \end{bmatrix} \qquad (38)$$

6. Calculate the change in the state vector $\delta\underline{x}(t_0)$.

$$\delta\underline{x}(t_0) = P \; H^{*T} \; Q^{-1} \; \underline{r} \qquad (39)$$

7. Calculate the estimated state vector $\underline{x}(t_0)$.

$$\underline{x}(t_0) = \underline{x}_r(t_0) + \delta\underline{x}(t_0) \qquad (40)$$

8. Check for convergence. For this study δx_i is compared to $\sqrt{P_{ii}}$. If the absolute value of the change in each element of the state vector is less than its associated standard deviation, the solution is assumed to have converged and the associated estimate is assumed to be the state estimate at the epoch time, t_0.

9. If the solution has not converged, the new solution replaces the reference orbit. This new reference orbit is propagated to each time, t_i, and new residuals are calculated as shown in Step 5. This process is repeated until convergence is achieved or a maximum number of iterations is exceeded. The maximum number of iterations used in this study is twenty.

The epoch time, t_0, in this filter is always taken as the time of the last measurement.

Since this filter uses only the last ten measurements, it is a finite memory filter and should not encounter problems with the co-variance matrix, P, becoming singular. A larger batch size or more frequent updates to the estimates may be implemented; however, a standard batch size of ten measurements per update is maintained in this study.

Some observations concerning the filter can be made. First, when using only the last ten measurements, the dimension of some of the matrices becomes rather large. The Q matrix is a 60 X 60 matrix in general; however, it is at worst block diagonal and in this case strictly a diagonal matrix. The P matrix is an 8 X 8 matrix which must be inverted. Both the P matrix and the H* matrix are calculated once per state estimate update and are then assumed to be constant for that update cycle. A more exact method would be to update the two matrices

each iteration. For this problem the possible decrease in the number of iterations was not worth the corresponding increase in computational time.

Bayes Filter

The Bayes Filter, or inverse covariance filter, used in this study is a recursive filter, providing a state estimate update after every measurement input into the filter. This filter propagates the estimated state vector and its associated covariance forward to the time of the current measurement. This estimate and the measurement are then combined to form a new estimate of the state vector along with its associated covariance matrix. The algorithm used in this study is listed below [Ref 13, 82-85].

1. Input the previous estimate, $\underline{x}(t_i - 1)$, new data, $\underline{z}(t_0)$, and its noise matrix, Q.

2. Propagate the state estimate and the covariance matrix to the time of the new measurement, t_i.

$$\underline{x}(t_i^-) = \underline{f}(\underline{x}(t_{i-1}), t_i - t_{i-1}) \tag{41}$$

$$P(t_i^-) = \phi(t_i, t_{i-1}) P(t_{i-1}) \phi^T(t_i, t_{i-1}) \tag{42}$$

The initial state vector in the filter is the first measurement. The initial covariance matrix input into the system is

$$P_{ij} = 1. \times 10^{-4} \quad i \neq j \tag{43}$$

$$P_{ii} = 1. \times 10^{-2} \tag{44}$$

3. Calculate the new covariance matrix, $P(t_i)$.

$$P(t_i) = \{P^{-1}(t_i^-) + \phi^T H^T Q^{-1} H\phi\}^{-1} \tag{45}$$

4. Calculate the gain matrix, G.

$$G = P(t_i) \ \Phi^T \ H^T \ Q^{-1} \tag{46}$$

5. Calculate the residual vector, $\underline{r}$.

$$\underline{r} = \underline{z}(t_i) - H\underline{x}(t_i^-) \tag{47}$$

6. Calculate the change in the state vector, $\delta\underline{x}$.

$$\delta\underline{x}(t) = \delta\underline{x}(-) + G(\underline{r} - H\Phi\delta\underline{x}(-)) \tag{48}$$

starting with

$$\delta\underline{x}(-) = \underline{0} \tag{49}$$

7. Check for convergence. For this study convergence is achieved
if

$$\underline{r} = H\Phi\delta\underline{x}(-) < \underline{\varepsilon} \tag{50}$$

where

$$\varepsilon_i = 1. \times 10^{-3} \tag{51}$$

If the solution converges, the state estimate is

$$\underline{x}(t_0) = \underline{x}(t_i-) + \delta\underline{x}(t) \tag{52}$$

8. If the solution has not converged, new residuals are calculated
based on the updated state estimate and steps 6 through 8 are repeated.
If the solution has not converged after ten iterations the algorithm
is exited and the new state estimate is calculated as shown in
equation (52).

20

The data storage requirements and the dimensions of the matrices are greatly reduced for this filter when compared to the least squares filter. The largest dimension of a matrix in this filter is 8 X 8. This filter provides a state estimate update after every measurement. This implies that the state estimate is more current than the least squares filter; however, this filter must generate an estimate ten times for every estimate generated by the least squares filter. Like the least squares filter, the gain and covariance matrix in this filter are calculated once per update cycle. These matrixes are then assumed to be constant for the remaining iterations. Also, like the least squares filter, the filter requires one 8 X 8 matrix inversion per update cycle.

Kalman Filter

The third filter investigated on this study is a Kalman Filter. The operation of the Kalman Filter is quite similar to the Bayes Filter. It is a recursive filter that provides a new state estimate following each measurement update. The algorithm used in this study is listed below [Ref 13, 90-91].

1 and 2 - same as Bayes Filter.

3. Calculate the Kalman Filter gain, K.

$$K = P(t_i-) \, \Phi^T H^T (Q + H\Phi P(t_i-)\Phi^T H^T)^{-1} \tag{53}$$

4. Calculate the new covariance matrix $P(t_i+)$.

$$P(t_i+) = P(t_i-) - KH\Phi P(t_i-) \tag{54}$$

21

5. Calculate the residuals, $\underline{r}$.

$$\underline{r} = \underline{z} - H\underline{x}(t_i-) \tag{55}$$

6. Calculate the change in the state vector, $\delta\underline{x}(+)$.

$$\delta\underline{x}(+) = \delta\underline{x}(-) + K(\underline{r} - H\Phi\delta\underline{x}(-)) \tag{56}$$

7. Check for convergence. The convergence check is

$$\underline{r} - H\Phi\delta\underline{x}(-) < \underline{\varepsilon} \tag{57}$$

where

$$\varepsilon_i = 1.0 \times 10^{-3} \tag{58}$$

If convergence is achieved, the new estimate is

$$\underline{x}(t_i+) = \underline{x}(t_i-) + \delta\underline{x}(+) \tag{59}$$

8. If convergence is not attained, calculate new residuals using the updated state vector estimate and repeat Steps 6 through 8. Again, the maximum number of iterations is 10.

The characteristics of the Kalman Filter are the same as the Bayes Filter except the Kalman Filter requires a 6 X 6 matrix inversion instead of an 8 X 8 matrix inversion.

A summary of the three filter characteristics is listed in Table I.

TABLE I

Filter Characteristics

Characteristics	Least Squares	Bayes	Kalman
Method of Update	Batch	Recursive	Recursive
Frequency of Updates	1 per 10 measurements	every measurement	every measurement
Storage Requirements	Current estimate and covariance plus last 10 measurements	Current estimate and covariance plus last measurements	
Dimension of Matrix Inversion	8 X 8	8 X 8	8 X 8

IV. Satellite Cases

Various satellite cases were investigated in this study to eval-
uate the performance of the three filters. The orbital elements for
each case are listed below along with an explanation of the objectives
of each case (see List of Symbols).

Case 1.

$$a_0 = 1.2 \text{ DU} = 7653.774 \text{ km}$$

$$e_0 = .1$$

$$i_0 = .5 \text{ rad} = 28.648°$$

$$\omega_0 = 1.0 \text{ rad} = 57.296°$$

$$\Omega_0 = 2.0 \text{ rad} = 114.592°$$

$$M_0 = 3.0 \text{ rad} = 171.887°$$

$$\Delta t = 10 \text{ TU} \quad = 134.686 \text{ min}$$

where

Δt is the time between measurement updates.

The satellite orbit is used to demonstrate the operation of the
filters under normal operation with no singularities in the orbital
elements. Normal operation is assumed to be one radar track every two
hours.

Case 2.

$$a_0 = 2.0 \text{ DU} = 12{,}756.286 \text{ km}$$

$$e_0 = .1$$

$$i_0 = 1.0 \text{ rad} = 57.286°$$

$$\omega_0 = 2.0 \text{ rad} = 114.592°$$

$$\Omega_0 = 3.0 \text{ rad} = 171.887°$$

24

$$M_0 = 1.0 \text{ rad} = 57.296°$$
$$\Delta_t = 50 \text{ TU} = 672.343 \text{ min}$$

The objective of this orbit is to investigate the effect on the estimators with a long time delay between updates. There are approximately two updates per day with this orbit.

Case 3.

$$a_0 = 1.15 \text{ DU} = 7335 \text{ km}$$
$$e_0 = .1$$
$$i_0 = .5 \text{ rad} = 28.648°$$
$$\omega_0 = 1.0 \text{ rad} = 57.296°$$
$$\Omega_0 = 2.0 \text{ rad} = 114.592°$$
$$M_0 = 3.0 \text{ rad} = 57.296°$$
$$\Delta_t = 10 \text{ TU} = 134.686 \text{ min}$$

This orbit is a low altitude orbit. This orbit should identify problems in estimating air drag. The perigee altitude for this orbit is 200 km. Also the drag coefficient of the satellite was increased by a factor of 10, from 0.01 to 0.1, to increase the effect of air drag.

Case 4.

$$a_0 = 1.2 \text{ DU} = 7653.774 \text{ km}$$
$$e_0 = 0.$$
$$i_0 = 0.$$
$$\omega_0 = 0.$$
$$\Omega_0 = 0.$$
$$M_0 = 0.$$
$$\Delta_t = 10 \text{ TU} = 134.686 \text{ min}$$

This orbit introduces singularities when estimating the classical elements from position and velocity data.

Case 5.

a_0 = 4 DU = 25500 km

e_0 = .7

i_0 = 1.1 rad = 63°

ω_0 = 4.7 rad = 270°

Ω_0 = 1.0 rad = 57°

M_0 = 0 rad = 0°

Δ_t = 10 TU = 134.686 min

This orbit simulates a highly eccentric orbit. To simulate tracking problems and observation problems, all data generated at altitudes greater than 6000 km were disregarded. In this case the Δ_t given will vary, depending upon the altitude.

The performance of the filters using each of the orbits is presented in Chapter V. The filters are evaluated for twenty measurement update cycles, which is two days for the high frequency tracks and ten days for the low frequency tracks.

V. Filter Performance Evaluation

The three filters used in this study are evaluated based on each filter's estimate of the covariance, the mean error of the state estimates, and the root mean square errors of the state estimates.

Covariance Analysis

Since the dynamics in this problem are non-linear, a Monte Carlo analysis is required to evaluate the covariance estimate of the three filters. The first step is to determine the number of runs required for the covariance from the Monte Carlo analysis to reach a constant value. The variance of the filter is given by the following equation:

$$var(x) = \sigma^2 - \bar{e}^2 \qquad (60)$$

where

$$\sigma^2 = \frac{1}{N-1} \sum_{j=1}^{N} (X_T - \hat{X}_j{}^2)^2 \qquad (61)$$

$$\bar{e} = \frac{1}{N} \sum_{j=1}^{N} (X_T - \hat{X}_j) \qquad (62)$$

σ^2 is the mean squared error

$\bar{e}$ is the mean error

N is the number of runs starting from 2

X_T is the true value of the state

$\hat{X}_j$ is the estimated value of the state

This analysis provides the diagonal elements of the filter covariance; the variance of the state estimates.

The Bayes and Kalman Filters are evaluated using twenty-five separate runs of Case I of the satellite orbits. The Least Squares Filter is evaluated using twenty-five runs of Case II of the satellite orbits. The mean squared error is calculated at the time of the last measurement update.

$$\Delta t = 200 \text{ TU} \approx 45 \text{ hrs}$$

The mean squared error σ^2 for each state is plotted as a function of the number of runs. Figure 3 represents a plot of the mean squared error of the inclination versus the number of runs for the Least Squares Filter. This plot shows the desired characteristic of approaching a constant value after about 12-14 runs. Plots for the semi-major axis and mean anomaly for each filter are shown in Figures 4-9. The plots for the remaining states are included in Appendix F. As can be seen in the plots (i.e., Fig 6) not all curves look like Figure 3. In some cases it is difficult to tell when and if the mean squared error has reached a nearly constant value. However, in most cases, nearly constant values are achieved after fifteen runs. Fifteen runs are used for all subsequent Monte Carlo analyses.

Next, the variance obtained from the Monte Carlo analysis is compared to the estimate of the variance from the filters. The variances of the semi-major axis and mean anomaly are used for comparison. Table II shows a comparison of the variances of these two elements for each filter. The final estimate for Case I is used for comparison.

As shown in the table, all three filters underestimate the variance of both elements. Similar results are obtained for the other four elements. This is probably due to the assumption of perfect dynamics
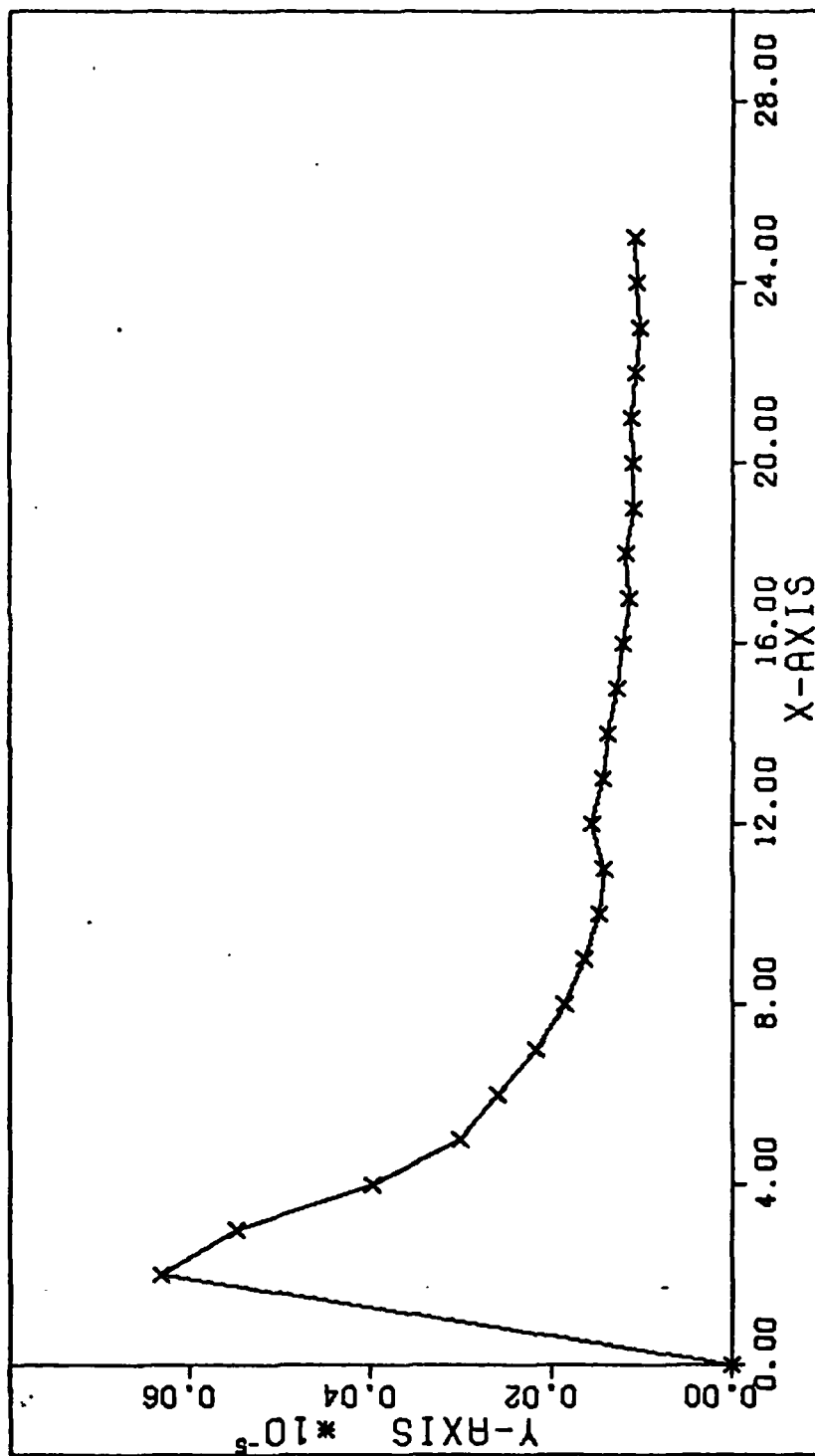
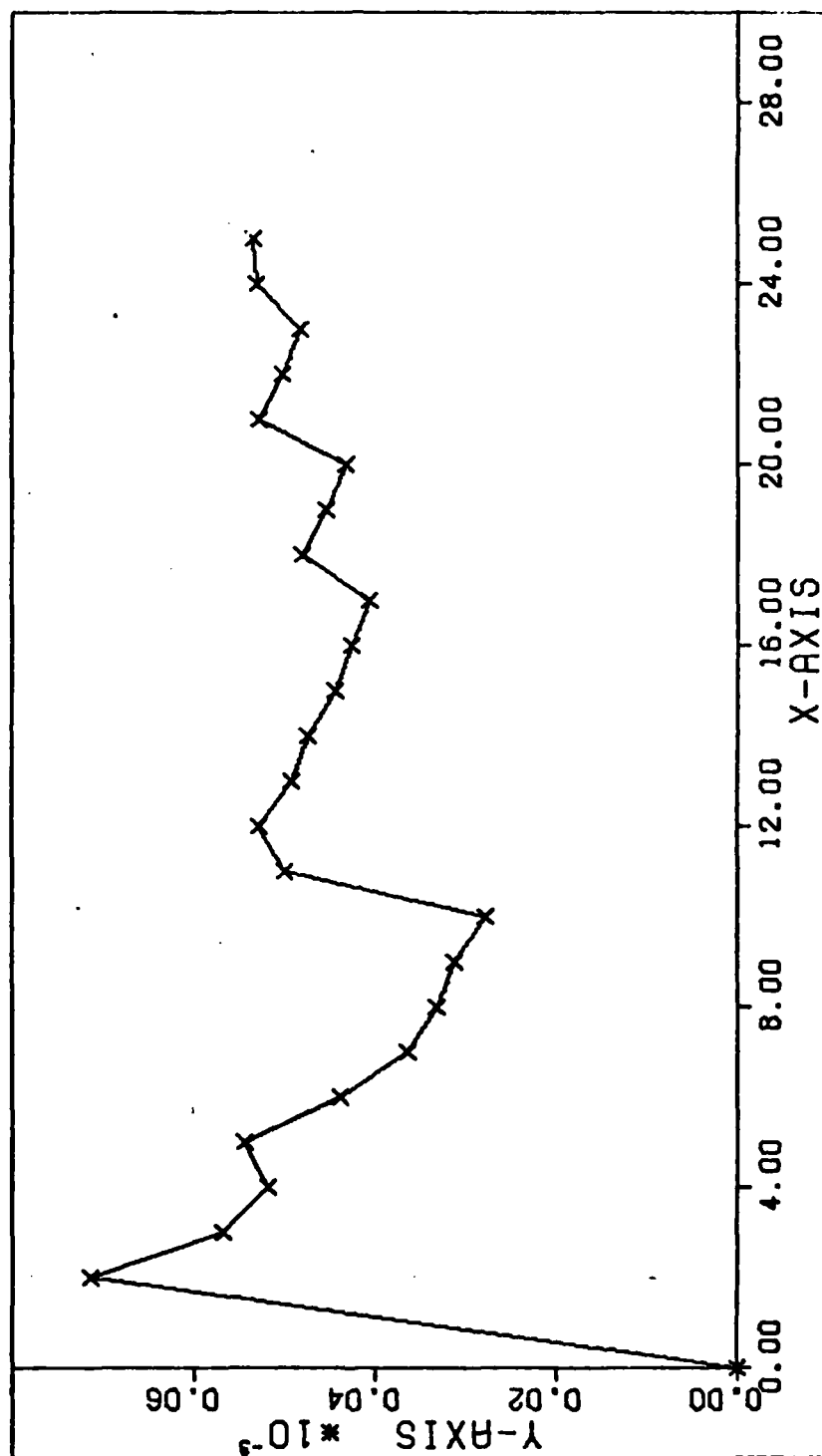Fig 3. σ_i^2 vs N, Least Squares Filter
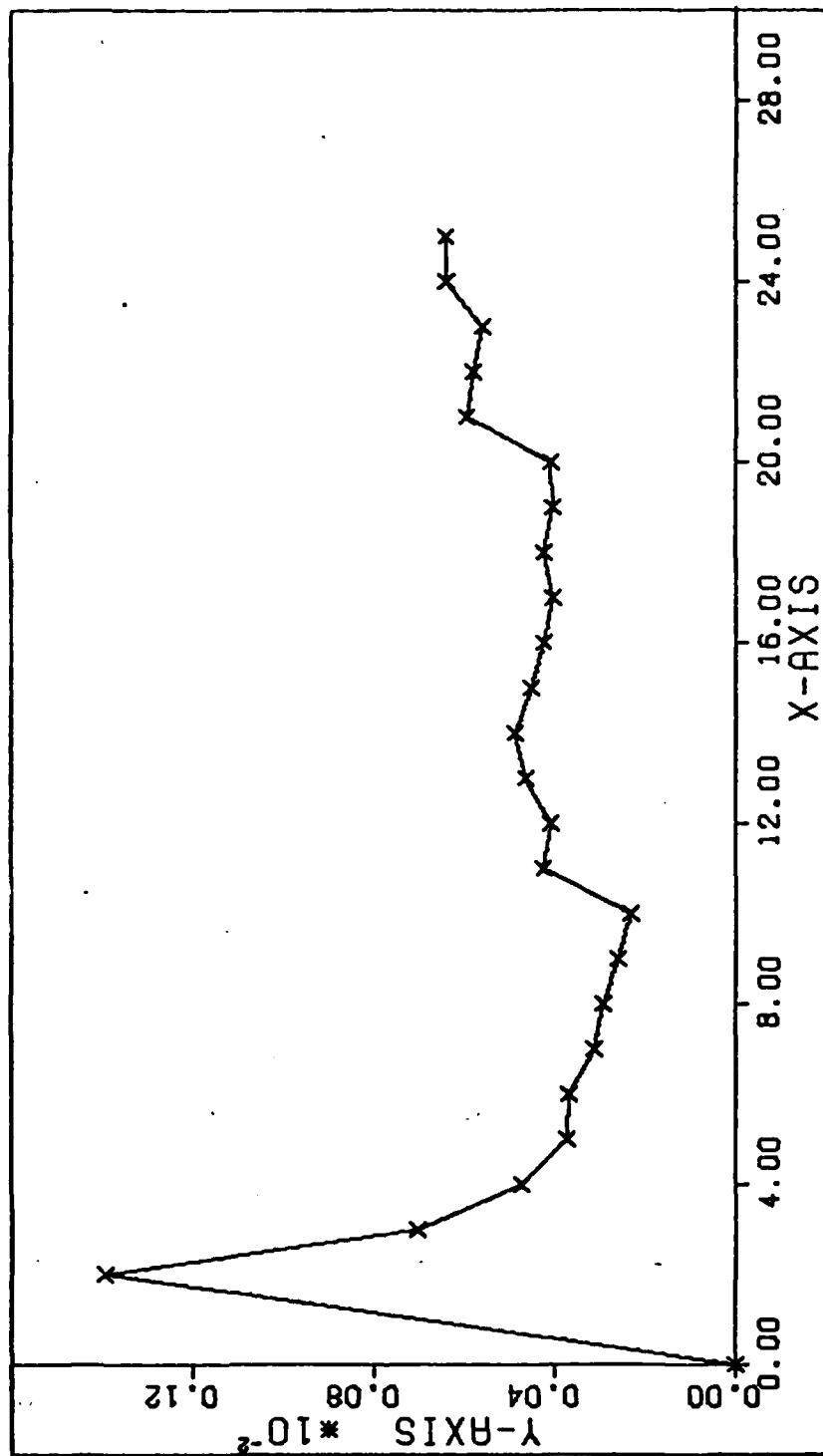
29

Fig 4. σ_a^2 vs N, Least Squares Filter

Fig 5. σ_M^2 vs N, Least Squares Filter

31
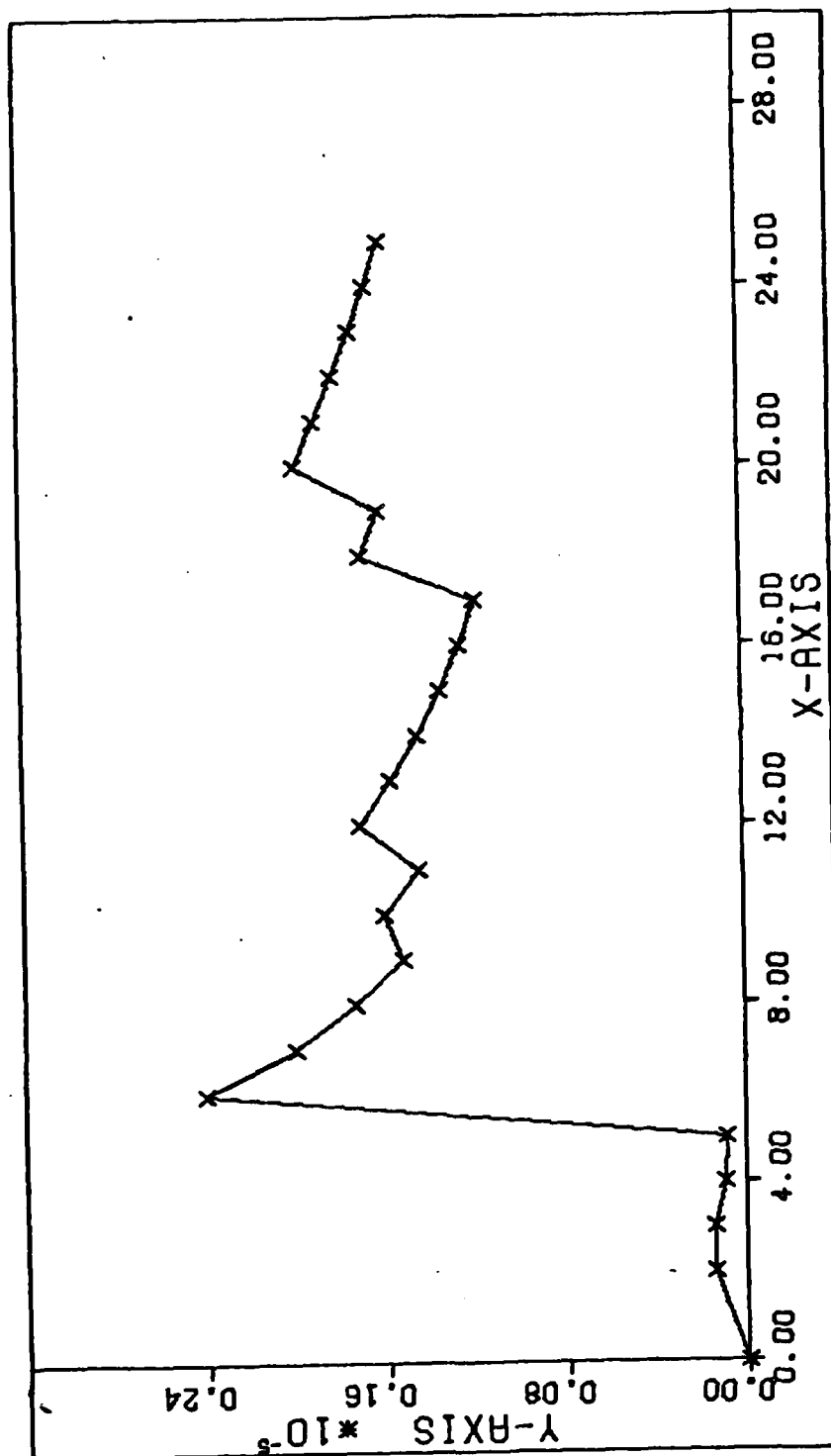
Fig 6. σ_a^2 vs N, Bayes Filter

32
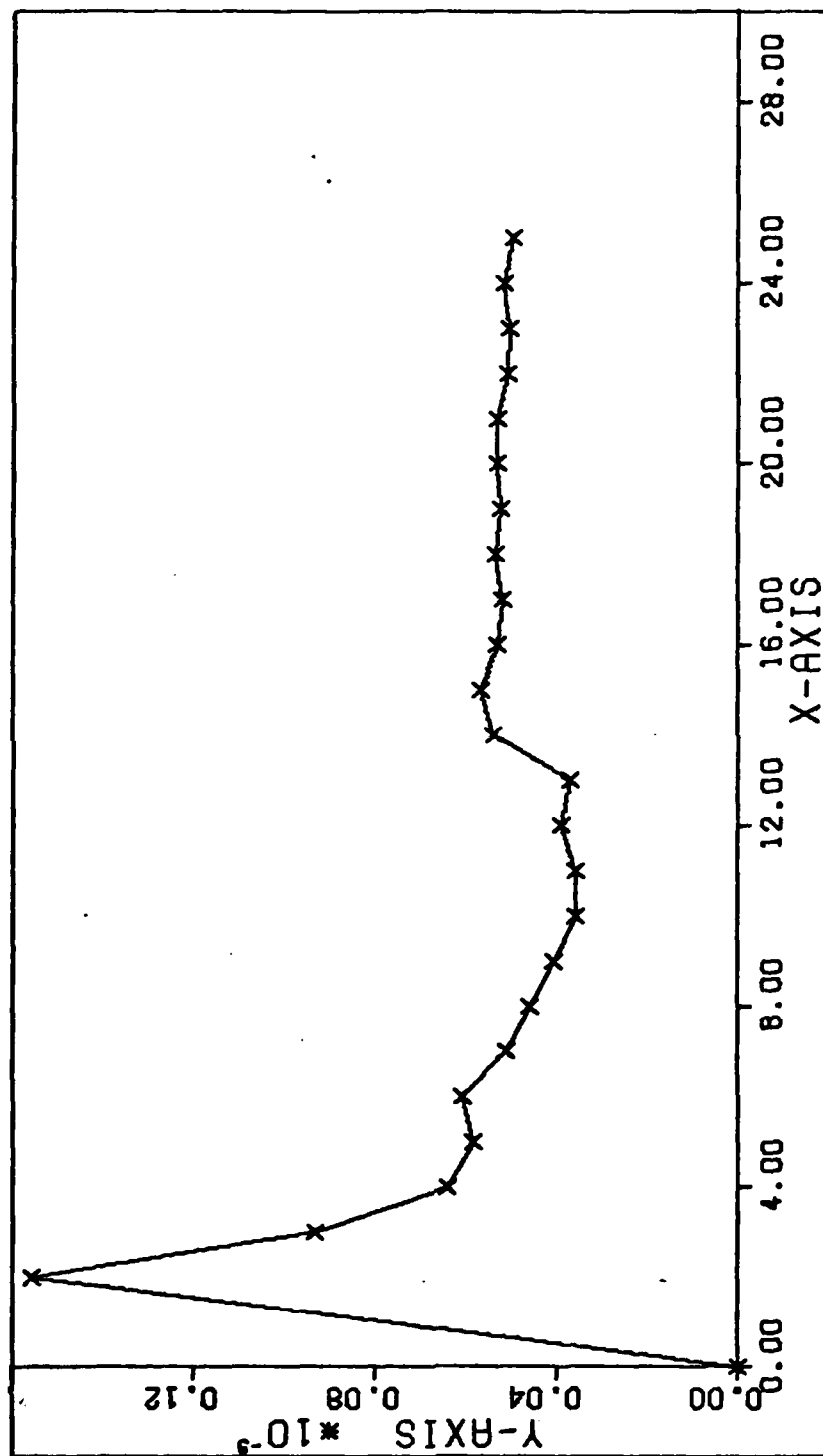
Fig 7. σ_M^2 vs N, Bayes Filter

33
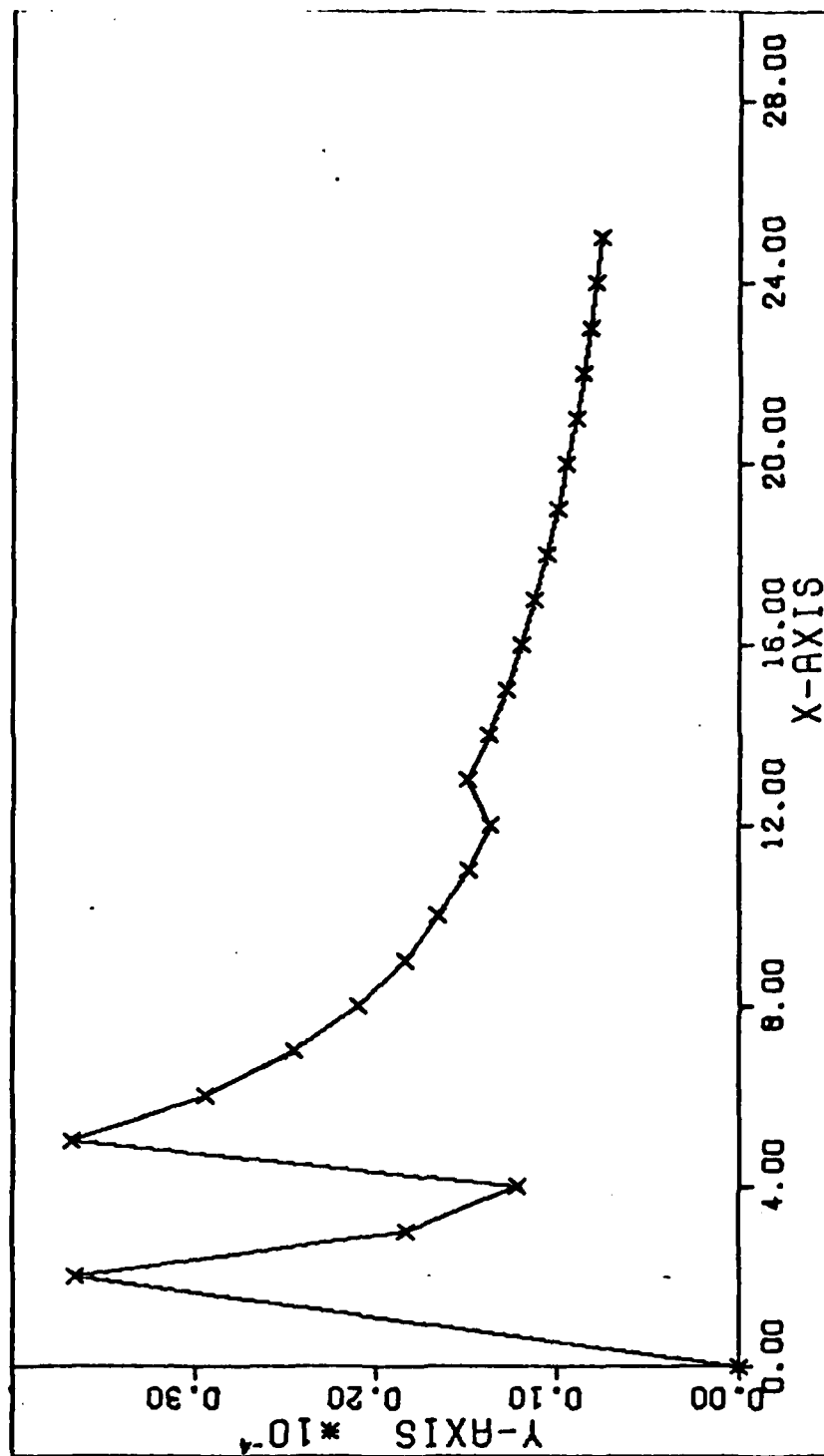
Fig 8. σ_a^2 vs N, Kalman Filter
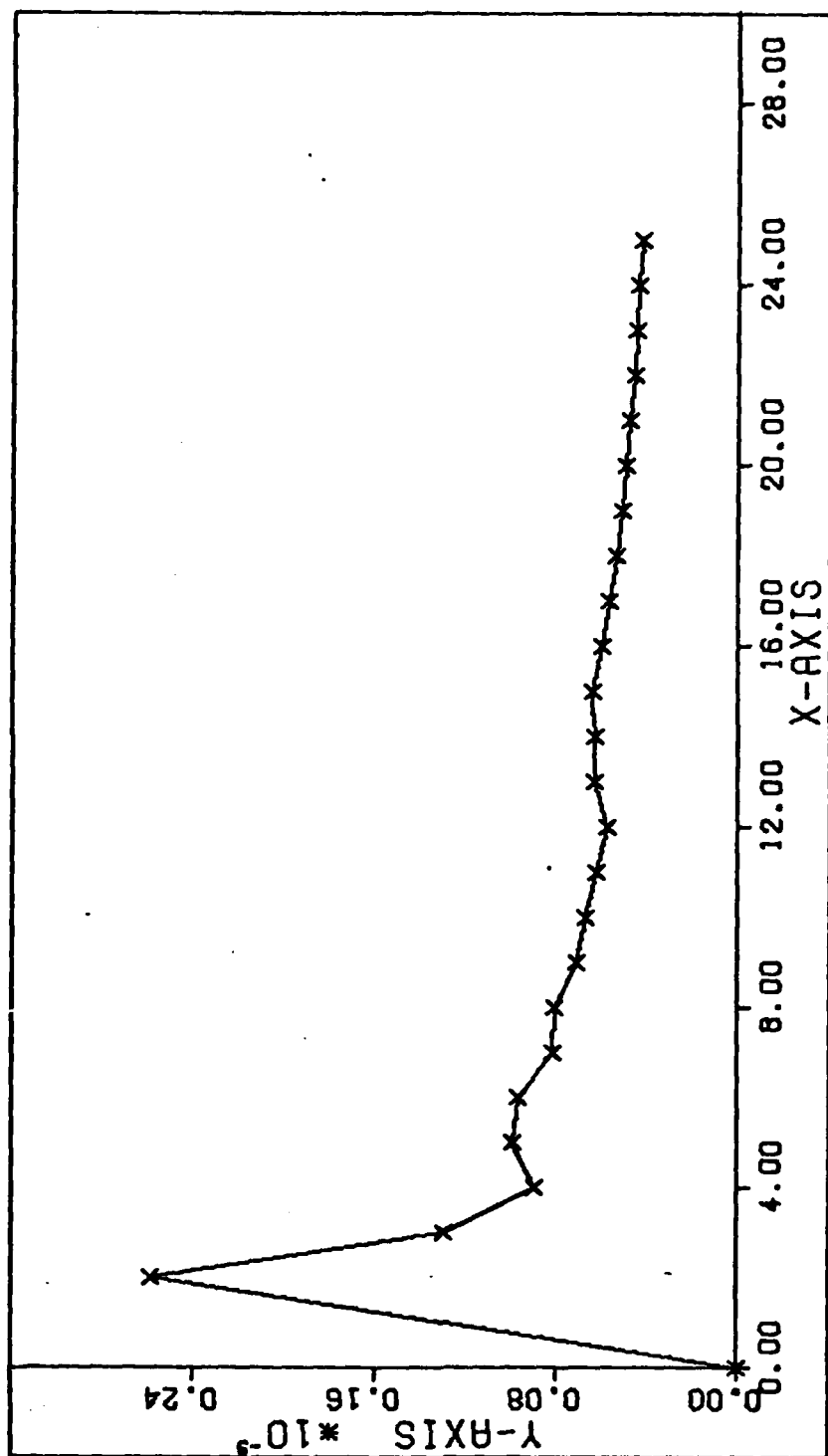
Fig 9. σ_M^2 vs N, Kalman Filter

35

TABLE II

Covariance Analysis

Filter	Semi-major Axis (DU^2)		Mean Anomaly (Rad^2)	
	Estimate	Monte Carlo	Estimate	Monte Carlo
Least Squares	1.7×10^{-11}	6.3×10^{-6}	4.7×10^{-9}	1.4×10^{-3}
Bayes	2.2×10^{-12}	1.2×10^{-6}	2.6×10^{-9}	5.3×10^{-5}
Kalman	2.2×10^{-12}	1.3×10^{-6}	2.5×10^{-9}	5.3×10^{-5}

in the filter models. The lack of process noise in the system could result in artificially low estimates of the covariance matrix. This also causes the filters to follow the model and ignore the measurement updates, resulting in slow convergence.

Also noted in Table II is the slightly better performance of the Bayes and Kalman filters compared to the Least Squares filter. This is in part due to the basic operation of the filters. The Least Squares filter is a batch estimator and updates the estimate after ten measurement updates. The filter minimizes the residuals over the last ten measurements. The Bayes and Kalman filters are recursive filters and minimize the residuals of the last measurement only.

Finally, the data in Table II indicates that the Kalman and Bayes filters provide similar results. This similarity will be investigated further in the following sections.

State Estimate Errors

Another measure of filter performance is the error in the state estimates. The errors evaluated in this section are the mean error, the standard deviation, and the root mean squared (rms) error.

The mean error given in the previous section is

$$\bar{e}_j = \frac{1}{N} \sum_{i=1}^{N} (x_T - \hat{x}_i)_j \tag{62}$$

This provides the mean error of the jth element based on N runs. As stated in the previous section, fifteen runs are used for the Monte Carlo analysis.

The standard deviation is the square root of the variance defined in the previous section and the rms error, σ, is the square root of the mean squared error σ^2 defined in the previous section.

Discussions of these errors for each satellite case are presented in the following sections.

Case I

This orbit is used to verify filter performance under normal operations. A measurement update is input every 10 time units, a little more than two hours (133 min). Twenty measurement updates are processed for filter evaluation.

Plots of mean error and mean error plus and minus rms error are presented for comparison. Plots of mean error plus and minus standard deviation may be more meaningful; however, for nearly zero-mean errors, there is little difference between rms error and standard deviation. The following plots show that the errors are nearly zero-mean.

Figures 10-12 are plots of the mean error and mean error plus and minus rms error of the semi-major axis for the three filters. The mean errors are nearly zero-mean. The Bayes and Kalman Filters demonstrate a large initial transient in the estimates. The mean error minus the rms error is nearly 800 km which is unacceptable for this problem. Both filters recover from these transients to errors of less than 50 km.
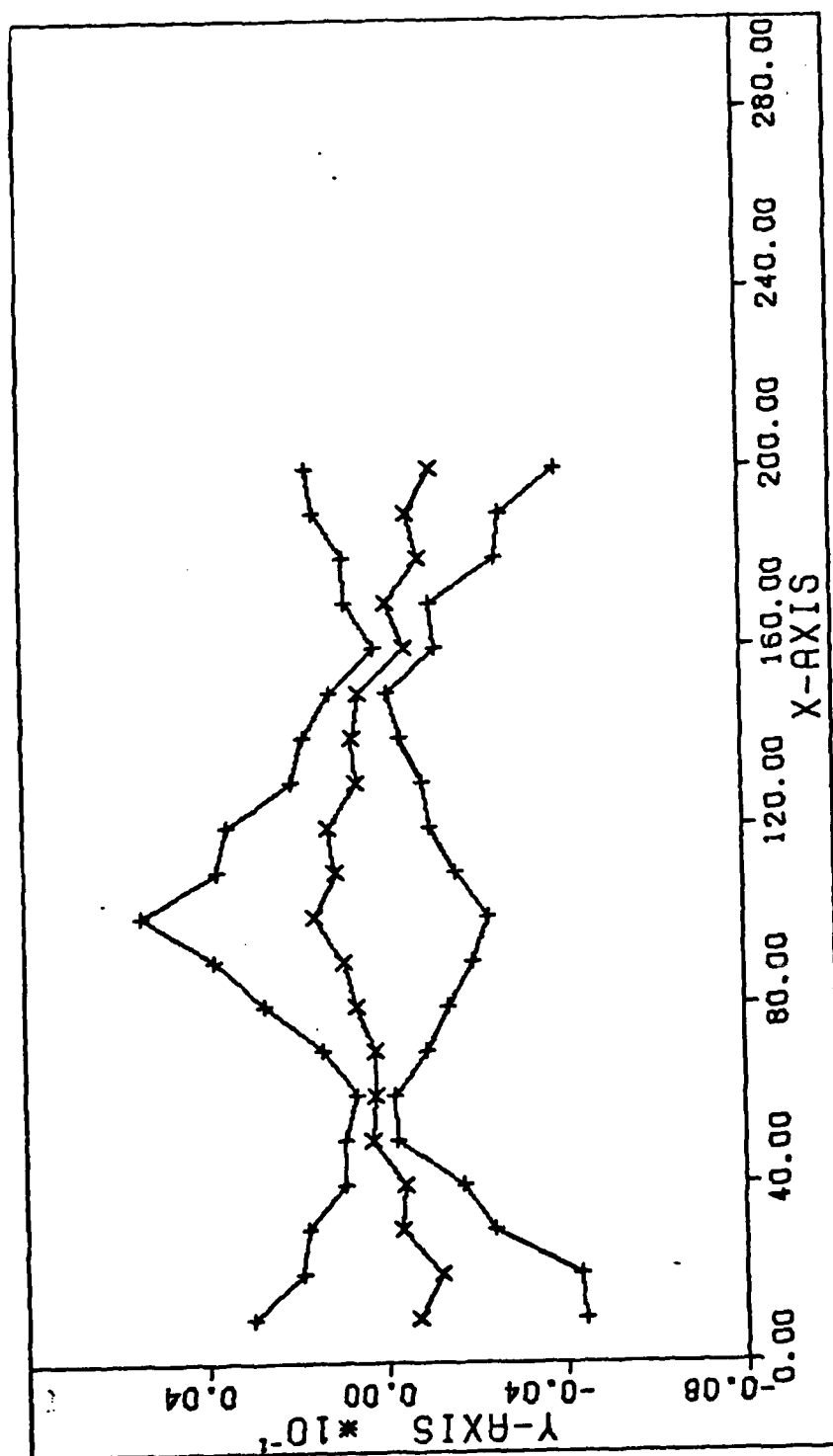
Fig 10. $e_a \pm \sigma_a$ vs t, Least Squares Filter – Case I
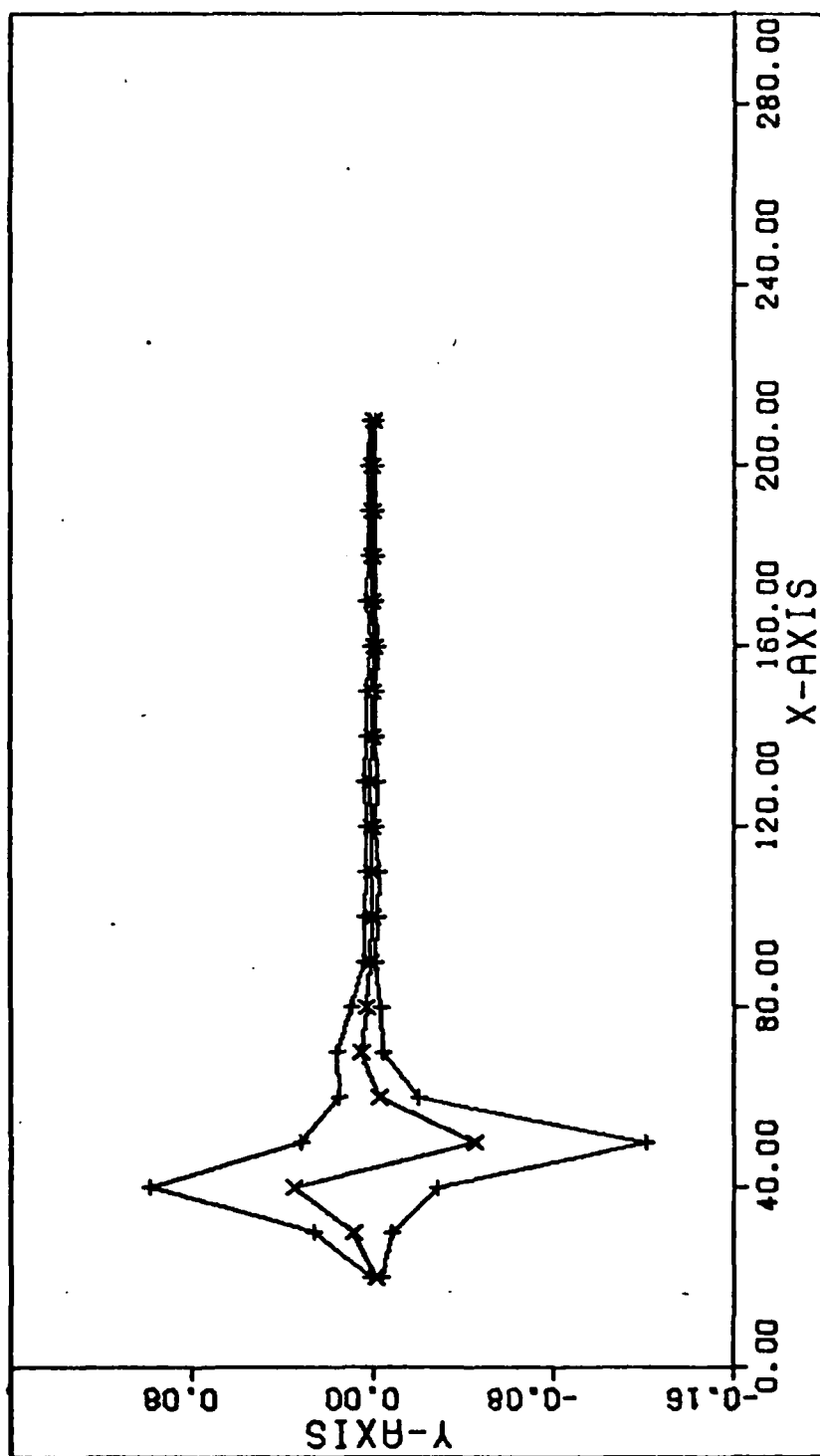
38

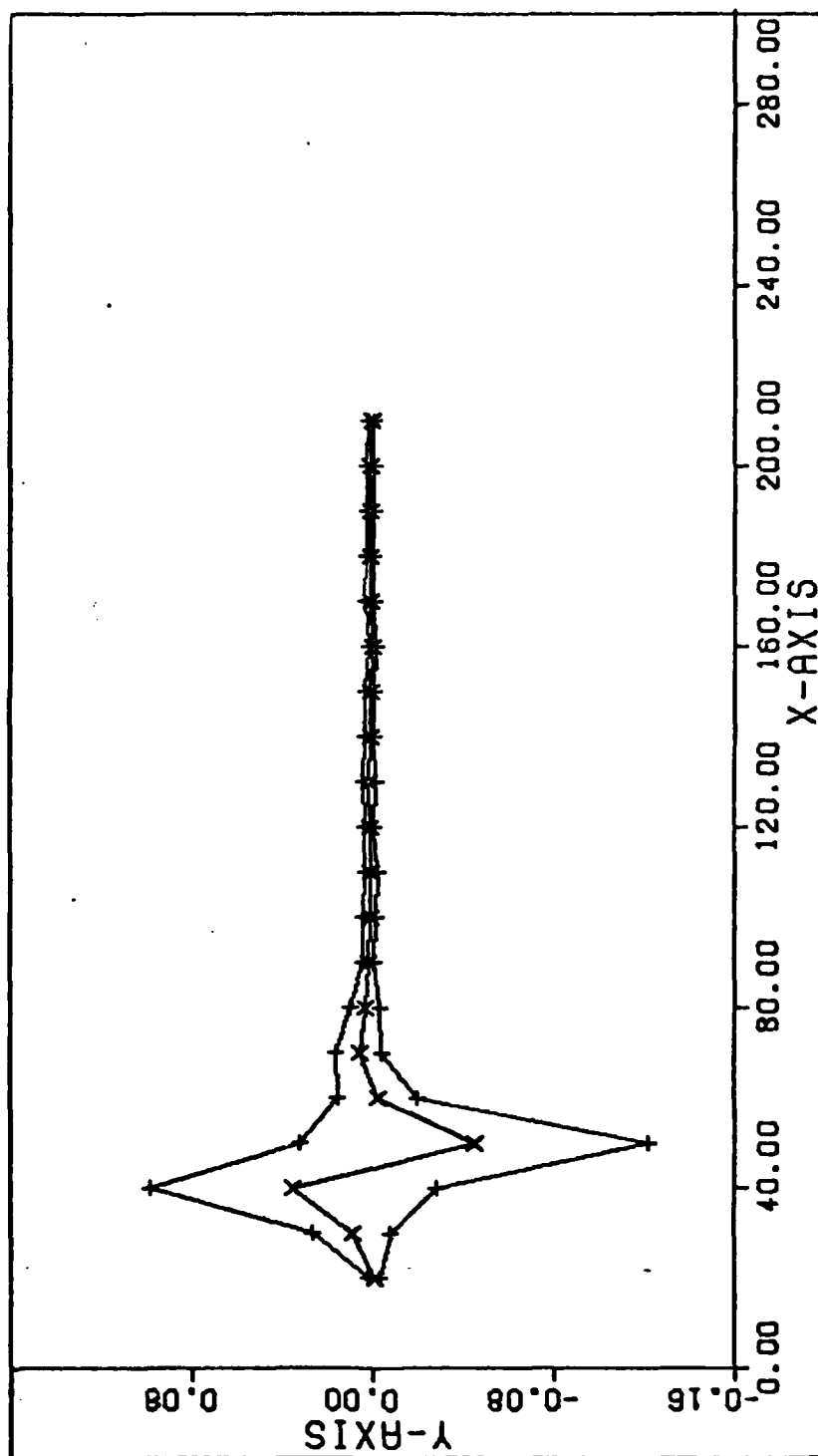Fig 11. $e_a \pm \sigma_a$ vs t, Bayes Filter - Case I

39

Fig 12. $e_a \pm \sigma_a$ vs t, Kalman Filter - Case I

Similar results are observed in the plots for mean anomaly for the Bayes and Kalman Filters (Figs 13 and 14).

The large initial transients could be due to two possible problems. First, there may be observability problems in estimating the derivative of the semi-major axis $\dot{a}$. The estimates of $\dot{a}$ in both the Bayes and Kalman Filters tend to track noise in the data. Second, the filters' initial estimate of the covariance matrices could be tuned to eliminate the large initial transients.

Another difficulty is the appearance of a bias in the estimation of the inclination (Figs 15-17). Also the Bayes ad Kalman Filters appear to be diverging in the estimate of the inclination. These problems will be investigated in Case II with a longer time scale.

The plots of mean error versus time for the remaining elements are contained in Appendix F. A comparison of the estimation results of the Bayes and Kalman Filters shows little or no difference. These similarities are also demonstrated in Table III, which presents the maximum mean error, maximum rms error, and maximum standard deviation for each element. Due to their similarities subsequent results will be presented for only the Bayes or Kalman Filter, but not both.

Case II

This orbit is input to evaluate the filter performance with a reduced rate of measurement updates. About two measurements per day are input to the filters. Also, the semi-major axis is two earth radii, so atmosphere effects will not be present. Only the Least Squares and Bayes Filters are evaluated for this case.

Figures 18 and 19, plots of the mean error in the semi-major axis and mean anomaly for the Least Squares Filter, indicate a periodic
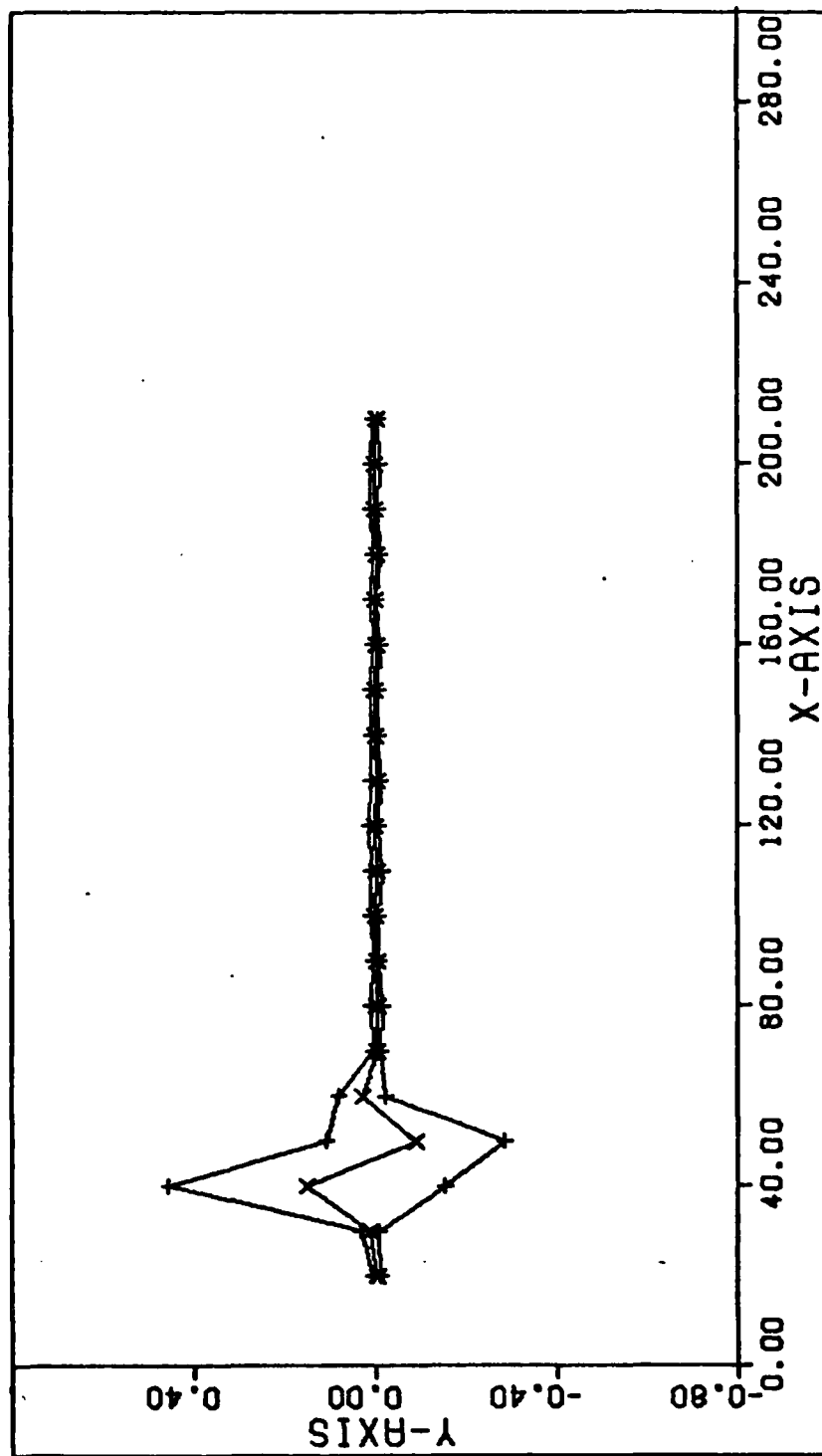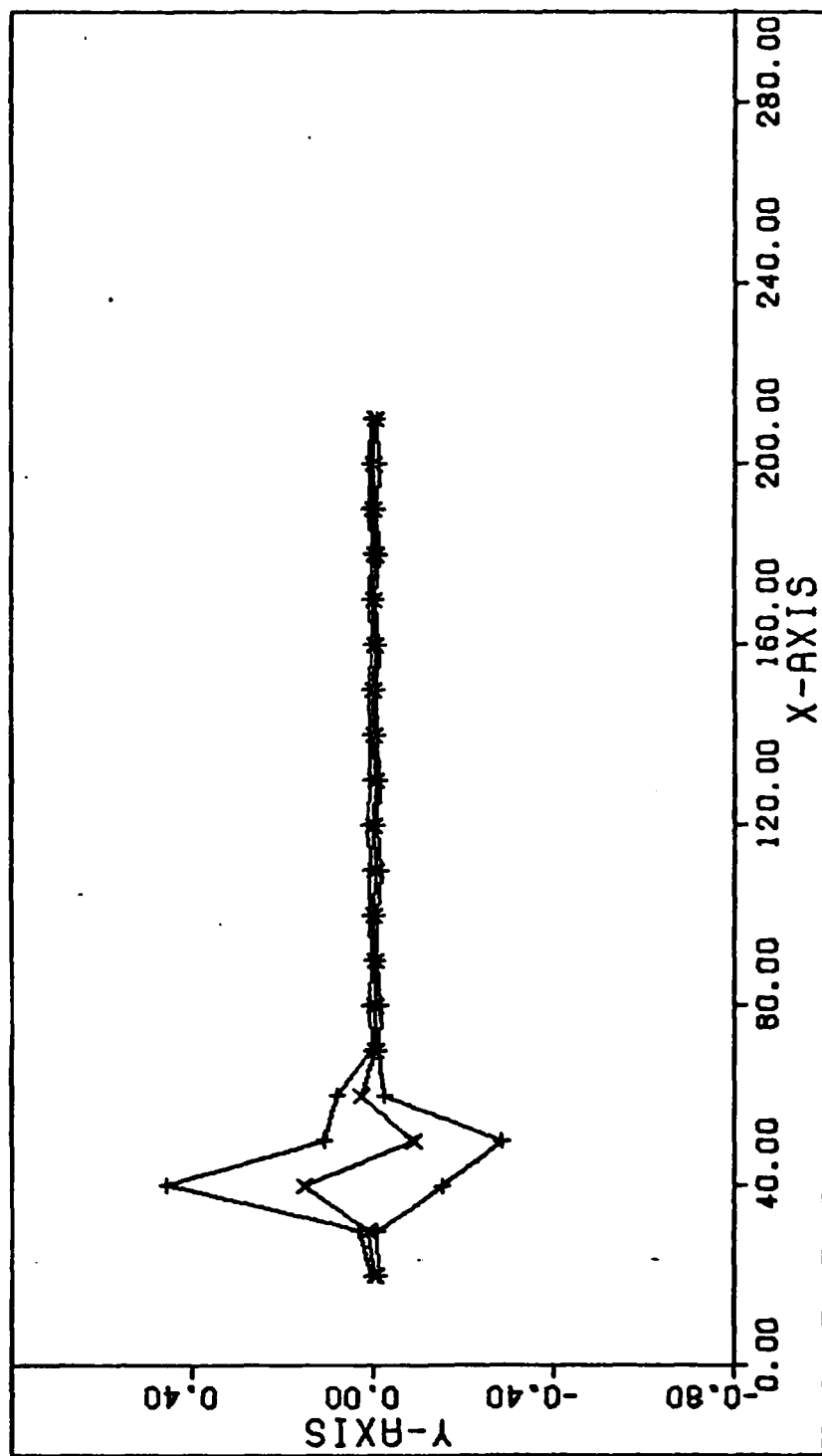
Fig 13. $e_M \pm \sigma_M$ vs t, Bayes Filter - Case I
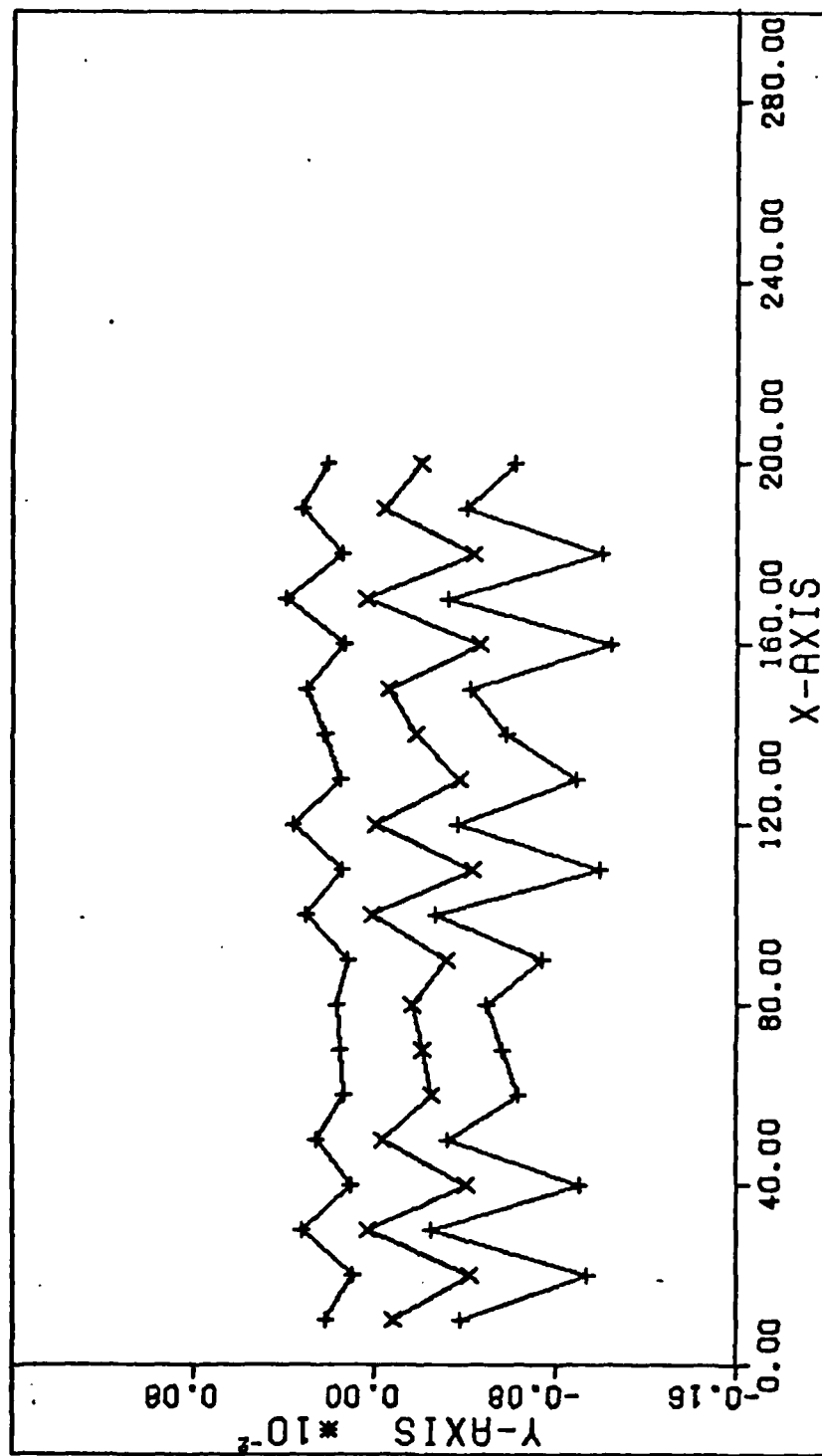
Fig 14. $e_M \pm \sigma_M$ vs t, Kalman Filter – Case I

43

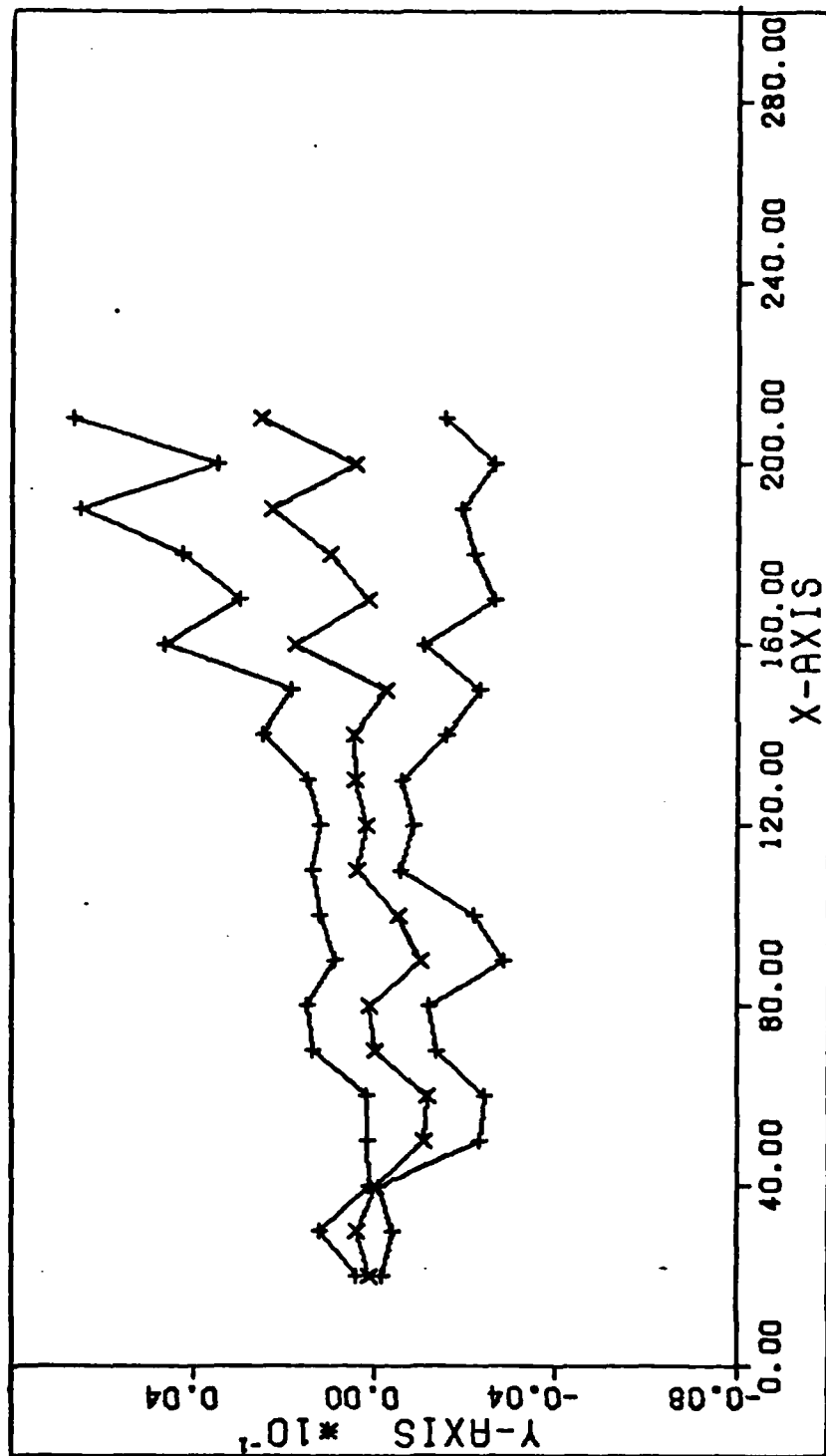Fig 15. $e_i \pm \sigma_i$ vs t, Least Squares Filter - Case I
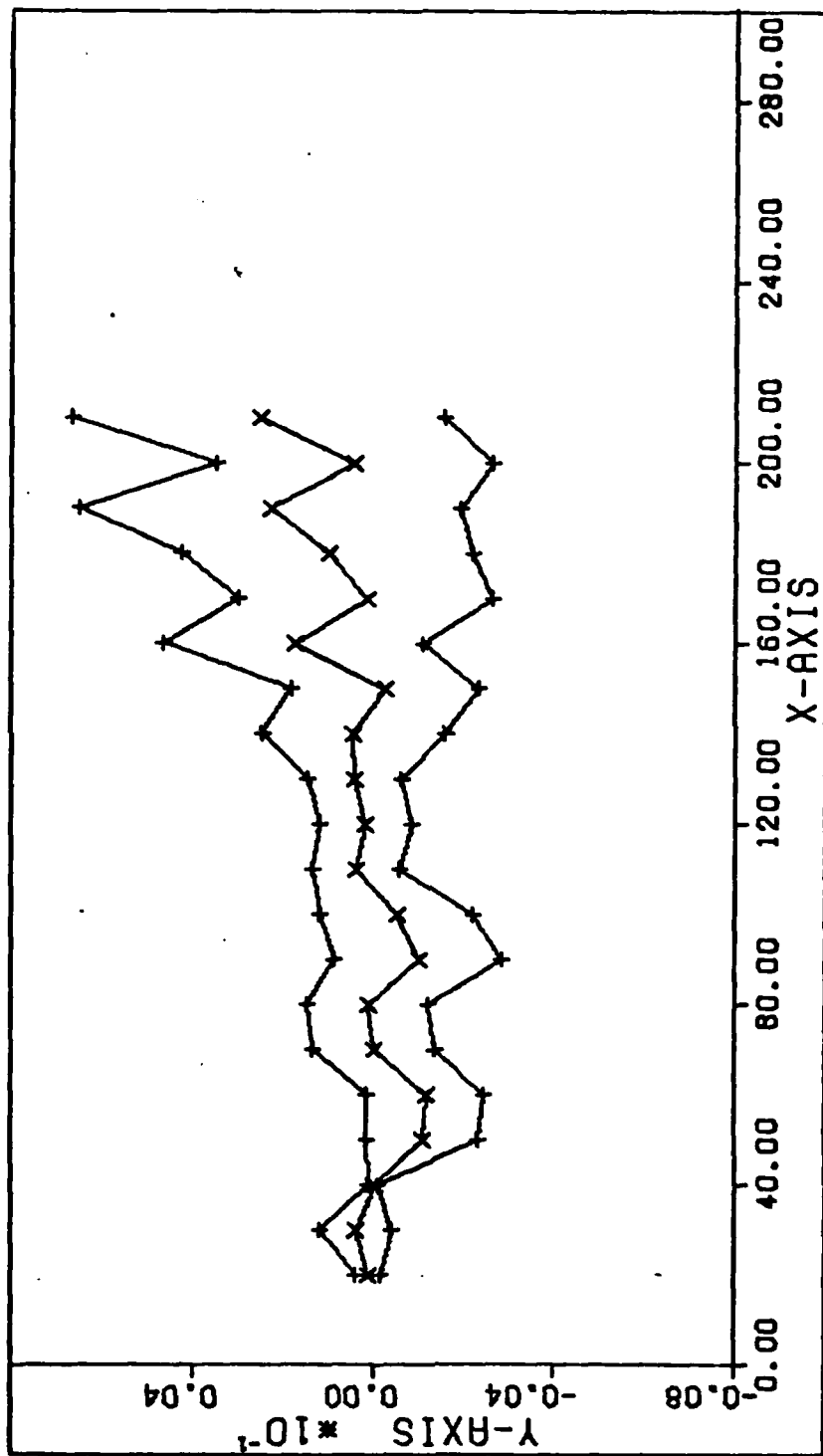
Fig 16. $e_i \pm \sigma_i$ vs t, Bayes Filter - Case I

Fig 17. $e_i \pm \sigma_i$ vs t, Kalman Filter - Case I

TABLE III

Maximum Estimation Errors - Case I

Least Squares Filter

Element	e_M (mean error)	σ_M (rms error)	Max Std Dev
a (km)	7.6	25.0	22.6 km
e	0.0009	0.0013	0.0012
i (deg)	0.03	0.03	0.02
ω (deg)	0.74	0.81	0.34
Ω (deg)	0.057	0.069	0.040
M (deg)	1.26	3.0	2.90

Bayes Filter

Element	e_M (mean error)	σ_M (rms error)	Max Std Dev
a (km)	286 (32)[1]	486 (42)[1]	395 (15)[1]
e	0.0008	0.0028	0.00265
i (deg)	0.14	0.24	0.18
ω (deg)	1.1	1.9	1.5
Ω (deg)	0.080	0.11	0.08
M (deg)	8.6 (0.20)[1]	17.2 (0.65)[1]	15.1 (0.63)[1]

Kalman Filter

Element	e_M (mean error)	σ_M (rms error)	Max Std Dev
a (km)	281 (36)[1]	485 (42)[1]	395 (15)[1]
e	0.0009	0.0028	0.00245
i (deg)	0.13	0.24	0.18
ω (deg)	1.1	1.9	1.5
Ω (deg)	0.08	0.11	0.10
M (deg)	8.6 (0.17)[1]	17.2 (0.65)[1]	15.1 (0.63)[1]

Note 1: Maximum values following initial transient.

variation with a period of about 500 TU, about five days. This is the frequency of the estimate update for this filter. The Bayes Filter estimates, which are updated every 50 TU, about twelve hours, do not show similar trends (Figs 20 and 21). These two plots again display large initial transients in the semi-major axis and the mean anomaly. The large transients are in the rms error and not in the mean error.

Figure 22, mean error in inclination versus time for the Bayes Filter, shows that the filter is again diverging in the estimate of the inclination.

The plots of mean error versus time for the remaining elements are contained in Appendix F. The maximum mean errors, rms errors, and standard deviations for Case II are shown in Table IV.

Case III

This orbit is used to evaluate filter performance with large perturbations due to air drag. The Least Squares and Kalman Filters were evaluated for this orbit. The perigee altitude of this orbit is 200 km and the apogee altitude is 1700 km. The drag coefficient, B, of the satellite is increased from 0.01 to 0.1 Kg/m^2. The non-circular orbit is used to provide variations in the air drag and thus the derivative of the semi-major axis. Plots of mean error and mean error plus and minus rms error in the semi-major axis verus time for the two filters are shown in Figures 23 and 24. Similar plots for the mean anomaly are shown in Figures 25 and 26.

Table V contains the maximum mean errors, rms errors, and standard deviations for each element for both filters.
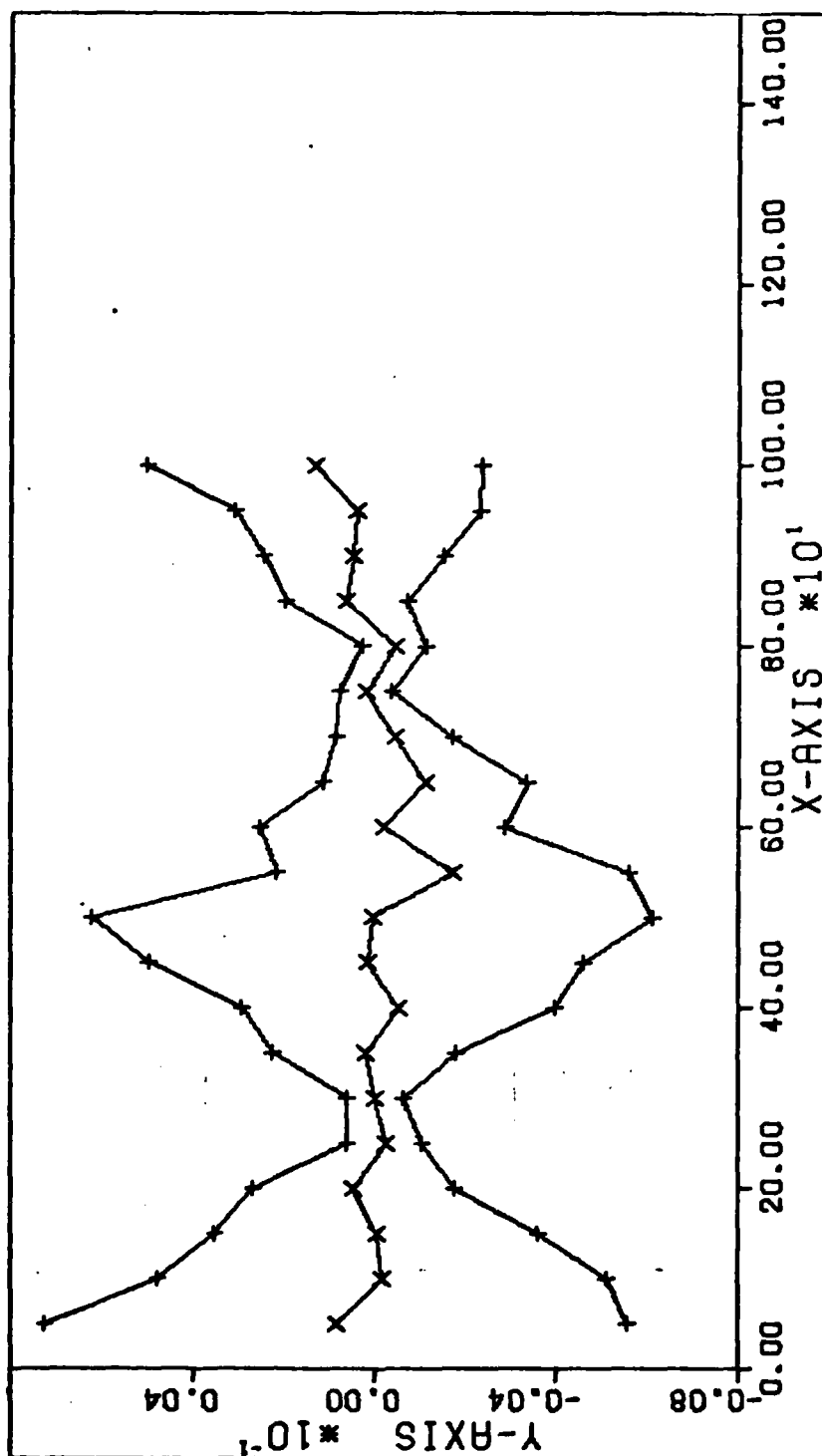
48

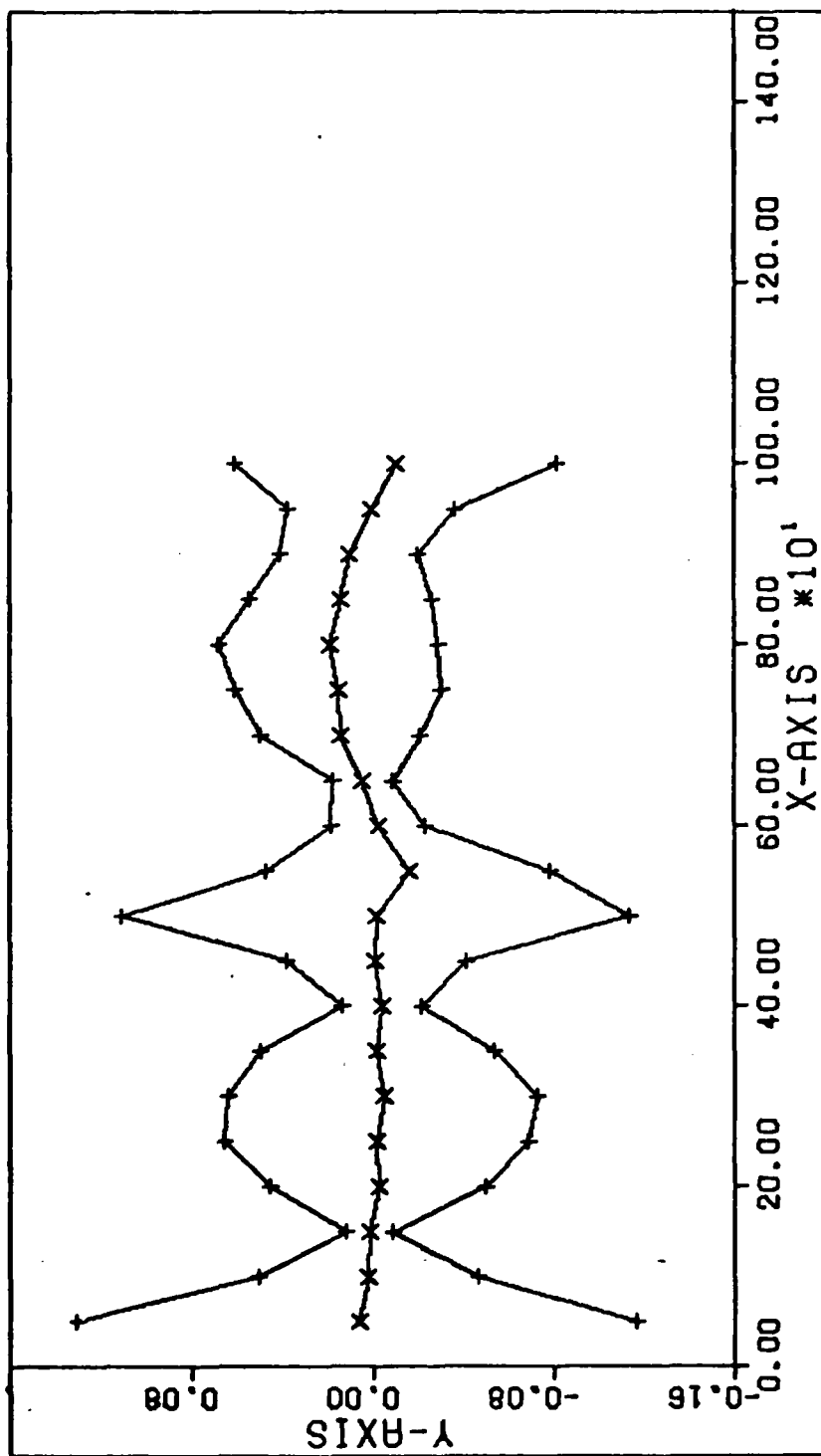Fig 18. $e_a \pm \sigma_a$ vs t, Least Squares Filter - Case II

Fig 19. $e_M \pm \sigma_M$ vs t, Least Squares Filter - Case II

50

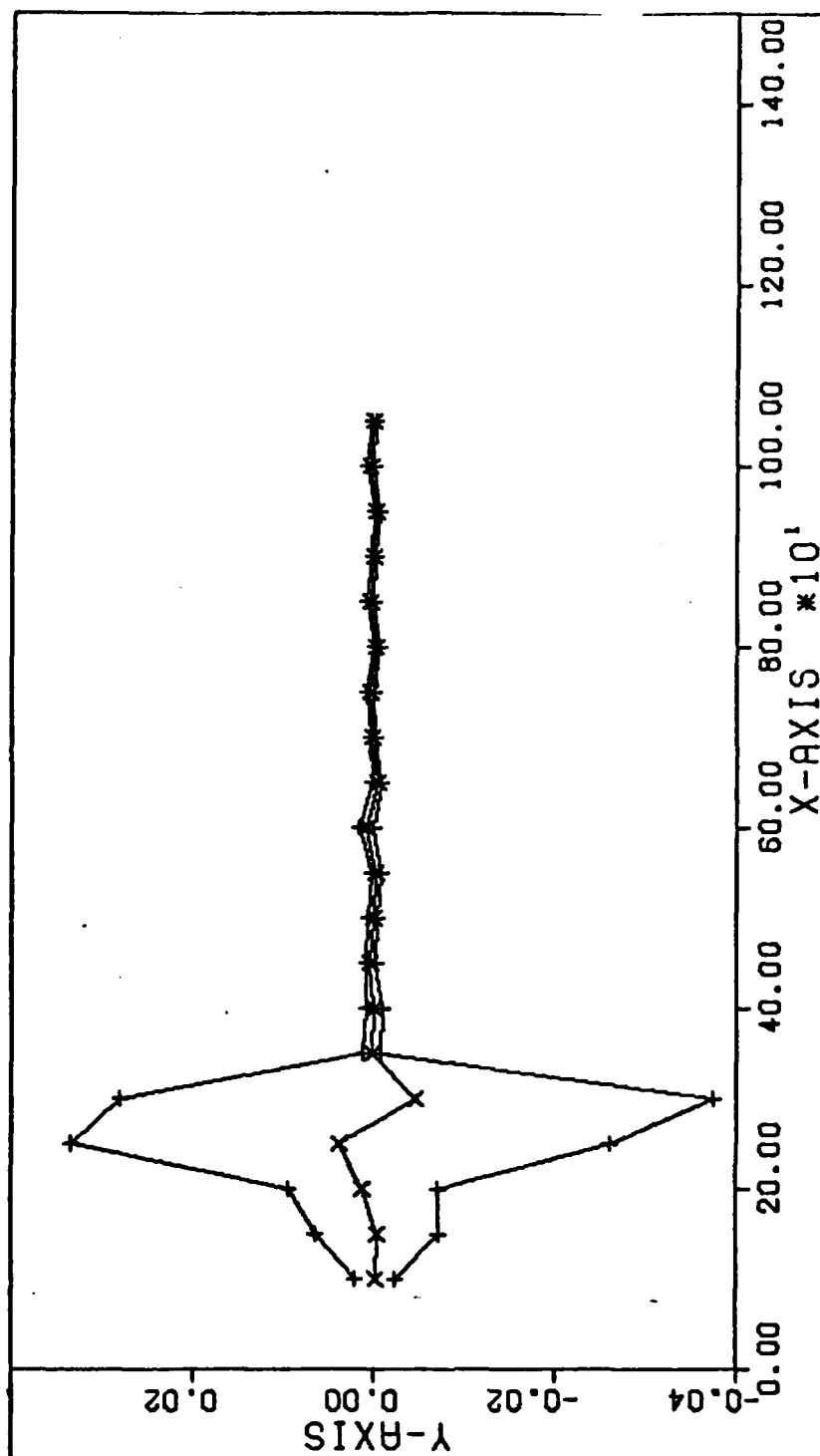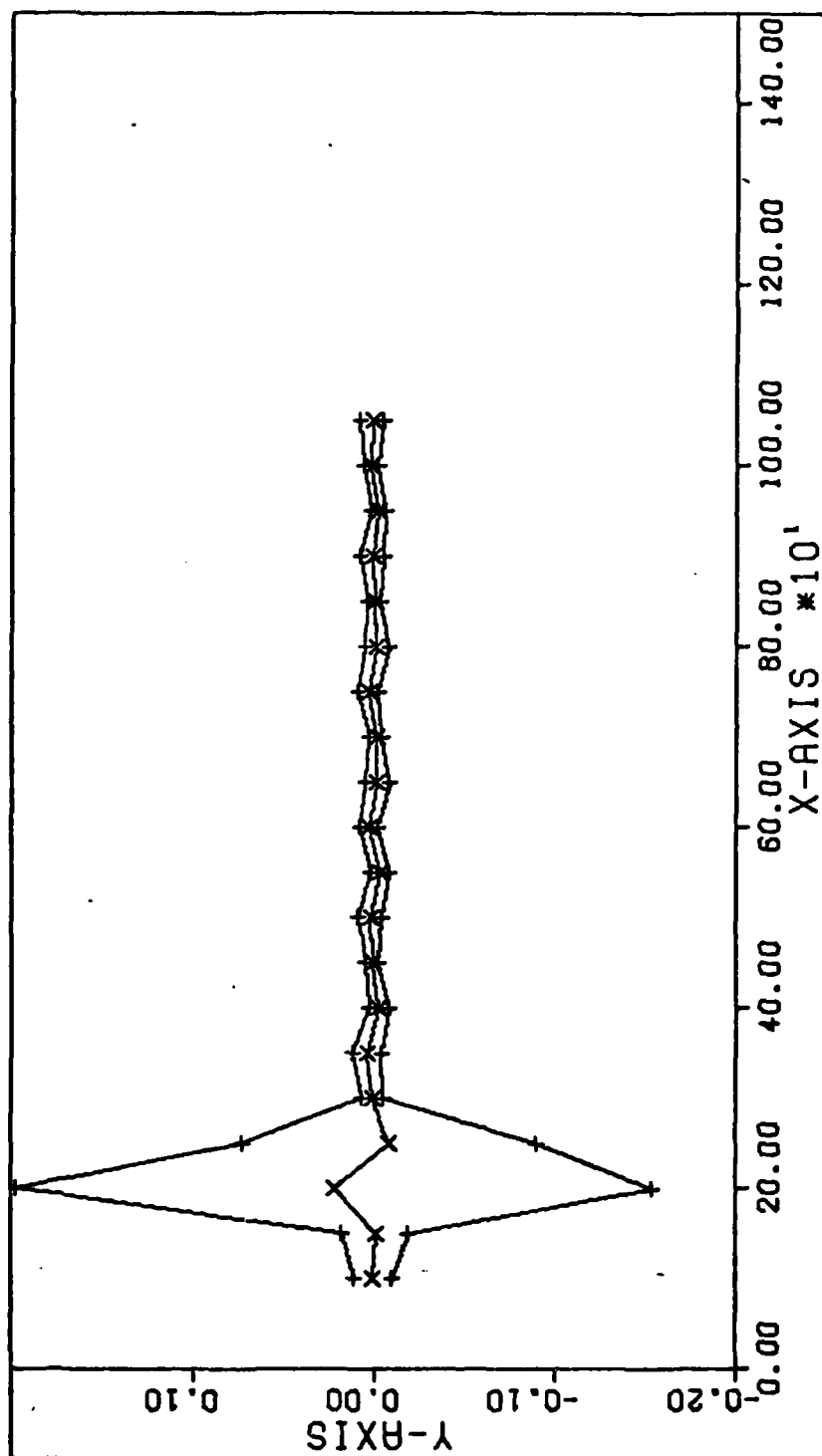Fig 20. $e_a \pm \sigma_a$ vs t, Bayes Filter - Case II

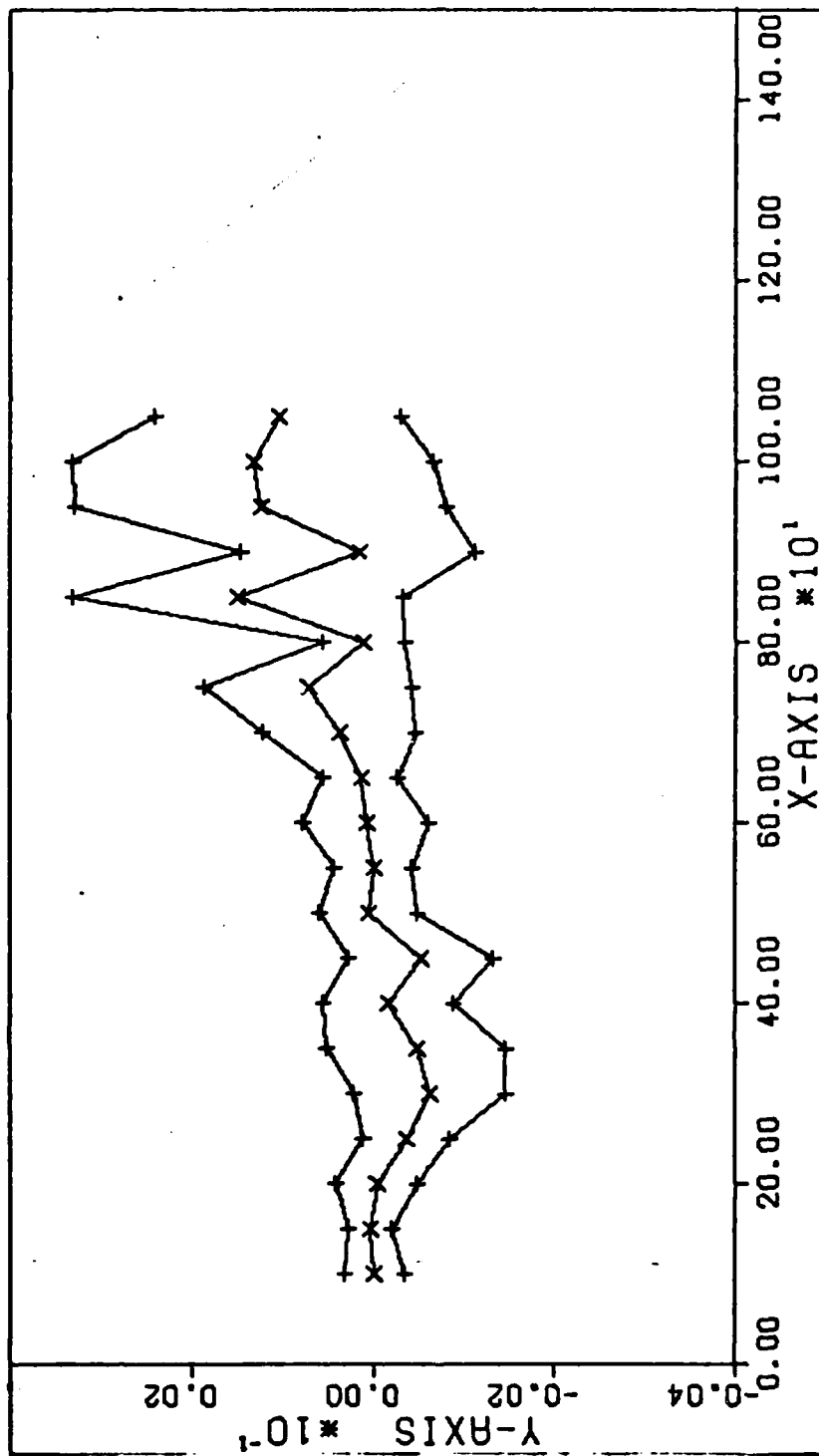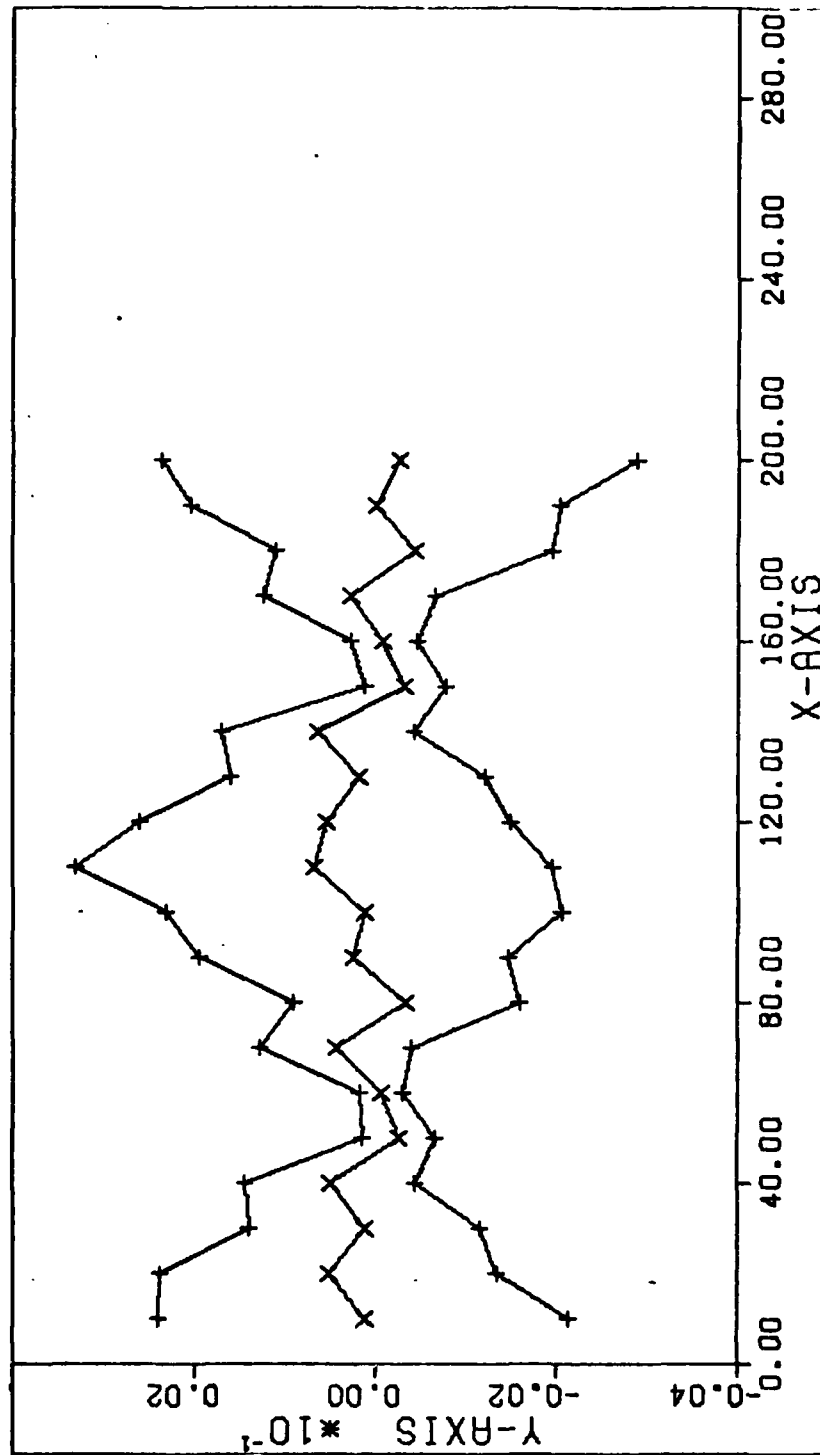Fig 21. $e_M \pm \sigma_M$ vs t, Bayes Filter - Case II

Fig 22. $e_i \pm \sigma_i$ vs t, Bayes Filter - Case II

TABLE IV

Maximum Errors - Case II

Least Squares Filter

Element	$\bar{e}_M$ (mean error)	σ_M (rms error)	Max Std Dev
a (km)	10.8	40.8	40.4
e	0.0014	0.0017	0.0010
i (deg)	0.09	0.032	0.031
ω (deg)	0.26	0.45	0.36
Ω (deg)	0.12	0.13	0.04
M (deg)	1.09	7.02	7.02

Bayes Filter

Element	$\bar{e}_M$ (mean error)	σ_M (rms error)	Max Std Dev
a (km)	30.0 (4.7)[1]	212 (5.9)[1]	204 (1.85)[1]
e	0.0006	0.0036	0.0012
i (deg)	0.08	0.12	0.09
ω (deg)	1.1	1.27	0.69
Ω (deg)	0.014	0.044	0.043
M (deg)	1.26 (0.23)[1]	10.1 (0.50)[1]	10.0 (0.38)[1]

Note 1: Maximum values following initial transients.

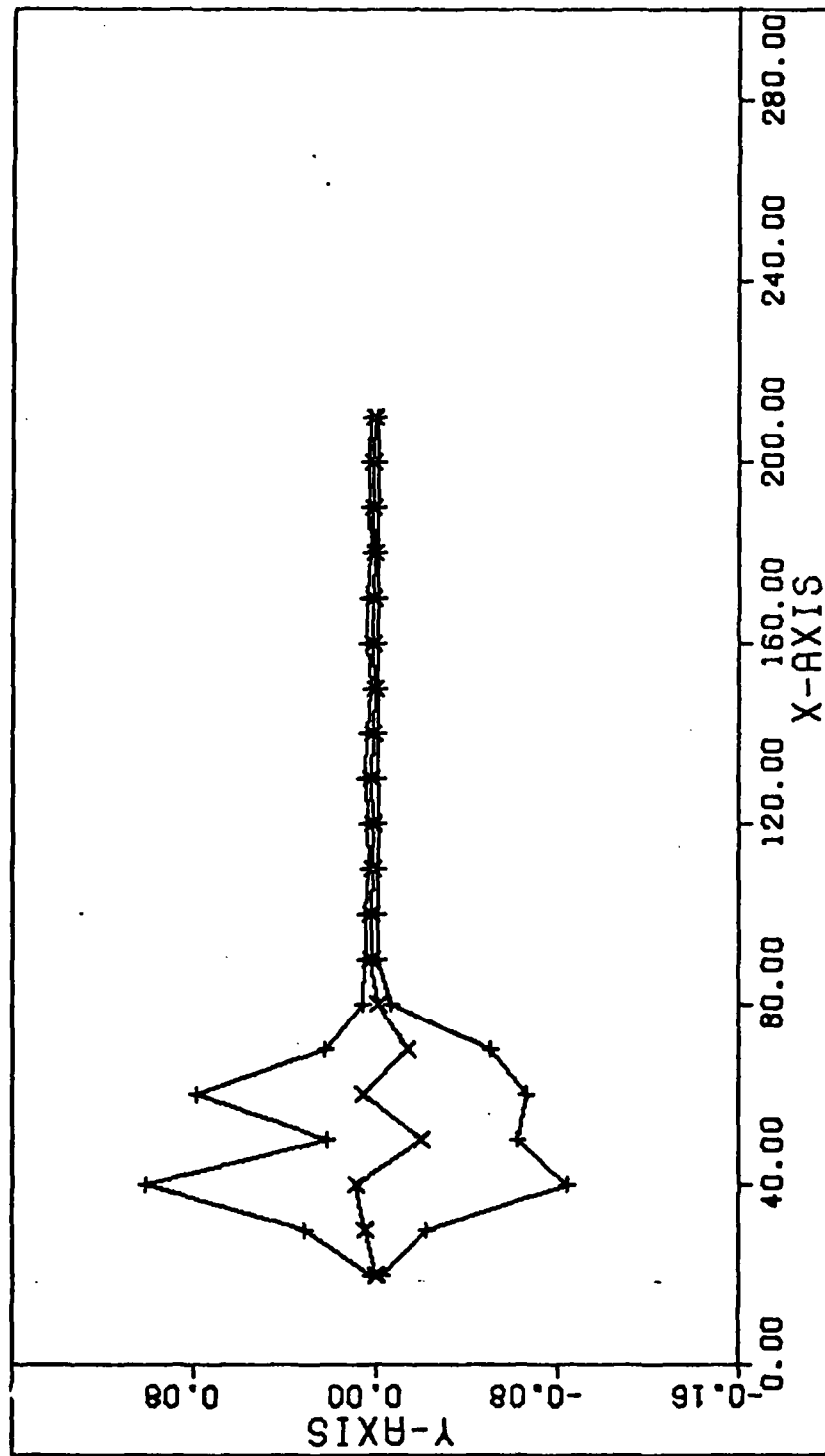Fig 23. $e_a \pm \sigma_a$ vs t, Least Squares Filter – Case III
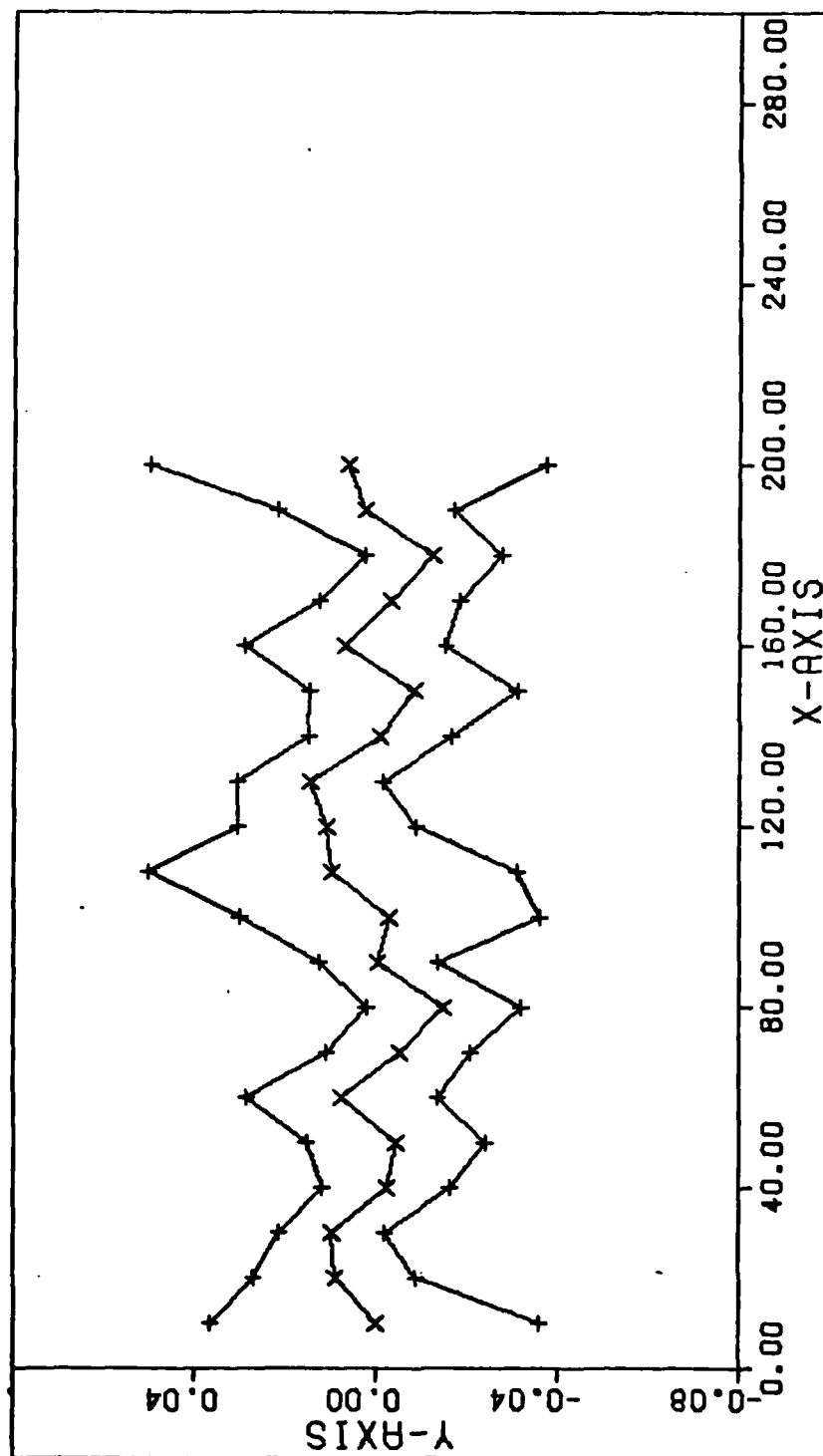
Fig 24. $e_a \pm \sigma_a$ vs t, Kalman Filter - Case III

56

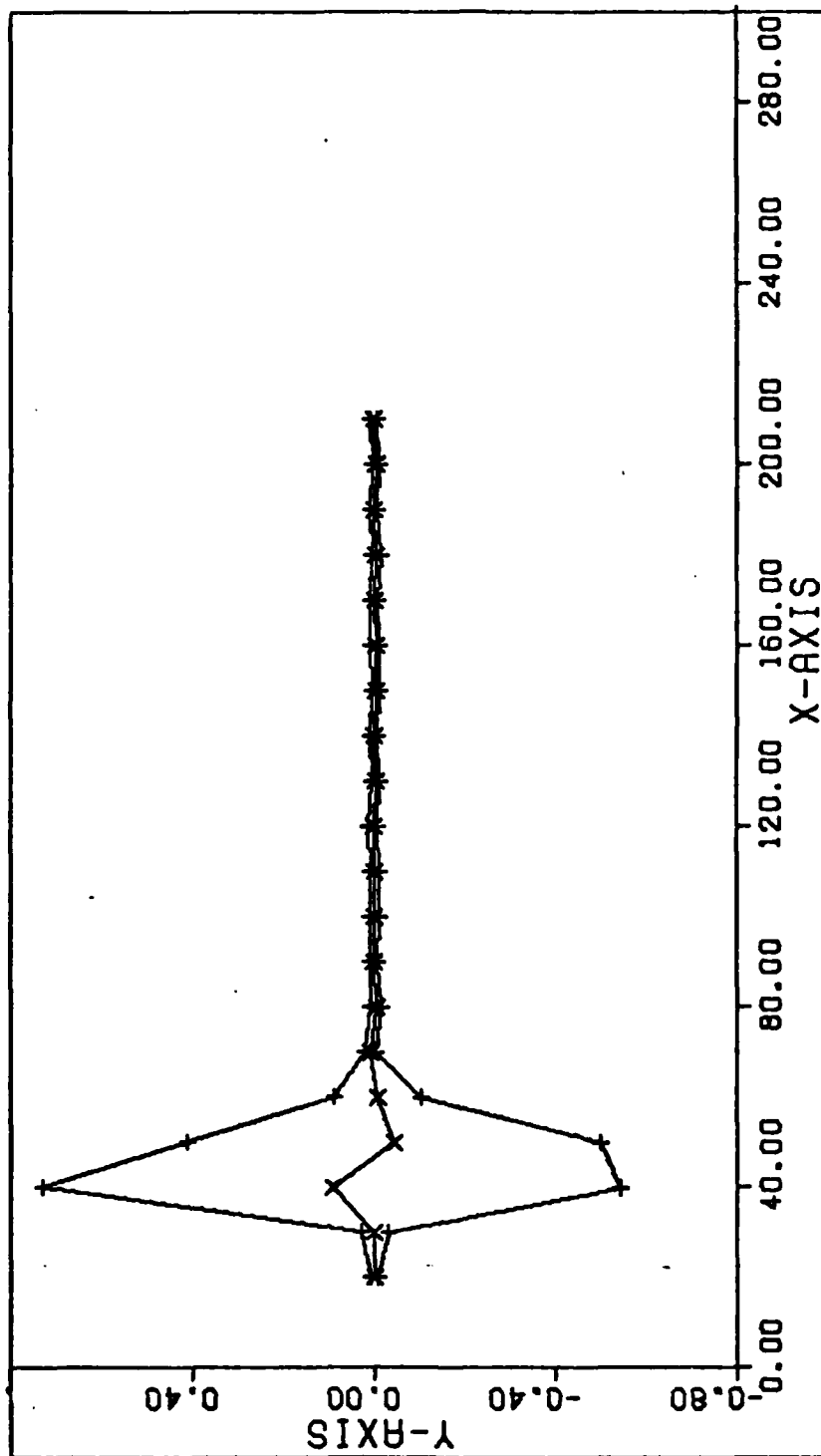Fig 25. $e_M \pm \sigma_M$ vs t, Least Squares Filter - Case III

57

Fig 26. $e_M \pm \sigma_M$ vs t, Kalman Filter - Case III

TABLE V

Maximum Errors - Case III

Least Squares Filter

Element	$\bar{e}_M$	σ_M	Max Std Dev
a (km)	4.33	16.0	15.0
e	0.001	0.001	0.001
i (deg)	0.003	0.12	0.03
ω (deg)	0.74	0.79	0.33
Ω (deg)	0.08	0.09	0.04
M (deg)	0.86	2.50	2.46

Kalman Filter

Element	$\bar{e}_M$	σ_M	Max Std Dev
a (km)	126 (12.6)[1]	588 (19.1)[1]	580 (14.0)[1]
e	0.0021	0.0036	0.0030
i (deg)	0.20	0.29	0.21
ω (deg)	1.43	1.98	1.32
Ω (deg)	0.09	0.14	0.11
M (deg)	5.27 (0.26)[1]	36.7 (0.60)[1]	36.1 (0.57)[1]

Note 1: Maximum values following initial transients.

Case IV

This orbit is used to demonstrate the effects of singularities on the estimators due to undefined components in the classical elements. The first singularity is due to a circular orbit. For a circular orbit, the argument of perigee is not defined since the perigee itself is not defined. Subsequently the mean anomaly is not defined. A zero inclination orbit presents a singularity in the right ascension of the ascending node since the ascending node is not defined.

It should be noted that these singularities are actually due to the transformation from position and velocity vectors to classical elements, and are not singularities in the orbit itself. The orbit is still defined by six elements; but, the classical elements do not uniquely define the orbit.

All the filters have difficulty with this orbit. The major problem is estimating the mean anomaly. Since this quantity is not uniquely defined, large residuals occur. The filters attempt to zero out these residuals by adjusting the mean motion, which in turn causes the semi-major axis to vary. The estimate of the semi-major axis diverges rapidly; and, in the case of this orbit, the filters eventually estimate a negative semi-major axis, halting program execution.

This represents a major problem for the filters used in this study. A possible solution to this problem is to use equinoctal orbital elements as the filter states [Ref 9; 44]. These elements do not have singularities due to circular orbits or zero inclination orbits. Classical elements could still be used as measurement updates. The only change would be the observation relationship, H. The actual estimator equations would not be changed.

60

Case V

This orbit presents observation problems to the estimators. Due to the highly eccentric orbit, the satellite is beyond the range of the radars most of the time; therefore, large data gaps are present in the data.

Attempting an observation every two hours, only one observation per day is obtained due to the range restrictions. Due to the long running time of the truth model to provide data for the filters, a Monte Carlo analysis for this case was not completed. A single run using the Kalman and Least Squares Filters shows no difficulty in estimating the orbital elements for this highly eccentric, low perigee orbit. Table VI shows the estimation errors for the two filters after twenty measurement updates, about twenty days.

TABLE VI

Estimation Errors for Case V

Element	Least Square	Kalman
a	25.5 km	57.0 km
e	0.001	0.0008
i	0.006°	0.03°
ω	0.20°	0.12°
Ω	0.97°	0.02°
M	3.15°	2.75°

It should be noted that these errors are only for one run and are not the result of a Monte Carlo analysis.

Discussion

As seen in the previous examples, all filters encounter problems in estimating the elements and the errors.

First, estimation was not possible with singularities in the classical elements. Second, the Bayes and Kalman Filters demonstrate large initial transients in the estimation problem. These initial transients are reduced. These transients are probably due to observability problems in the derivative of the semi-major axis and an improperly tuned filter.

Next, the in-track errors in the estimates are too large for SDC application. This may be due to using too large errors in the initial radar data or failure of the filters to converge within the specified number of iteration.

Finally, the Bayes and Kalman Filters track noise in the estimates of the derivatives of the semi-major axis and the eccentricity. The wrong sign on these values would greatly effect the ability of the filters to propagate the states forward and predict the satellite's position for radar acquisition.

In spite of the problems listed above, the potential of using two-body elements has been demonstrated in this study. If the problems listed above can be eliminated, any of the filters evaluated could be used by SDC for orbital estimation.

Another characteristic noted in the filter performance is the tendency of the gain matrices in the Kalman and Bayes Filters to approach steady state for a particular orbit.

As shown in Chapter III, the gains for the Bayes and Kalman are re-evaluated for every measurement update. After several measurements the gain matrices change very little from update to update. This is due to the nearly constant values of the orbital elements. If a pre-determined gain can be stored in the computer a significant reduction in computer time can be achieved. In the case of the Kalman Filter, no matrix inversions would be required. The covariance update would be given by

$$P(+) = P(-) - KH\Phi P(-) \tag{63}$$

and the change in the state estimate would be given by

$$\delta\underline{x}(+) = \delta\underline{x}(1-1) + K(\underline{r} - H\Phi\delta\underline{x}(-)) \tag{64}$$

The calculation of the gain

$$K = P(-)\Phi^T H^T (Q + H\Phi H^T\Phi)^{-1} \tag{65}$$

would not be required for every measurement update.

VI. Conclusions and Recommendations

Conclusions

The following conclusions are drawn from the filter performance analysis completed in this study:

1. The feasibility of using two-body classical orbital elements as measurement updates for orbital element estimation is demonstrated by all three filters.

2. All three filters diverge when estimating the elements of a circular orbit.

3. In-track errors in the filter estimates are too large for SDC requirements and techniques must be developed to reduce the error.

4. All filters underestimate the covariance of the estimates.

5. The Kalman and Bayes Filters are similar and differences in their performance can not be detected.

6. All three filters track noise in the estimation of the derivative of the semi-major axis.

7. The Bayes and Kalman Filters have large initial transients in the estimation of the semi-major axis and the mean anomaly. These transients are reduced with further updates.

Recommendations

1. Change the filter states to equinoctal orbital elements to eliminate problems due to singularities in the classical elements.

2. Add process noise to the filter dynamics and tune the filters to improve covariance estimates and remove initial transients.

3. Re-program the Least Squares Filter to improve computational efficiency by taking advantage of symmetry and zeroes in the matrices.

4. Modify the Bayes and Kalman Filters to provide batch estimates of the derivative of the semi-major axis.

5. Obtain actual satellite data for further filter evaluation.

6. Investigate the possibility of using a constant gain matrix for each orbit in the Bayes and Kalman Filters.

7. Investigate other methods of estimating the air drag such as parameter identification.

8. Change the Bayes and Kalman Filters from infinite memory filters to finite or fading-memory filters.

9. Investigate the estimation of the two-body orbital elements from radar data to gain insight into evaluating the measurement noise used in the filters.

Bibliography

1. Baker, Robert M. L., Jr. <u>Astrodynamics</u>. New York: Academic Press, 1967.

2. Baker, Robert M. L., Jr. and Maud W. Makemson. <u>An Introduction to Astrodynamics</u> (Second Edition). New York: Academic Press, 1967.

3. Bate, Roger R., Donald D. Mueller, and Jerry E. White. <u>Fundamentals of Astrodynamics</u>. New York: Dover Publications, Inc., 1971.

4. Brouwer, Dirk and Gerald M. Clemence. <u>Methods of Celestial Mechanics</u>. New York: Academic Press, 1961.

5. Danby, John M. A., <u>Fundamentals of Celestial Mechanics</u>. New York: The MacMillan Company, 1962.

6. Gaposchkin, E. M., <u>Smithsonian Standard Earth III</u>, SAO Special Report 353. Smithsonian Institution Astrophysical Observatory: Cambridge, Massachusetts, 1973.

7. Jacchia, L. G., "A Variable Atmospheric-Density Model from Satellite Acceleration", Journal of Geophysical Research, 2775-2782. September 1960.

8. Johnson, Francis J., <u>Satellite Environment Handbook</u>. Stanford University Press, 1961.

9. Koskela, Paul E., <u>Astrodynamic Analysis for the Advanced Orbit/ Ephemers Subsystem</u>, Aeronutronic Publication No. U-4180. Newport Beach, California: Philco-Ford Corporation, 1967.

10. Maybeck, Peter R. Lecture Notes distributed in EE765, Stochastic Estimation and Control I. School of Engineering, Air Force Institute of Technology, Wright-Patterson AFB, Ohio, 1979.

11. Maybeck, Peter R. Lecture Notes distributed in EE766, Stochastic Estimation and Control II. School of Engineering, Air Force Institute of Technology, Wright-Patterson AFB, Ohio, 1979.

12. Wiesel, Capt William. Lecture Notes distributed in MC636, Numerical Methods of Orbit Determination. School of Engineering, Air Force Institute of Technology, Wright-Patterson AFB, Ohio, 1979.

13. Wiesel, Capt William. Lecture Notes distributed in MC731, Advanced Astrodynamics. School of Engineering, Air Force Institute of Technology, Wright-Patterson AFB, Ohio, 1979.

14. ADCOM DCD 8. <u>Mathematical Foundation for SCC Astrodynamic Theory</u>. Peterson AFB, Colorado: Aerospace Defense Command, United States Air Force, 1977.

Appendix A

Coordinate Frame Transformations

There are two coordinate frame transformations required in this study. The first is a transformation from the perifocal to the geocentric-equatorial coordinate frame [Fig 27]. It is used in the generation of the satellite's initial position and velocity vector from the input orbital elements. The transformation is given by [Ref 3, 80-83]:

$$\begin{bmatrix} X \\ Y \\ Z \end{bmatrix} = [R] \begin{bmatrix} X\omega \\ Y\omega \\ Z\omega \end{bmatrix} \tag{62}$$

where

R is the direction cosine matrix between the two frames. The elements of R are

$R_{11} = \cos \Omega \cos \omega - \sin \Omega \sin \omega \cos i$

$R_{12} = -\cos \Omega \sin \omega - \sin \Omega \cos \omega \cos i$

$R_{13} = \sin \Omega \sin i$

$R_{21} = \sin \Omega \cos \omega + \cos \Omega \sin \omega \cos i$

$R_{22} = -\sin \Omega \sin \omega + \cos \Omega \cos \omega \cos i$

$R_{23} = -\cos \Omega \sin i$

$R_{31} = \sin \omega \sin i$

$R_{32} = \cos \omega \sin i$

$R_{33} = \cos i$

The angles i, Ω , ω are the inclination, right ascension and argument of perigee.
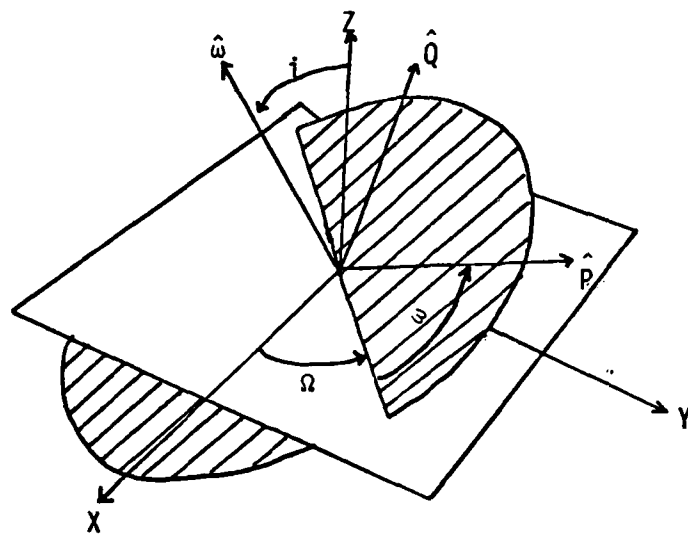
Figure 27. Relationship Between Perifocal
and Geocentric Equitorial Frames

The second coordinate frame transformation is from the local horizon coord^{j}nate frame. This transformation is used to rotate the geopotential acceleration terms into the geocentric-equatorial frame for integration. The rotation is given by [Ref 9; 91].

$$\begin{bmatrix} X \\ Y \\ Z \end{bmatrix} = [T] \begin{bmatrix} X_h \\ Y_h \\ Z_h \end{bmatrix} \tag{63}$$

where

$$[T] = \begin{bmatrix} \cos\alpha\cos\delta & -\sin\alpha & -\cos\alpha\sin\delta \\ \sin\alpha\cos\delta & \cos\alpha & -\sin\alpha\sin\delta \\ \sin\delta & 0 & \cos\delta \end{bmatrix} \tag{64}$$

where

α is the geocentric right ascension

δ is the geocentric declination

Appendix B

Position and Velocity Data from Classical Elements

In this study, a satellite's initial position and velocity vectors are derived from an input orbit. The equations needed for this transformation are presented below [Ref 3, 72-73]:

$$P = a(1-e^2) \tag{65}$$

$$E - e \sin E = M \tag{66}$$

$$\cos \nu = \frac{e - \cos E}{e \cos E - 1} \tag{67}$$

$$r = \frac{P}{1 + e \cos \nu} \tag{68}$$

$$\sin \nu = \frac{a\sqrt{1-e^2}}{r} \sin E \tag{69}$$

$$\underline{r} = r \cos \nu \; \hat{P} + r \sin \; \hat{Q} \tag{70}$$

$$\underline{v} = \frac{\sqrt{\mu}}{P} [-\sin \nu \; \hat{P} + (e + \cos \nu) \; \hat{Q}] \tag{71}$$

The position and velocity vector are then transformed from the perifocal to the geocentric-equatorial coordinate frame.

It should be noted that equation (66) is known as Kepler's equation and a closed form solution for the eccentric anomaly, E, cannot be obtained. A Newton iteration scheme is used to evaluate E, using Eo = M as an initial guess.

Appendix C

Geopotential Constants and Legendre Polynomials

Listed below are the geopotential coefficients for the zonal and sectoral harmonies used in this study [Ref 6]:

$$J_2 = 1.082637 \times 10^{-6} \qquad (72)$$

$$J_3 = -2.541 \times 10^{-6} \qquad (73)$$

$$J_4 = -1.618 \times 10^{-6} \qquad (74)$$

$$C_{22} = 1.5362 \times 10^{-6} \qquad (75)$$

$$S_{22} = -.86358 \times 10^{-6} \qquad (76)$$

Also, the following Legendre polynomials are required for evaluation of the perturbing accelerations due to the geopotential [Ref 9; 90-91]:

$$P_0 = 1 \qquad (77)$$

$$P_1 = \sin \delta \qquad (78)$$

$$P_2 = \frac{1}{2}[-1 + 3 \sin^2\delta] \qquad (79)$$

$$P_3 = \frac{1}{3}[-2 \sin \delta + 5 P_2 \sin \delta] \qquad (80)$$

$$P_4 = \frac{1}{4}[-3 P_2 + 7 P_3 \sin \delta] \qquad (81)$$

$$P_2^2 = 3 \cos^2 \delta \qquad (82)$$

$$\cos \delta \ P_2^{\prime} = 3 \sin \delta \cos \delta \qquad (83)$$

$$\cos \delta \ P_3^{\prime} = \sin \delta \cos \delta \ P_2^{\prime} + 3 \cos \delta \ P_2 \qquad (84)$$

$$\cos \delta \ P_4^{\prime} = \sin \delta \cos \delta \ P_3^{\prime} + 4 \cos \delta \ P_3 \qquad (85)$$

$$\cos \delta \ P_2^{2\prime} = -2 \sin \delta \ \frac{P_2^2}{\cos \delta} \qquad (86)$$

where

δ is the geodetic declination of the satellite.

Appendix D

Orbital Elements from Position and Velocity Data

The estimators in this study use classical orbital elements as measurement updates. These elements are calculated from the position and velocity data from the truth model. Prior to calculating the elements, noise is added to the data. The following equations are used to obtain classical elements from thegeocentric-equatorial position and velocity data [Ref 3; 62-63]:

$$\underline{h} = \underline{r} \times \underline{v} \tag{87}$$

$$\underline{n} = \underline{k} \times \underline{h} \tag{88}$$

$$\underline{e} = \frac{1}{\mu} \left[(v - \frac{\mu}{r}) \underline{r} - (\underline{r} \cdot \underline{v}) \underline{v} \right] \tag{89}$$

$$e = |\underline{e}| \tag{90}$$

$$p = h^2/\mu \tag{91}$$

$$a = \frac{p}{(1-e^2)} \tag{92}$$

$$\cos i = \frac{h_k}{h} \quad 0 < i < 180 \tag{93}$$

$$\cos \Omega = \frac{n_j}{n} \quad \text{If } n_j > 0, \ \Omega < 180° \tag{94}$$

$$\cos \omega = \frac{\underline{n} \cdot \underline{e}}{ne} \quad \text{If } e_k > 0, \ \omega < 180° \tag{95}$$

$$\cos \nu = \frac{\underline{e} \cdot \underline{r}}{er} \quad \text{If } \underline{r} \cdot \underline{v} > 0, \ \nu_0 < 180° \tag{96}$$

$$\cos E = \frac{e + \cos \nu}{1 + e \cos \nu} \tag{97}$$

$$M = E - e \sin E \tag{98}$$

where

    $\underline{h}$ is the angular momentum vector

    $\underline{n}$ is the nodal vector

    The eccentric anomaly, E, should be in the same half-plane as the true anomaly, ν_o.

    This method provides a set of osculating elements which match the orbit at the time the position and velocity is generated.

Appendix E

Derivation of State Transition Matrix

The state transition matrix, Φ, is calculated from equation (16) in Chapter III.

$$\Phi = \nabla \cdot \underline{f}$$

or,

$$\Phi = \begin{bmatrix} \partial f_1/\partial x_1 & \frac{\partial f_1}{\partial x_2} & \cdots \cdots \cdots & \frac{\partial f_1}{\partial x_8} \\ \partial f_2/\partial x_1 & \cdots \cdots \cdots \cdots & \frac{\partial f_2}{\partial x_8} \\ \vdots & & \\ \partial f_8/\partial x_1 & \cdots \cdots \cdots \cdots & \frac{\partial f_8}{\partial x_8} \end{bmatrix} \tag{99}$$

where

$$\underline{x}(t) = \underline{f}(\underline{x}(t_0), t)$$

is an approximate solution to the non-linear system.

The equations for the state dynamics presented in Chapter III (equation (16)) are listed below:

$$f_1 = a(t) = a_0 + \dot{a}(t - t_0) \tag{100}$$

$$f_2 = e(t) = e_0 + \dot{e}(t - t_0) \tag{101}$$

$$f_3 = i(t) = i_0 \tag{102}$$

$$f_4 = \omega(t) = \omega_0 + \dot{\omega}(t - t_0) \tag{103}$$

$$f_5 = \Omega(t) = \Omega_0 + \dot{\Omega}(t - t_0) \tag{104}$$

$$f_6 = M(t) = M_0 + n_k(t - t_0) + \frac{1}{2}\dot{n}(t - t_0)^2 \tag{105}$$

$$f_7 = \dot{a}(t) = \dot{a}_0 \tag{106}$$

$$f_8 = \dot{e}(t) = \dot{e}_0 \tag{107}$$

where

$$n_k = n + \dot{\varepsilon} \tag{108}$$

$$\dot{\omega} = \frac{-3n\, J_2\, r_e^2}{2a^2(1-e^2)^2} \left(\frac{5}{2} \sin^2 i - 2\right) \tag{109}$$

$$\dot{\Omega} = \frac{-3n\, J_2\, r_e^2}{2a^2(1-e^2)^2} \cos i \tag{110}$$

$$\dot{n} = \frac{-3}{2} \frac{n}{a}\, \dot{a} \tag{111}$$

$$\dot{\varepsilon} = \frac{-3n\, J_2 r_e^2}{2a^2(1-e^2)^{3/2}} \left(\frac{3}{2} \sin^2 i - 1\right) \tag{112}$$

Evaluation of the partial derivative provides the following elements to the Φ matrix:

$$\Phi_{ii} = 1 \quad i = 1, 8 \tag{113}$$

$$\phi_{1,7} = \phi_{2,8} = t - t_0 \tag{114}$$

$$\phi_{4,1} = \frac{21}{4} \frac{n\, J_2\, r_e^2}{a^3(1-e^2)^2} \left(\frac{5}{2} \sin^2 i - 2\right)(t - t_0) \tag{115}$$

$$\phi_{4,2} = \frac{-6n\, J_2\, r_e^2 e}{a^2(1-e^2)^3} \left(\frac{5}{2} \sin^2 i - 2\right)(t - t_0) \tag{116}$$

$$\phi_{4,3} = \frac{15n\, J_2\, r_e^2}{2a^2(1-e^2)^2} (\sin i \cos i)(t - t_0) \tag{117}$$

$$\phi_{5,1} = \frac{21n\, J_2\, r_e^2}{4a^2(1-e^2)^2} (\cos i\ (t - t_0) \tag{118}$$

$$\phi_{5,2} = \frac{6n\, J_2\, r_e^2 e}{a^2(1-e^2)^3} (\cos i\ (t - t_0) \tag{119}$$

$$\phi_{5,3} = \frac{3n\, J_2\, r_e^2}{2a^2(1-e^2)^2} \sin i\ (t - t_0) \tag{120}$$

$$\phi_{6,1} = \frac{3}{2} \frac{n}{a} (t - t_0) + \frac{21n\, J_2\, r_e^2}{4a^3(1-e^2)^2} \left(\frac{3}{2} \sin^2 i - 1\right)(t - t_0) \tag{121}$$

$$\phi_{6,2} = \frac{-9n \ J_2 \ r_e^2 e}{2a^2(1-e^2)^{5/2}} \ (\frac{3}{2} \sin^2 i - 1)(t - t_0) \tag{122}$$

$$\phi_{6,3} = \frac{-9n \ J_2 \ r_e^2}{2a^2(1-e^2)^{3/2}} \ \sin i \cos i \ (t - t_0) \tag{123}$$

$$\phi_{6,7} = \frac{-3}{4} \frac{n}{a} \ (t - t_0)^2 \tag{124}$$

The remaining terms in the ϕ matrix are all zero.

Appendix F

Plots for Filter Performance Analysis

The following plots are presented to supplement the discussion
and data presented in Chapter V. The plots are the mean error and
mean error plus and minus rms error versus time. As stated in
Chapter V, the rms error is nearly equal to the standard deviation.
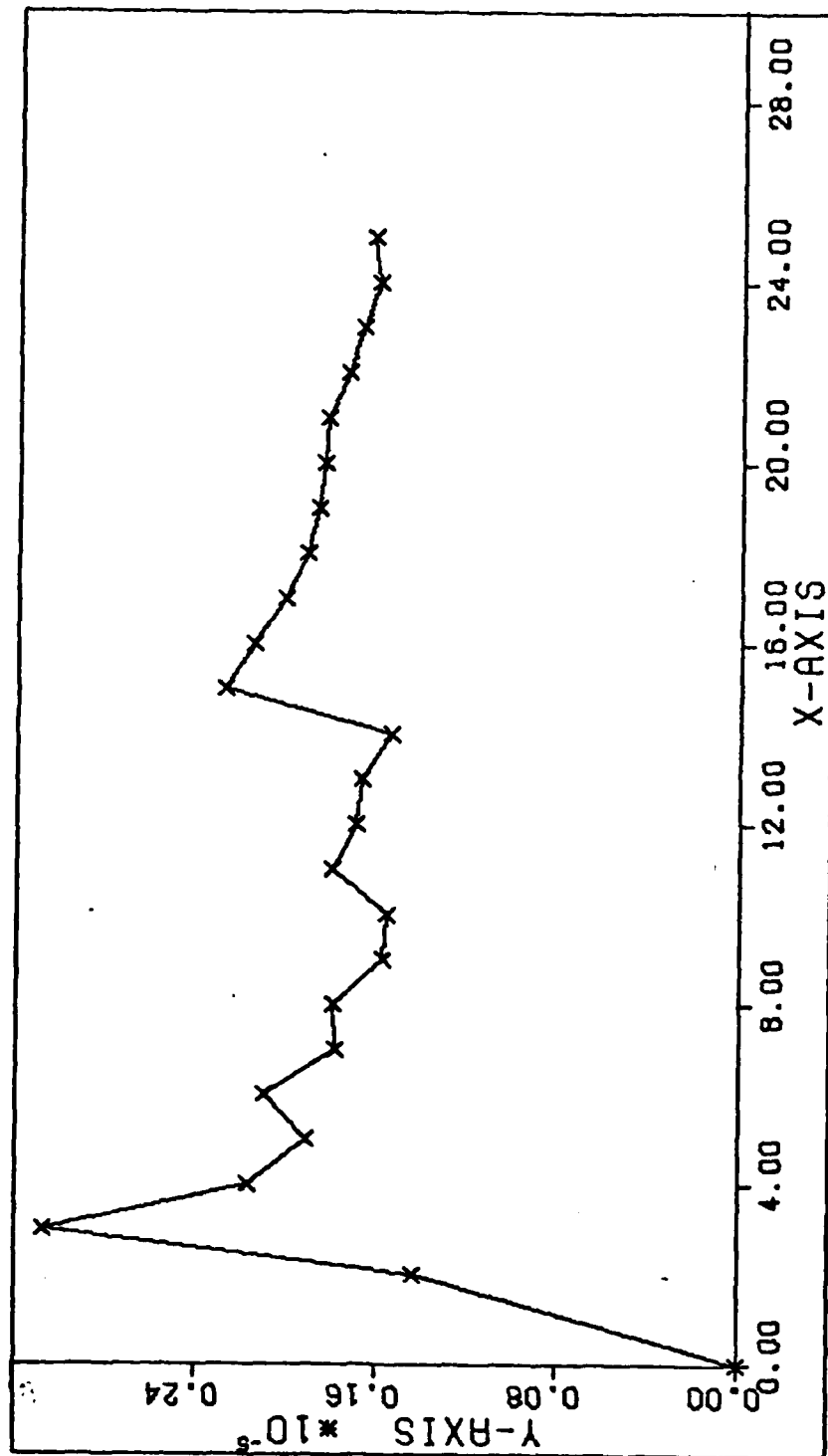
Fig 28. σ_e^2 vs N, Least Squares Filter
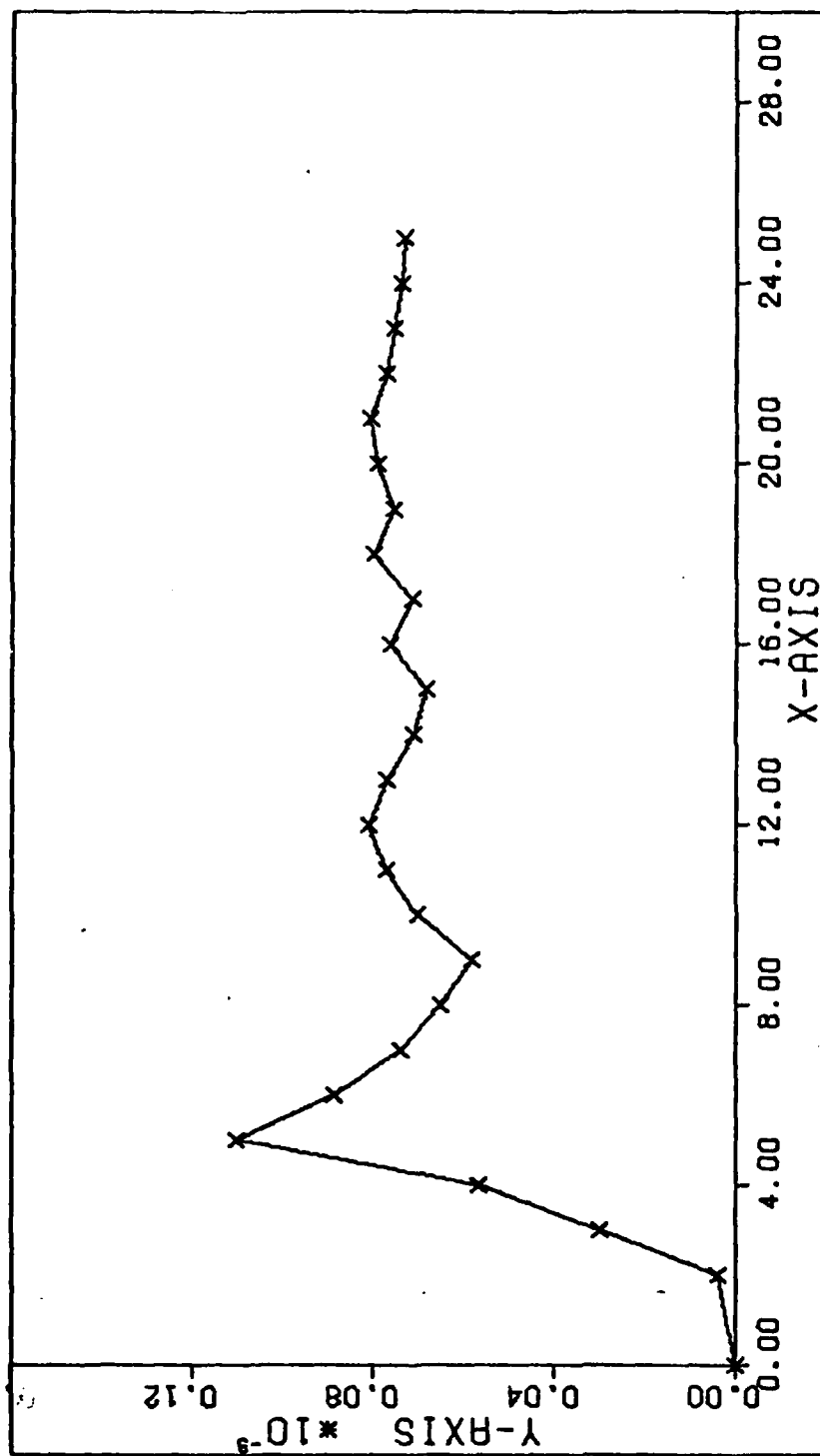
Fig 29. σ_ω^2 vs N, Least Squares Filter
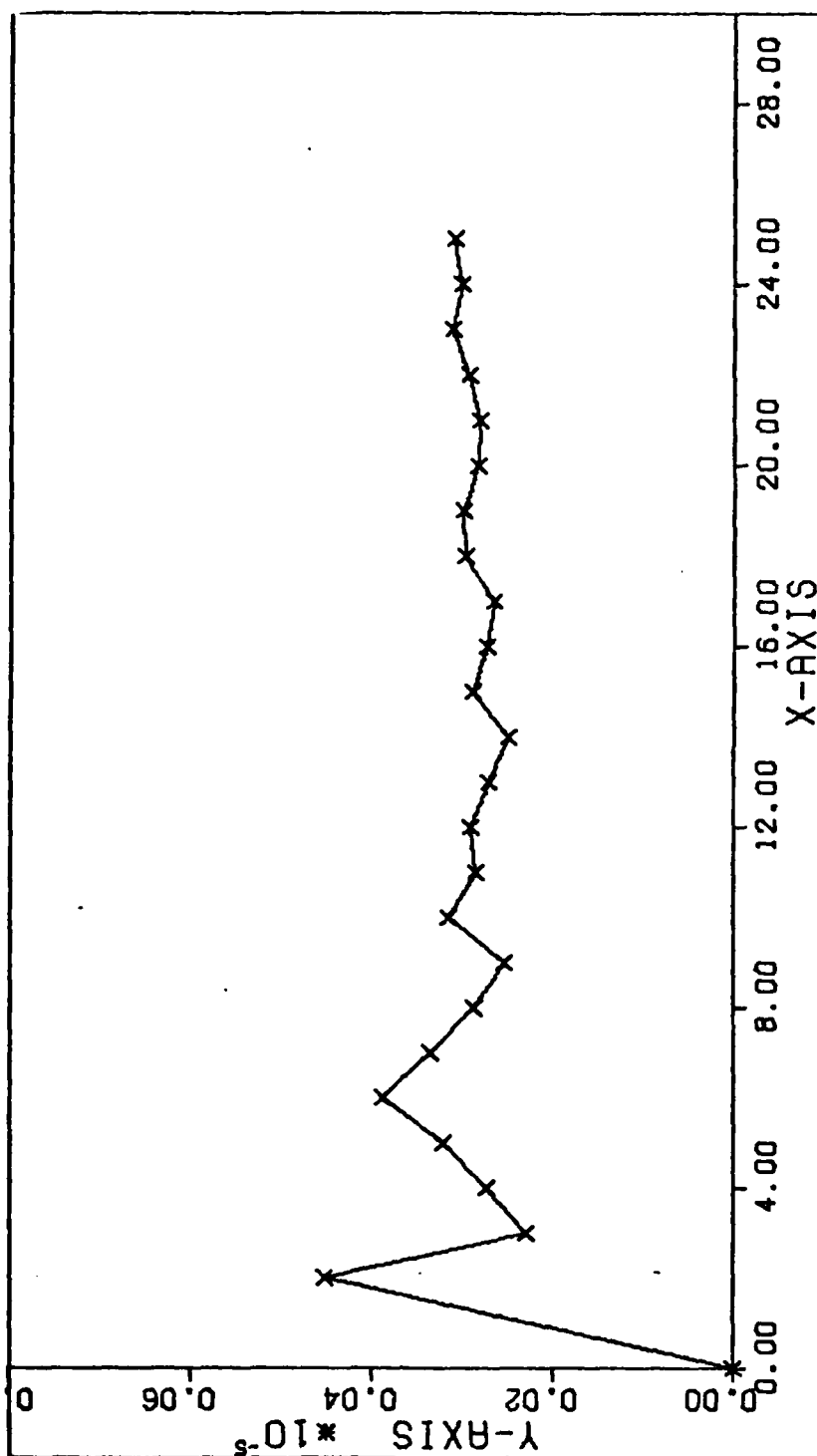
Fig 30. σ_Ω^2 vs N, Least Squares Filter
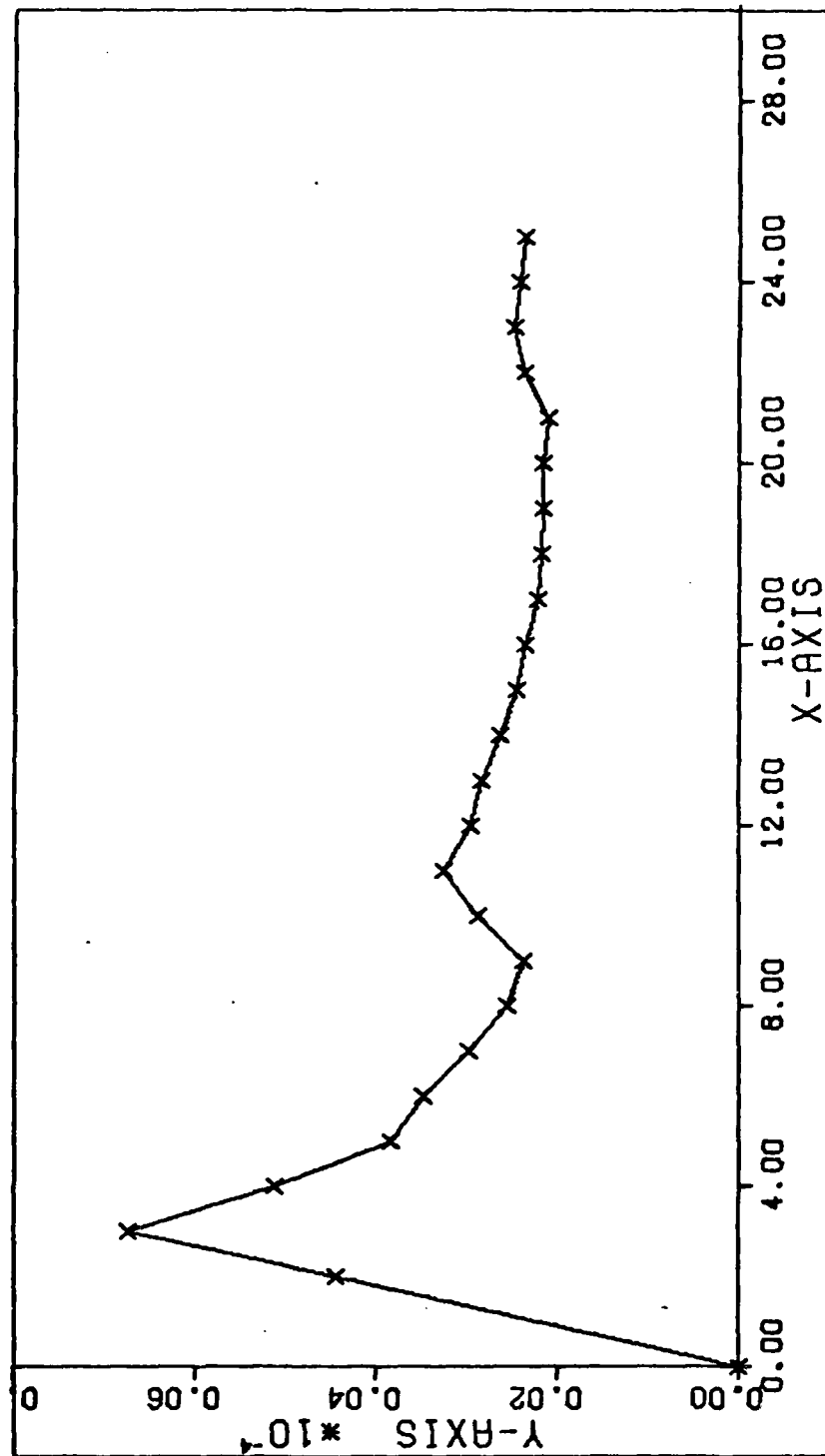
Fig 31. σ_e^2 vs N, Bayes Filter
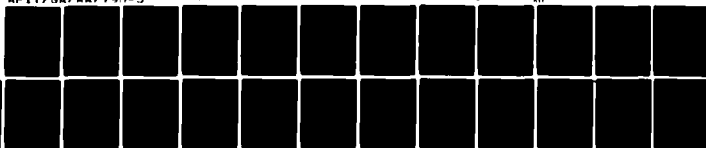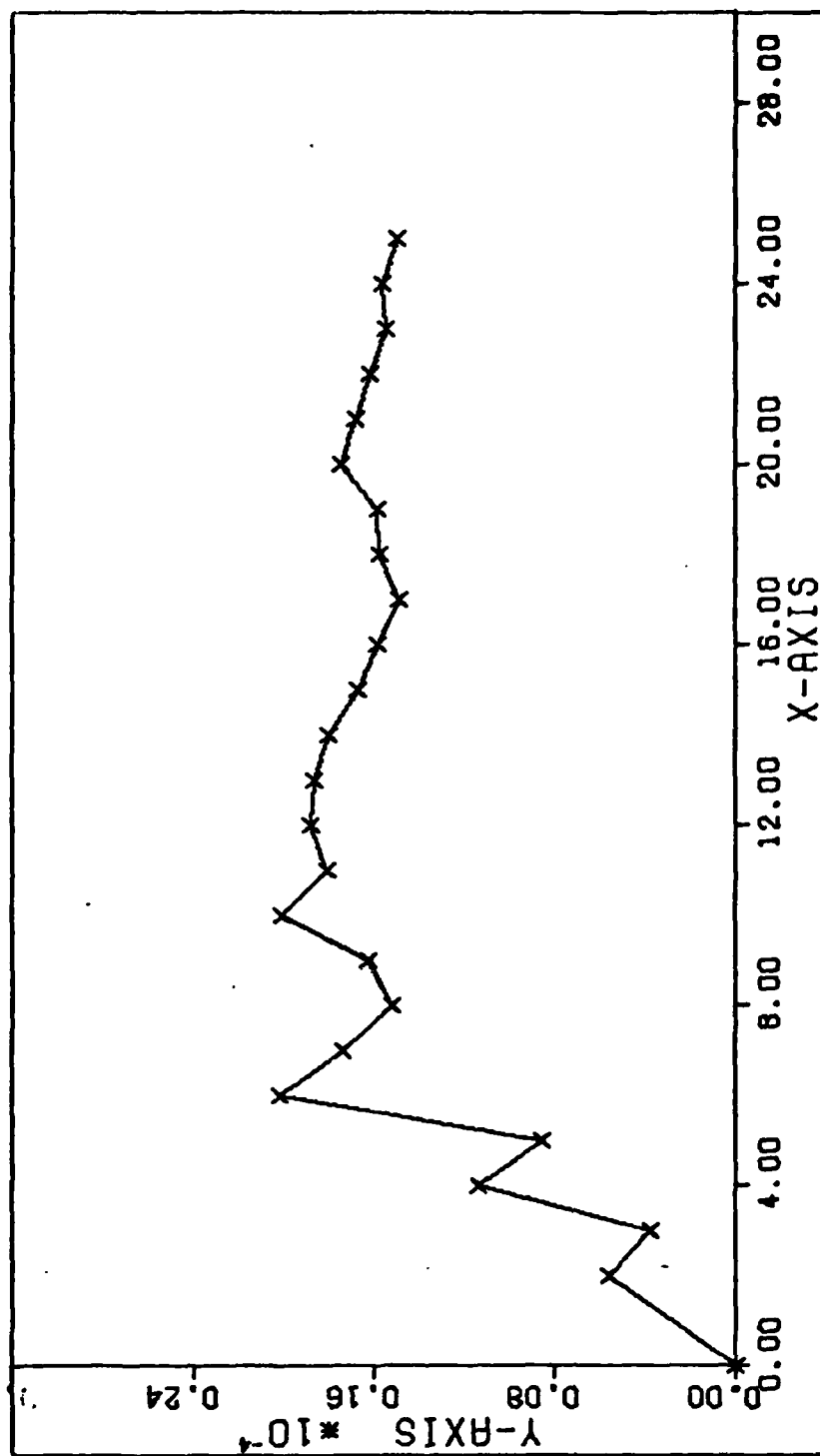
Fig 32. σ_i^2 vs N, Bayes Filter

84
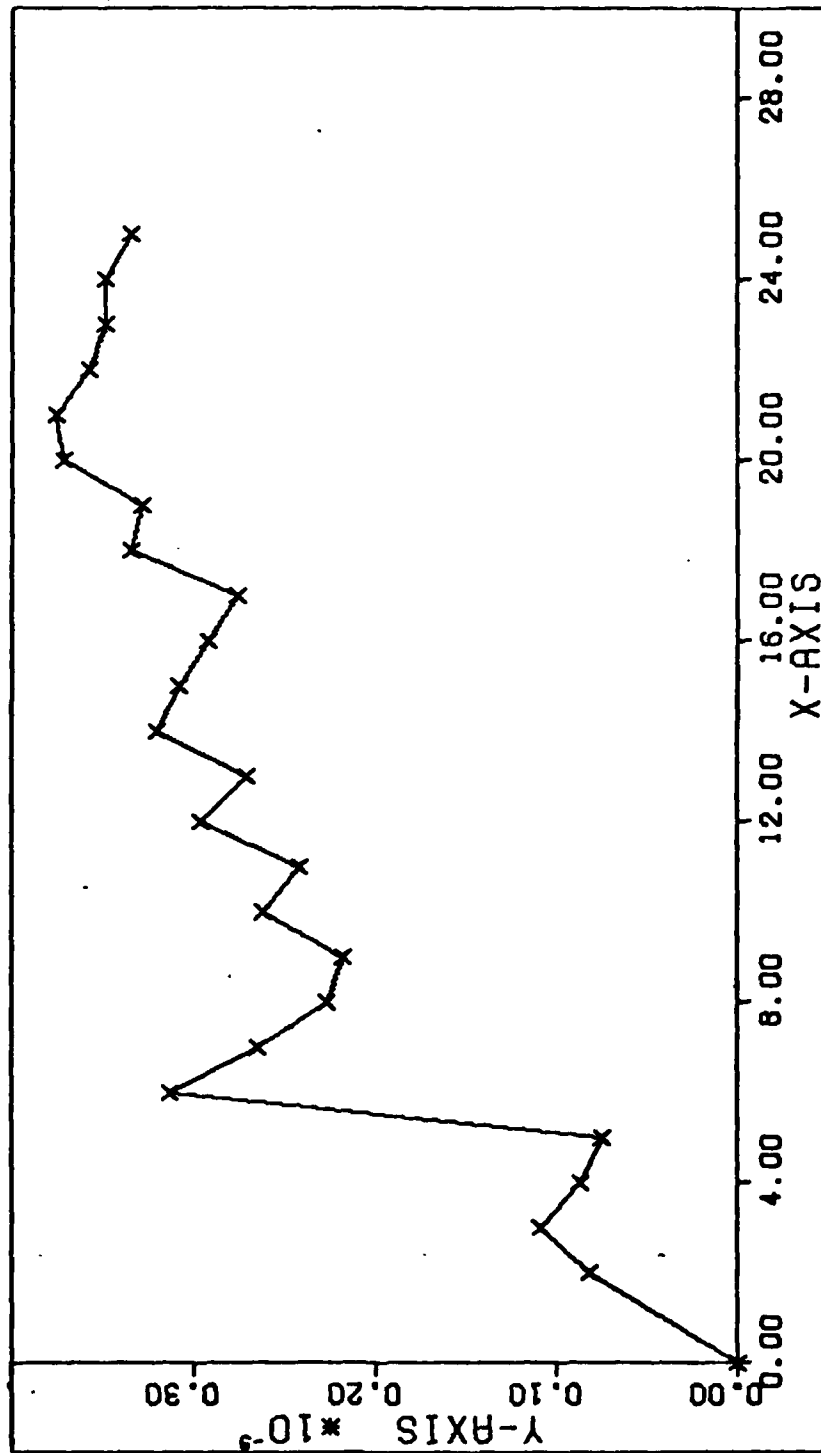
Fig 33. σ_ω^2 vs N, Bayes Filter
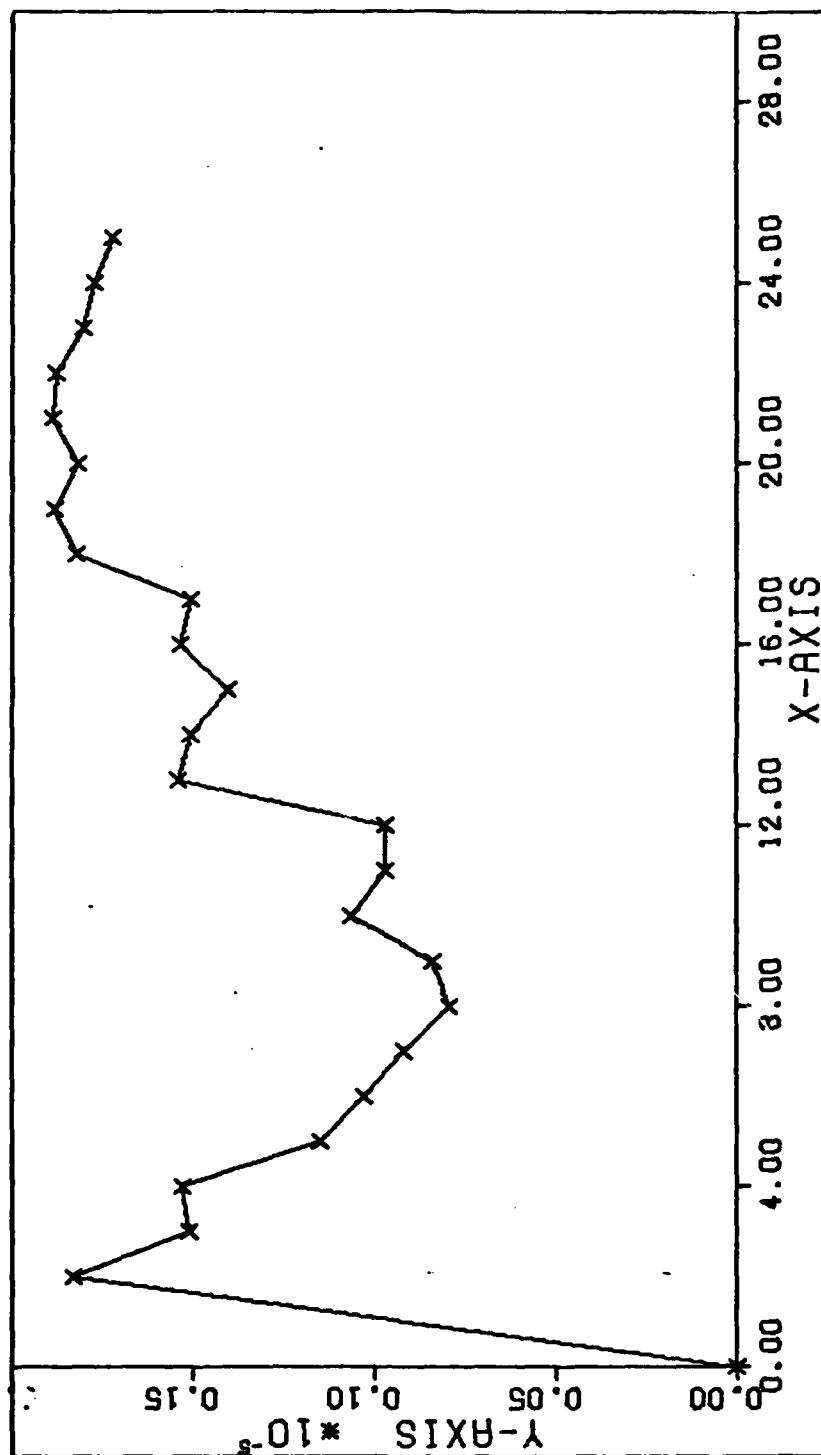
Fig 34. σ_Ω^2 vs N, Bayes Filter
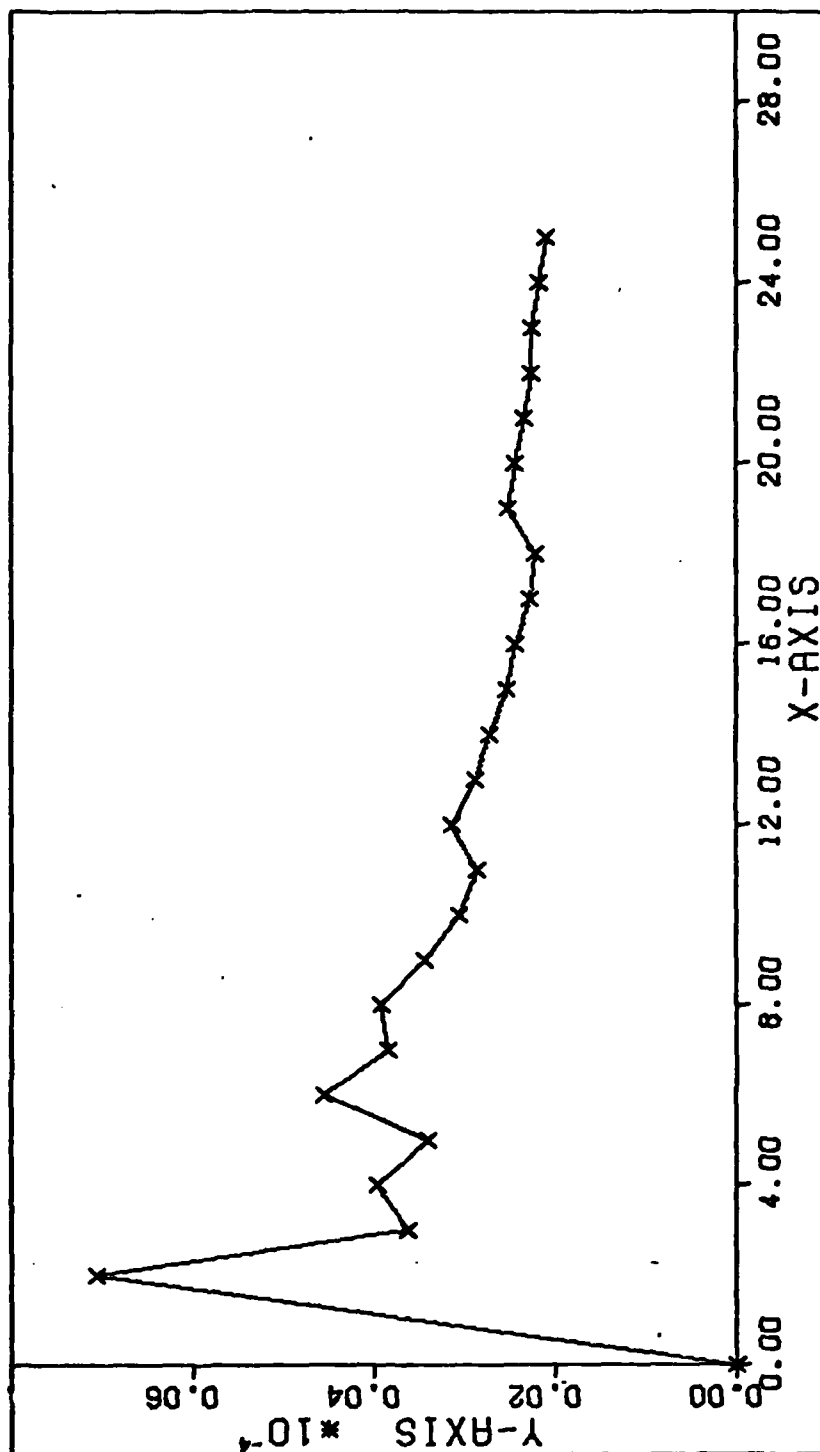
Fig 35. σ_e^2 vs N, Kalman Filter
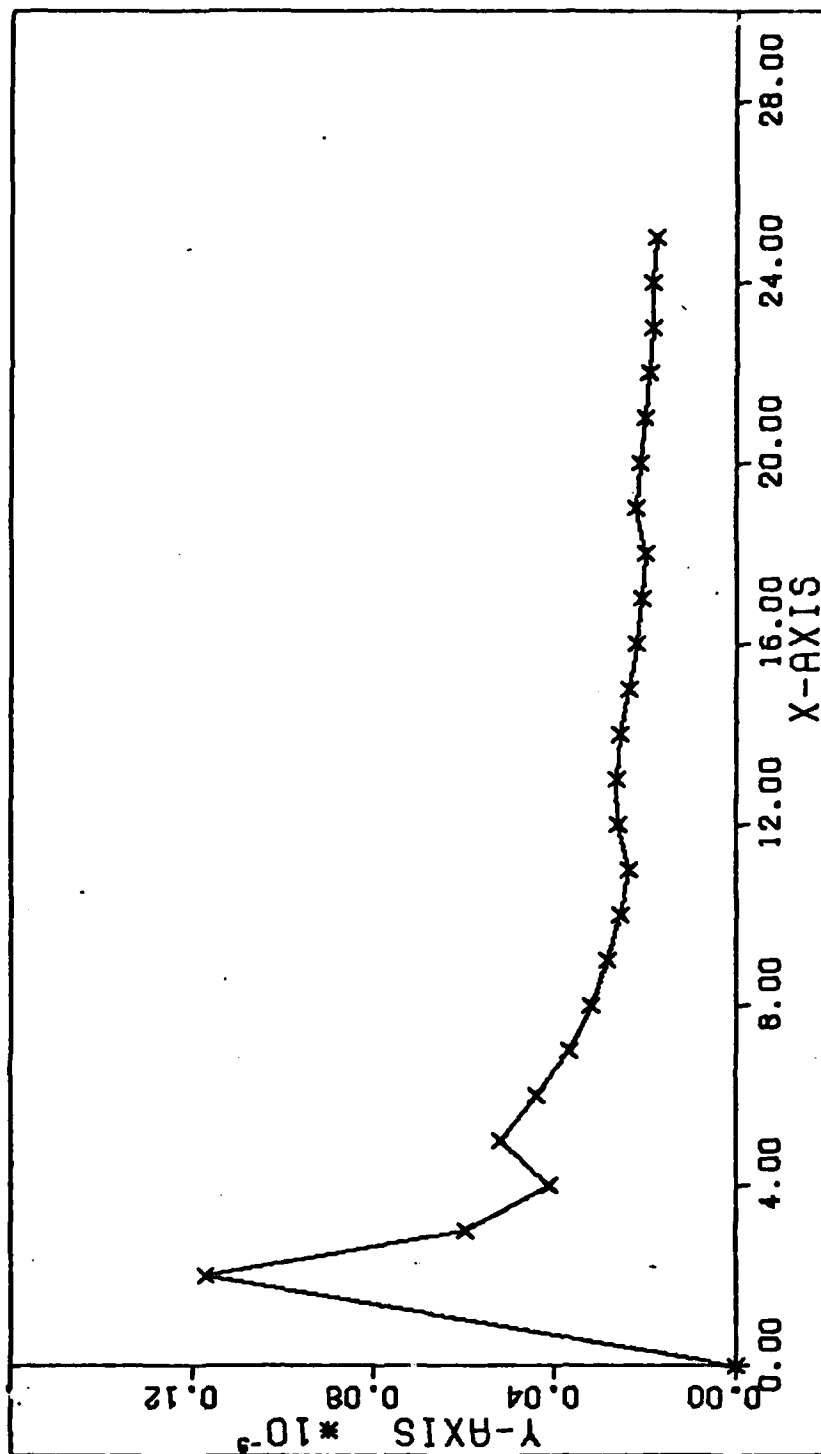
Fig 36. σ_1^2 vs N, Kalman Filter
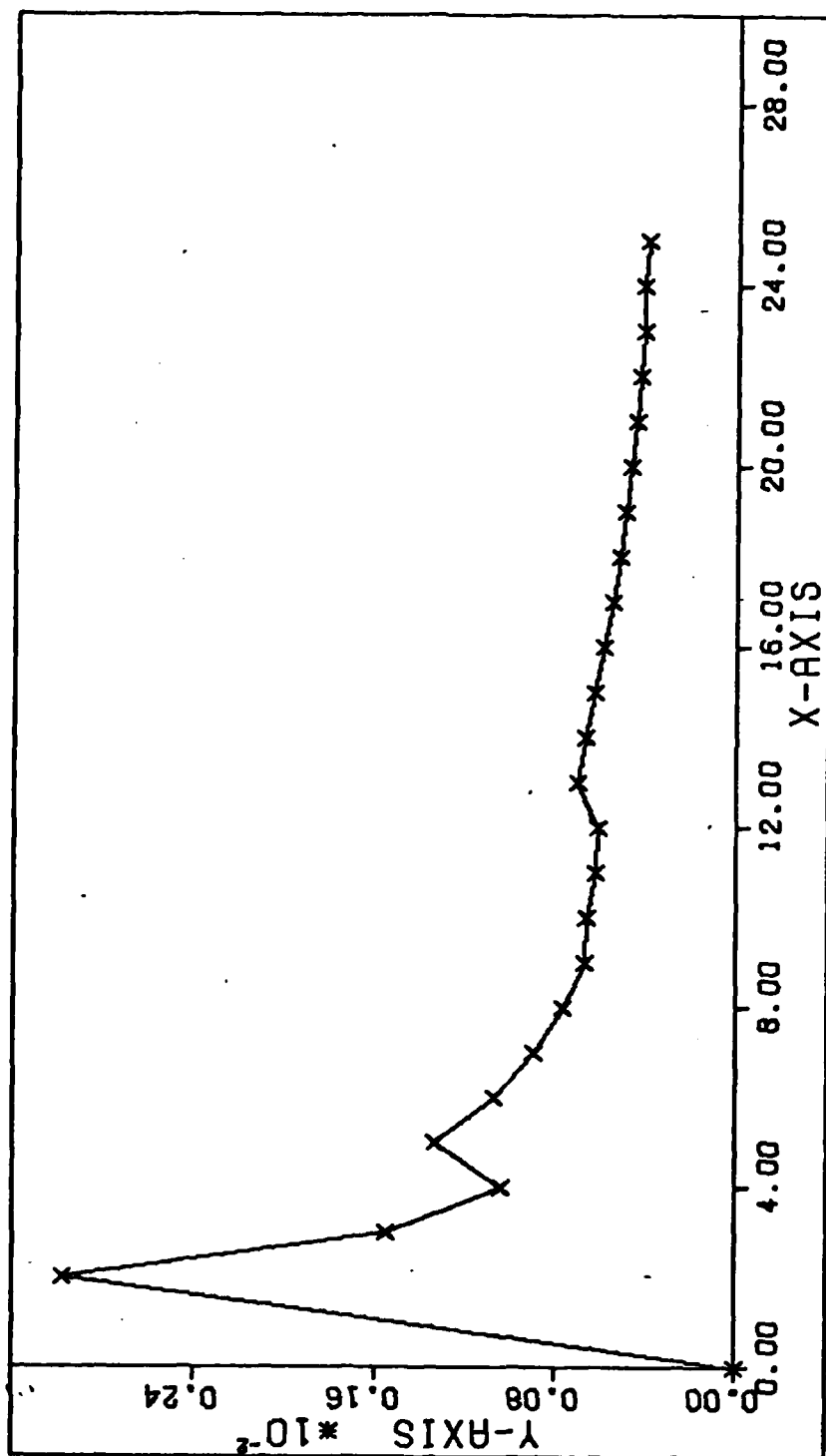
Fig 37. σ_ω^2 vs N, Kalman Filter
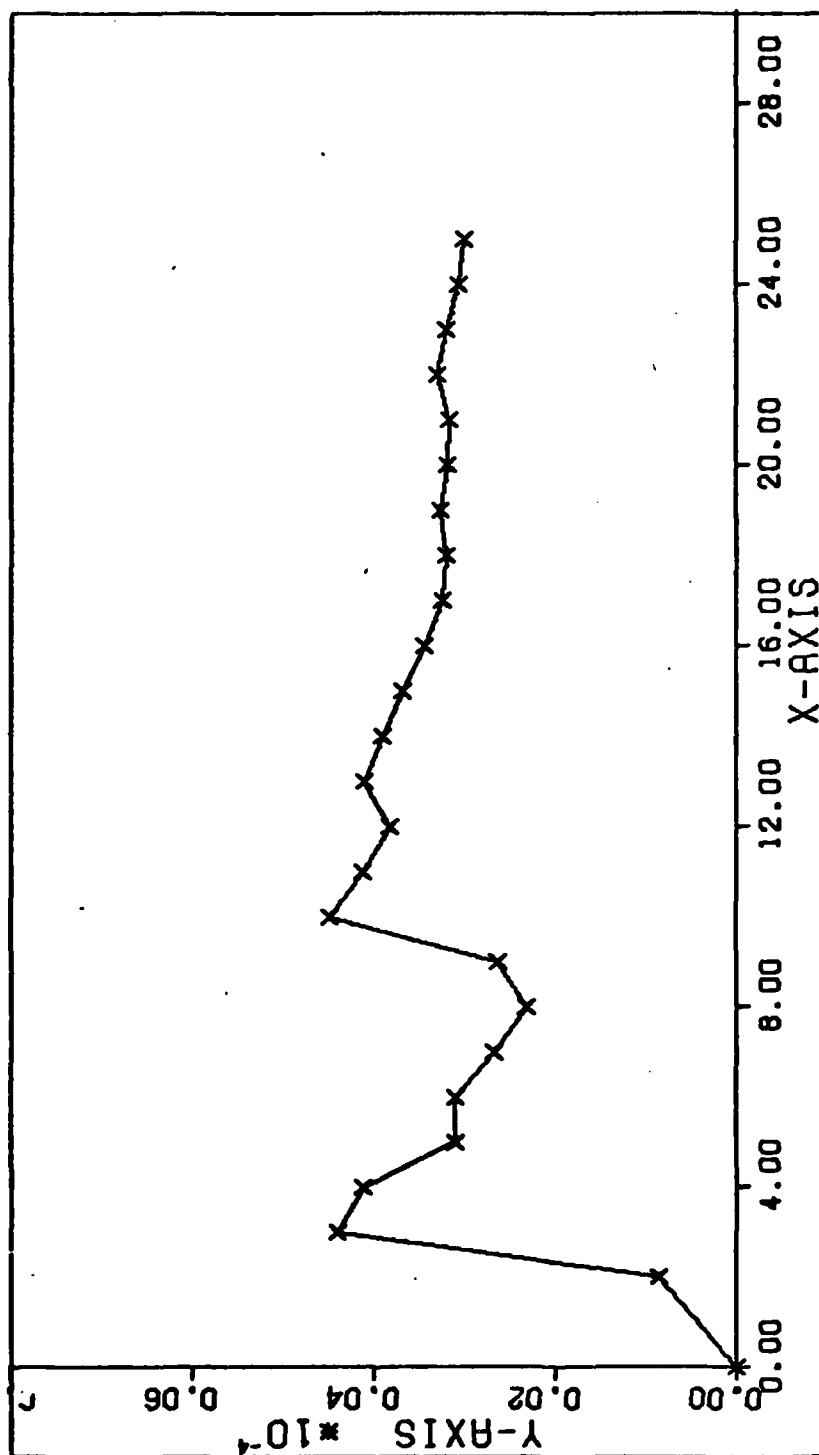
Fig 38. σ_Ω^2 vs N, Kalman Filter
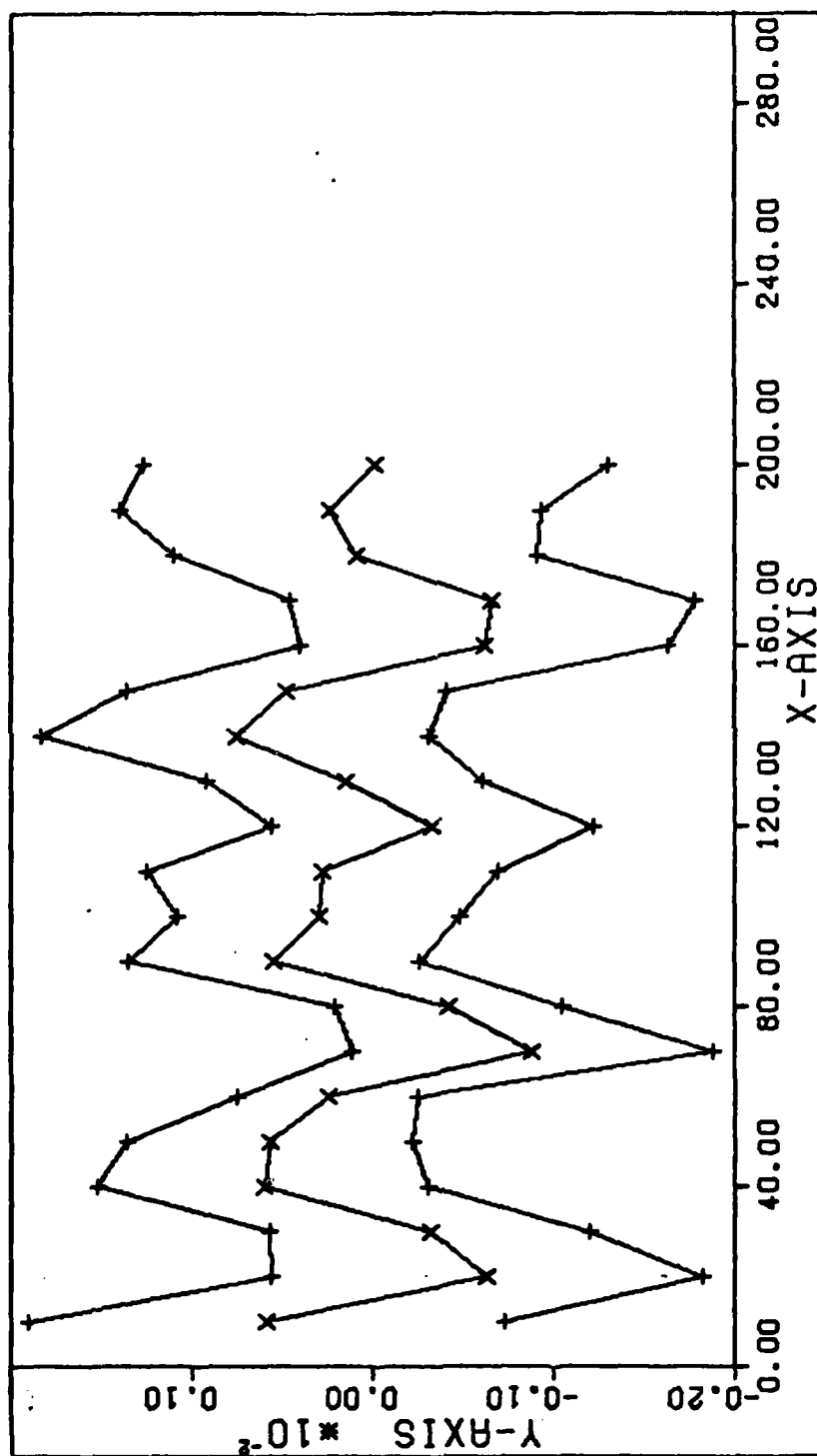
Fig 39. $e_e \pm \sigma_e$ vs t, Least Squares Filter - Case I

Fig 40. $e_\omega \pm \sigma_\omega$ vs t, Least Squares Filter – Case I

92
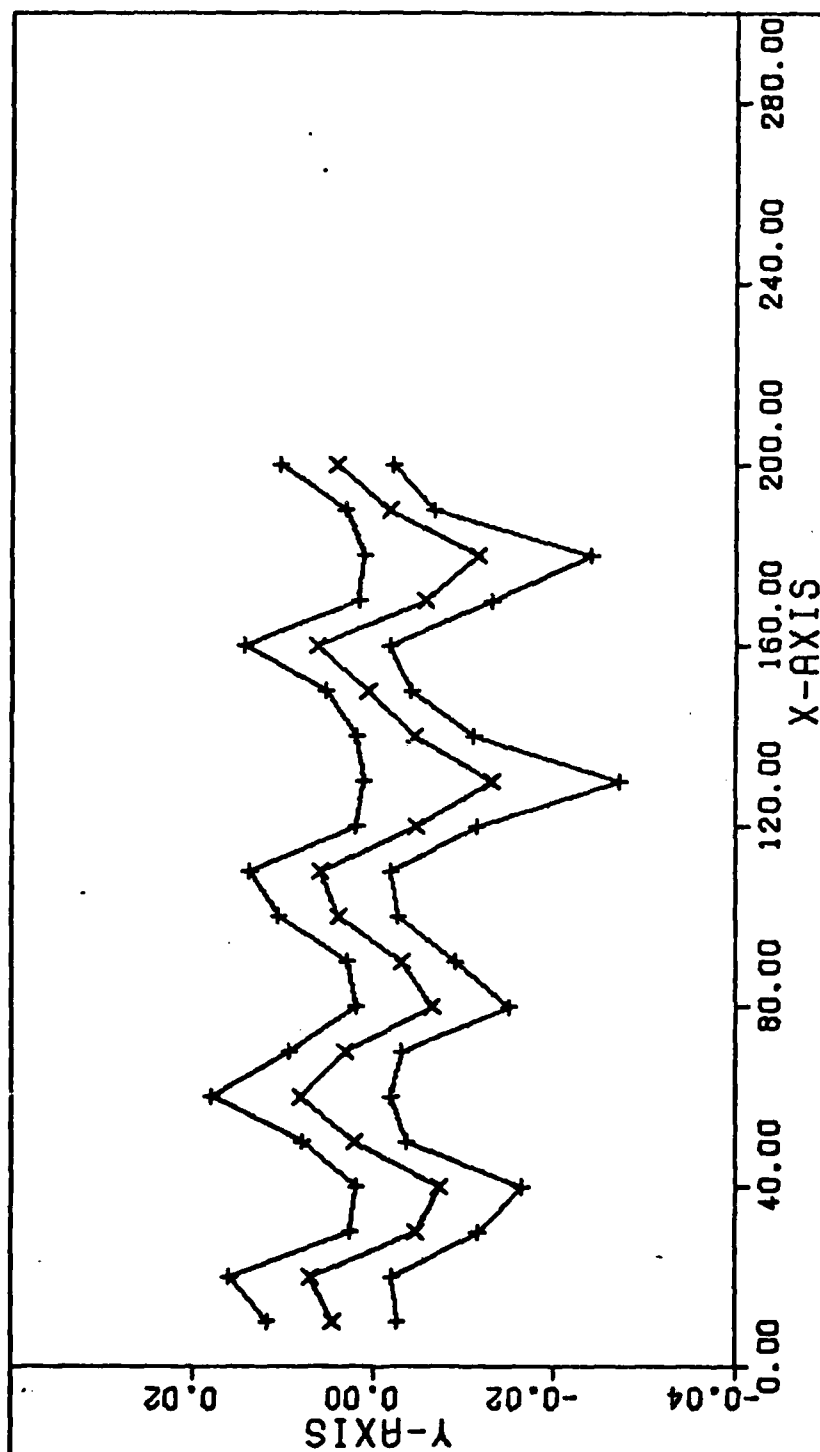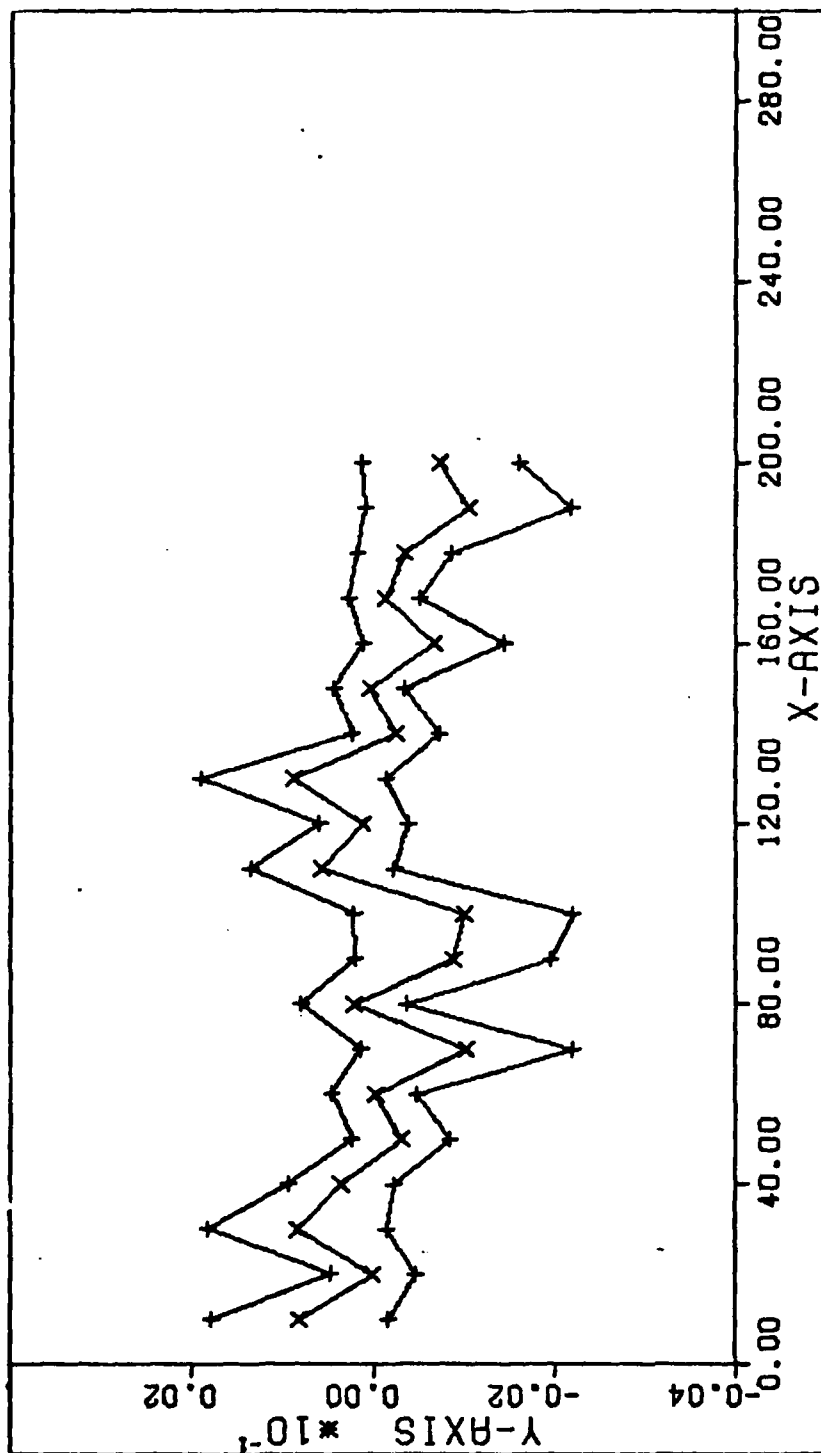
Fig 41. $e_\Omega \pm \sigma_\Omega$ vs t, Least Squares Filter - Case I
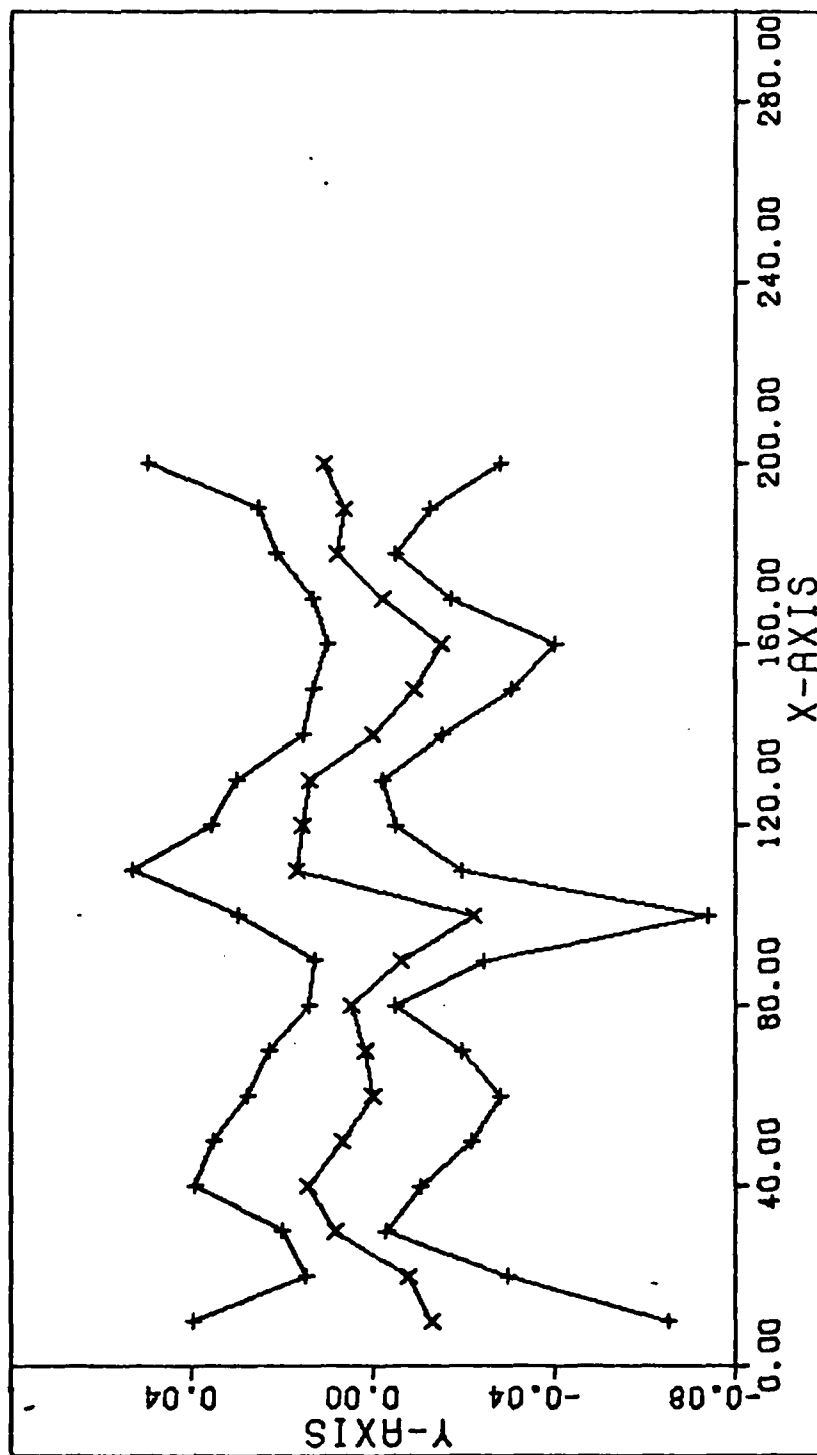
Fig 42. $e_M \pm \sigma_M$ vs t, Least Squares Filter - Case I

94
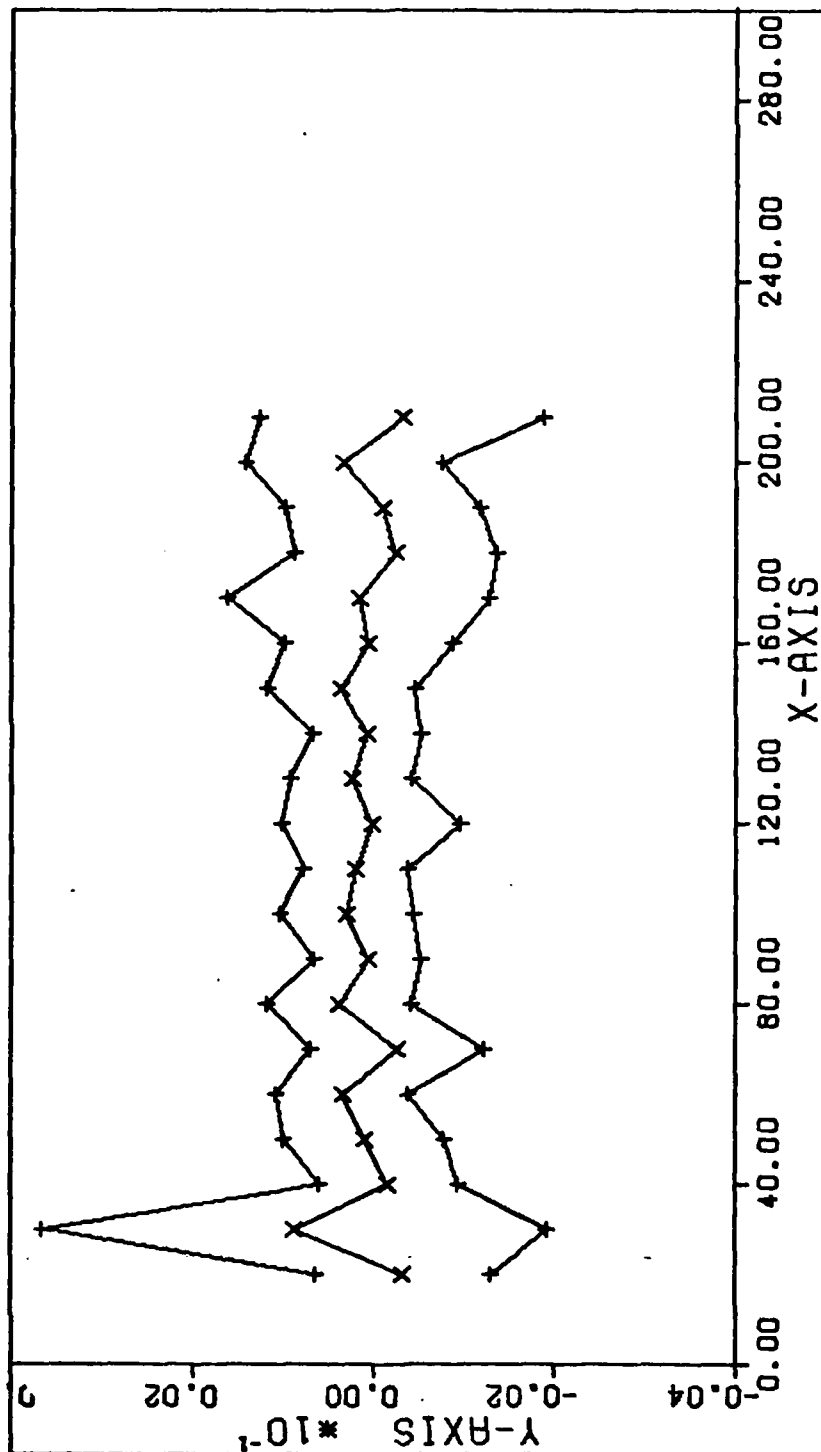
Fig 43. $e_e \pm \sigma_e$ vs t, Bayes Filter - Case I

95
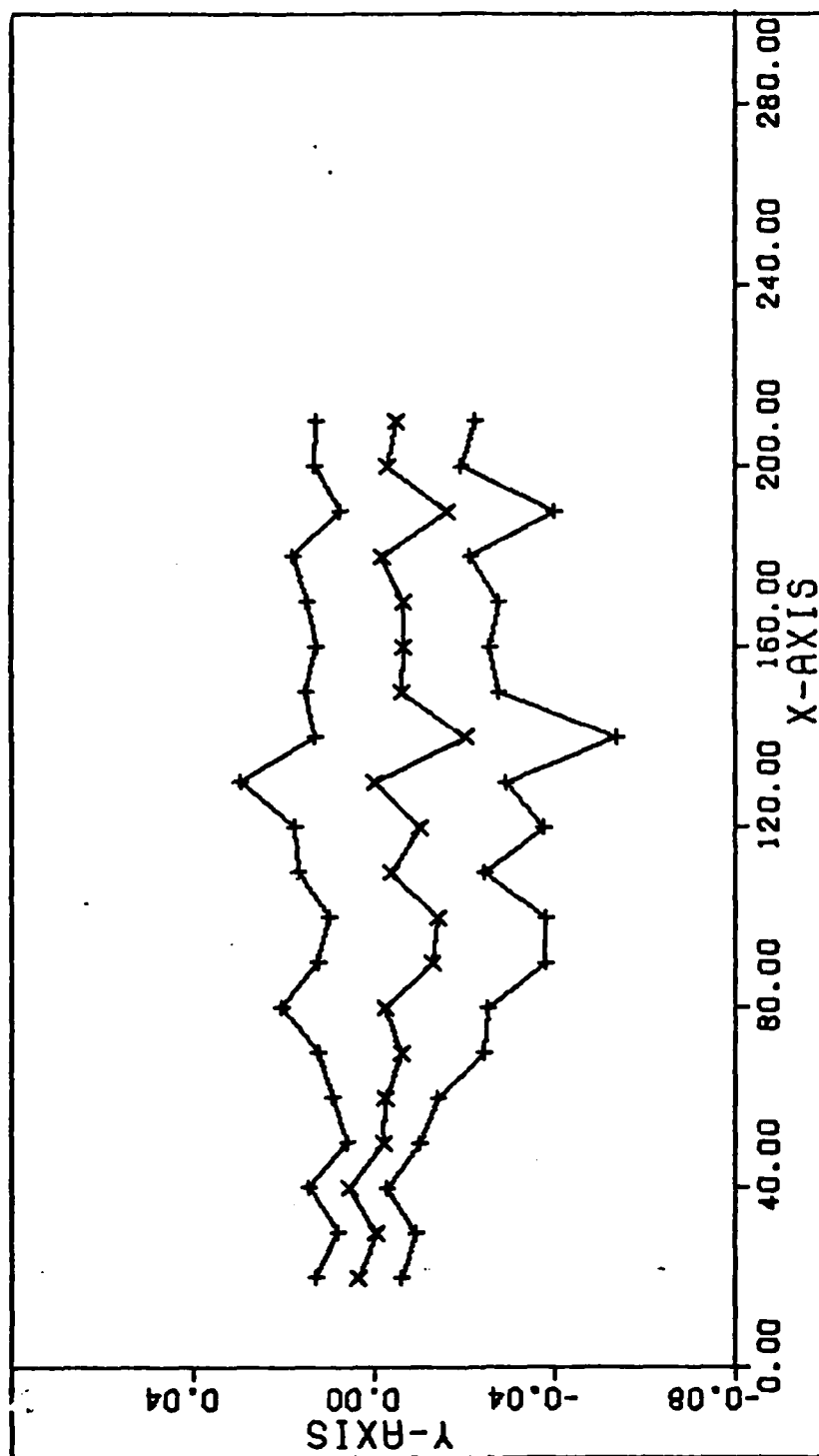
Fig 44. $e_\omega \pm \sigma_\omega$ vs t, Bayes Filter - Case I
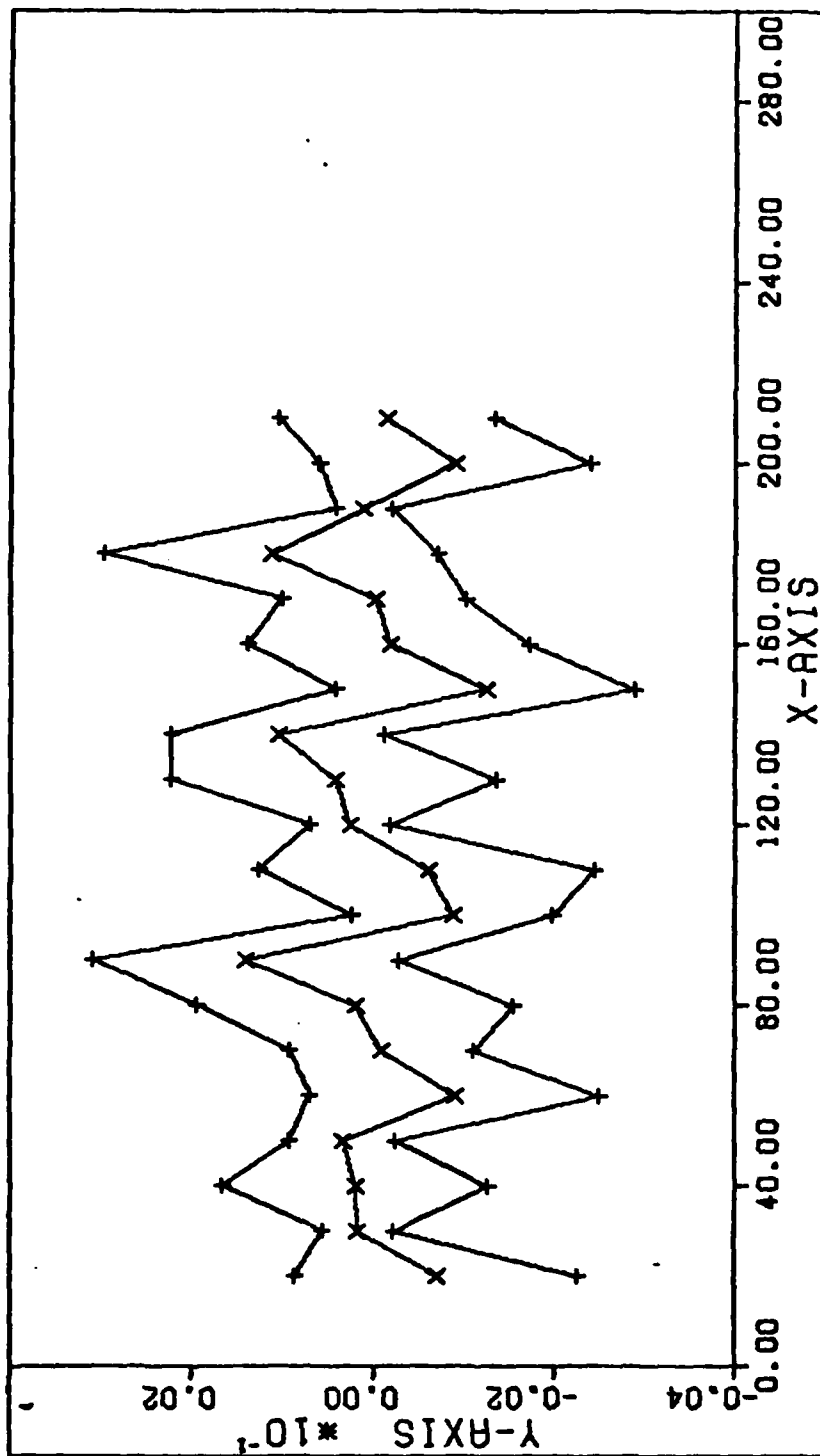
Fig 45. $e_\Omega \pm \sigma_\Omega$ vs t, Bayes Filter - Case I

97
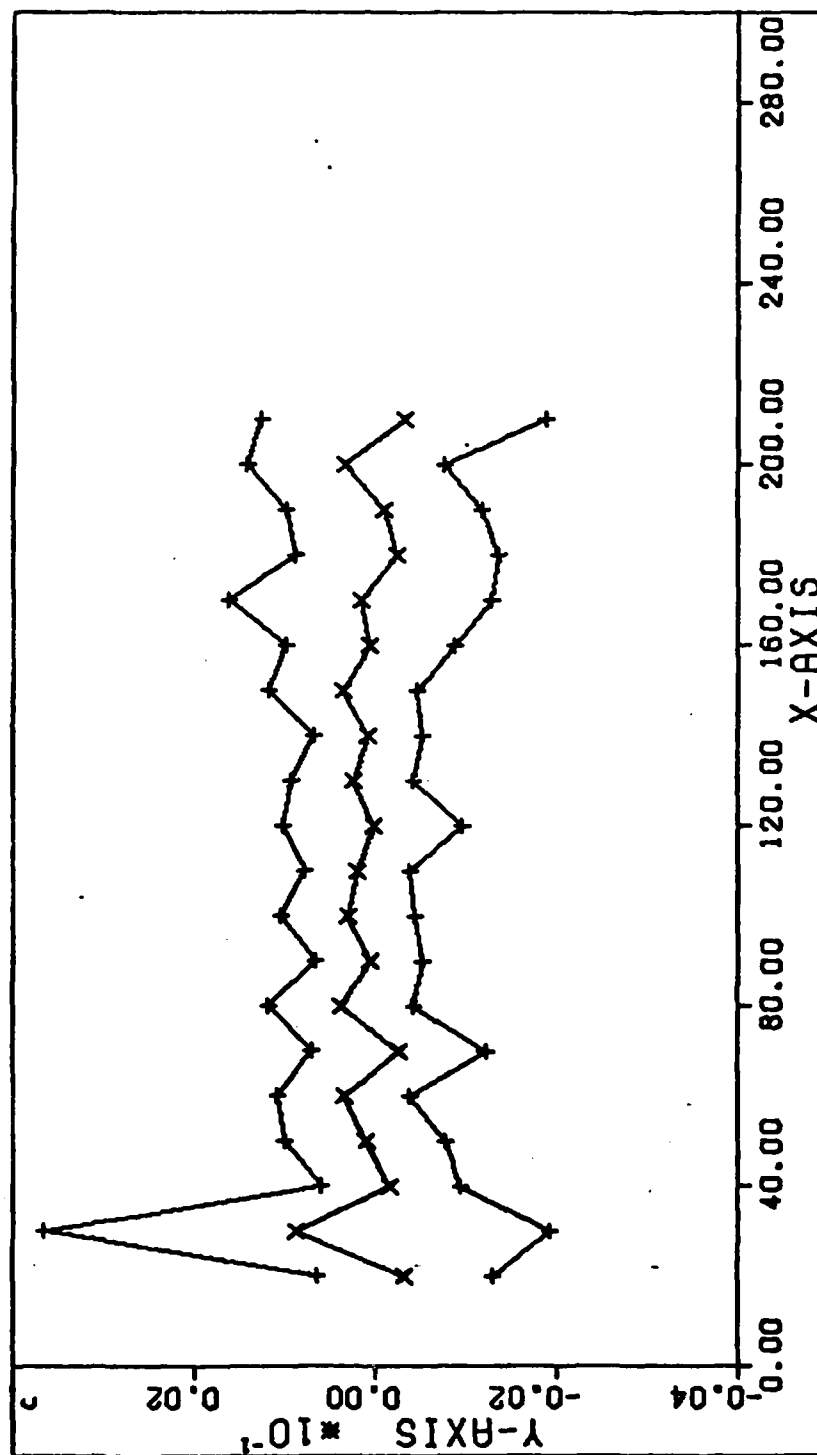
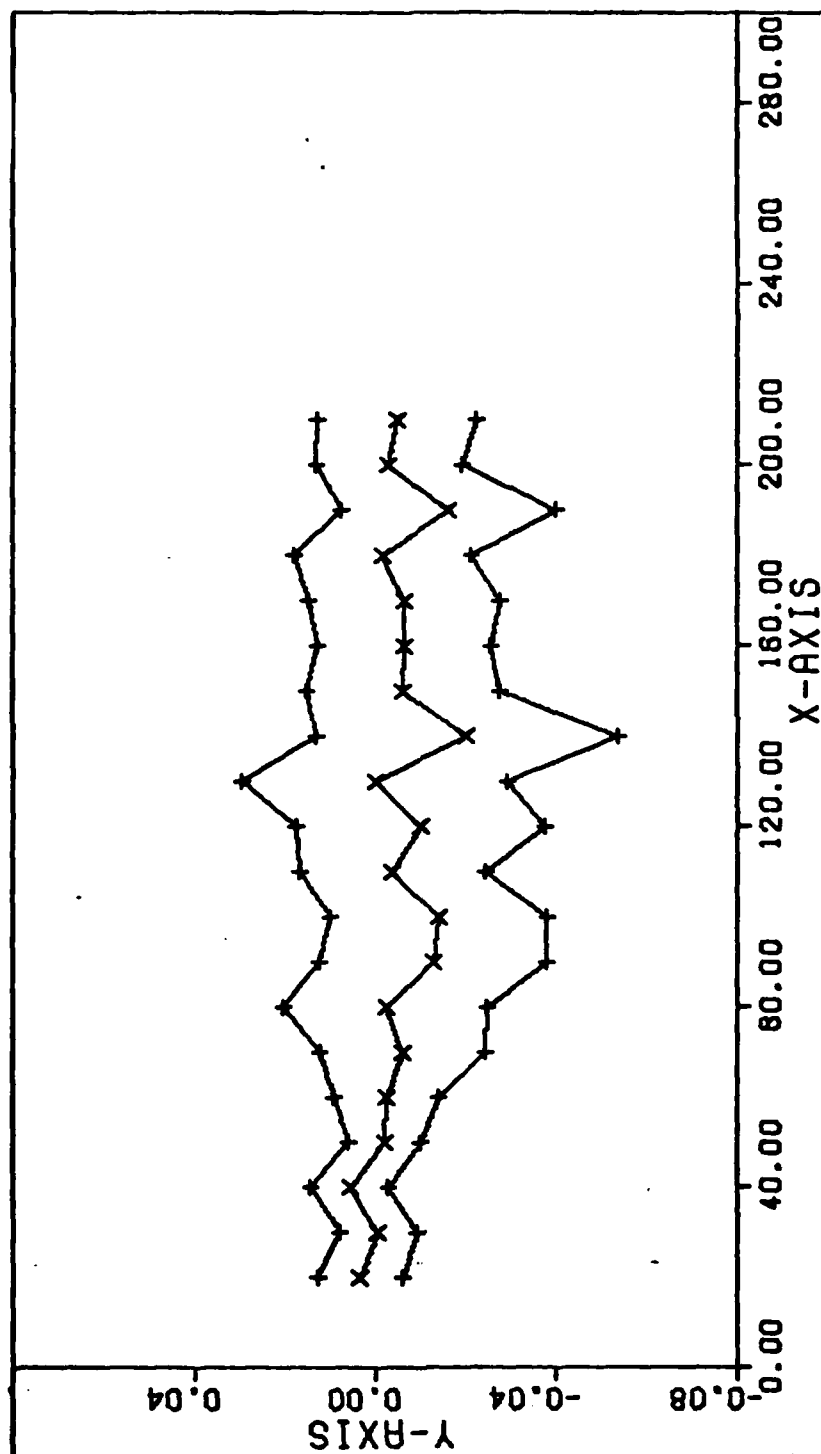Fig 46. $e_e \pm \sigma_e$ vs t, Kalman Filter - Case I
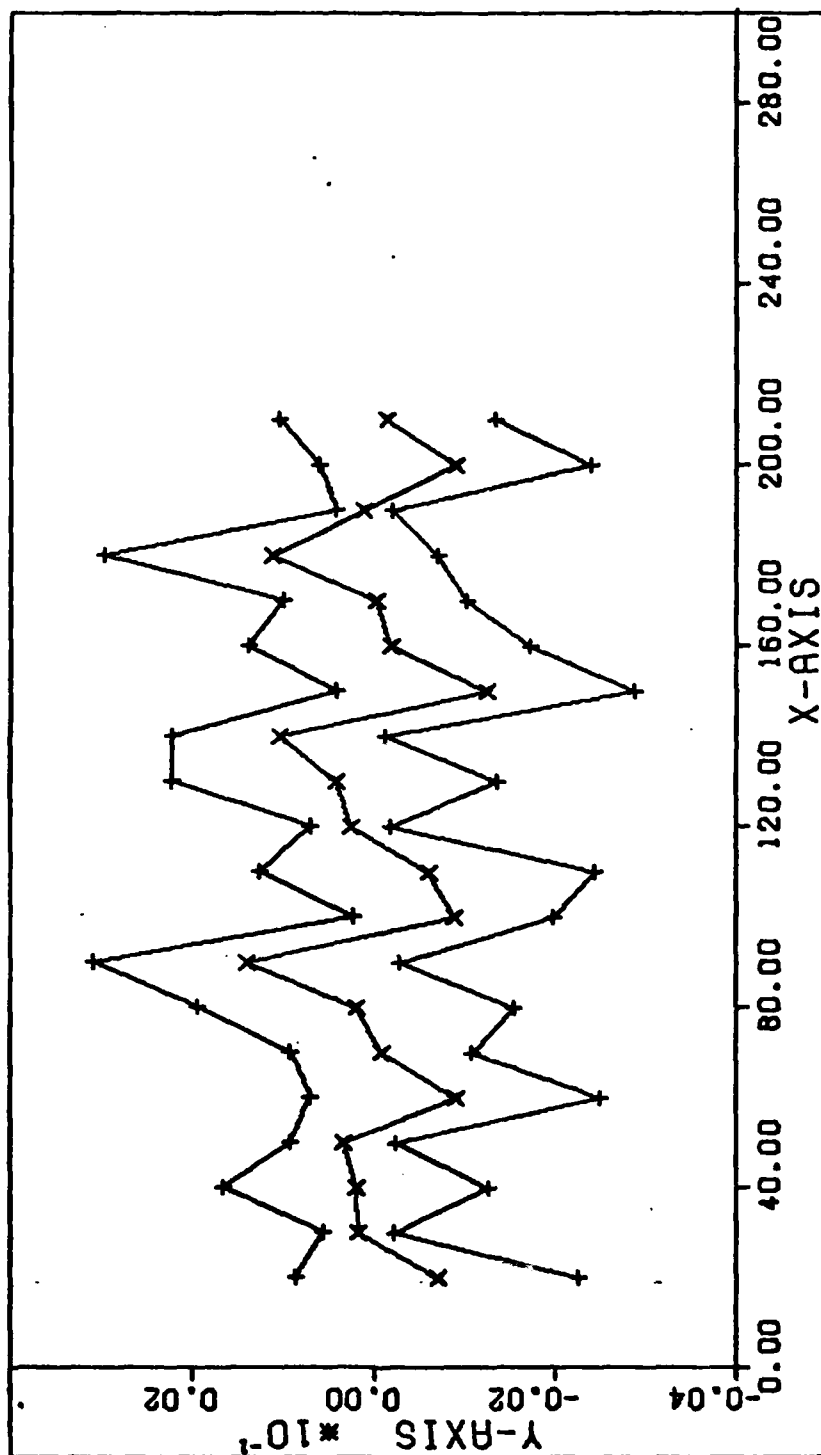
Fig 47. $e_\omega \pm \sigma_\omega$ vs t, Kalman Filter - Case I

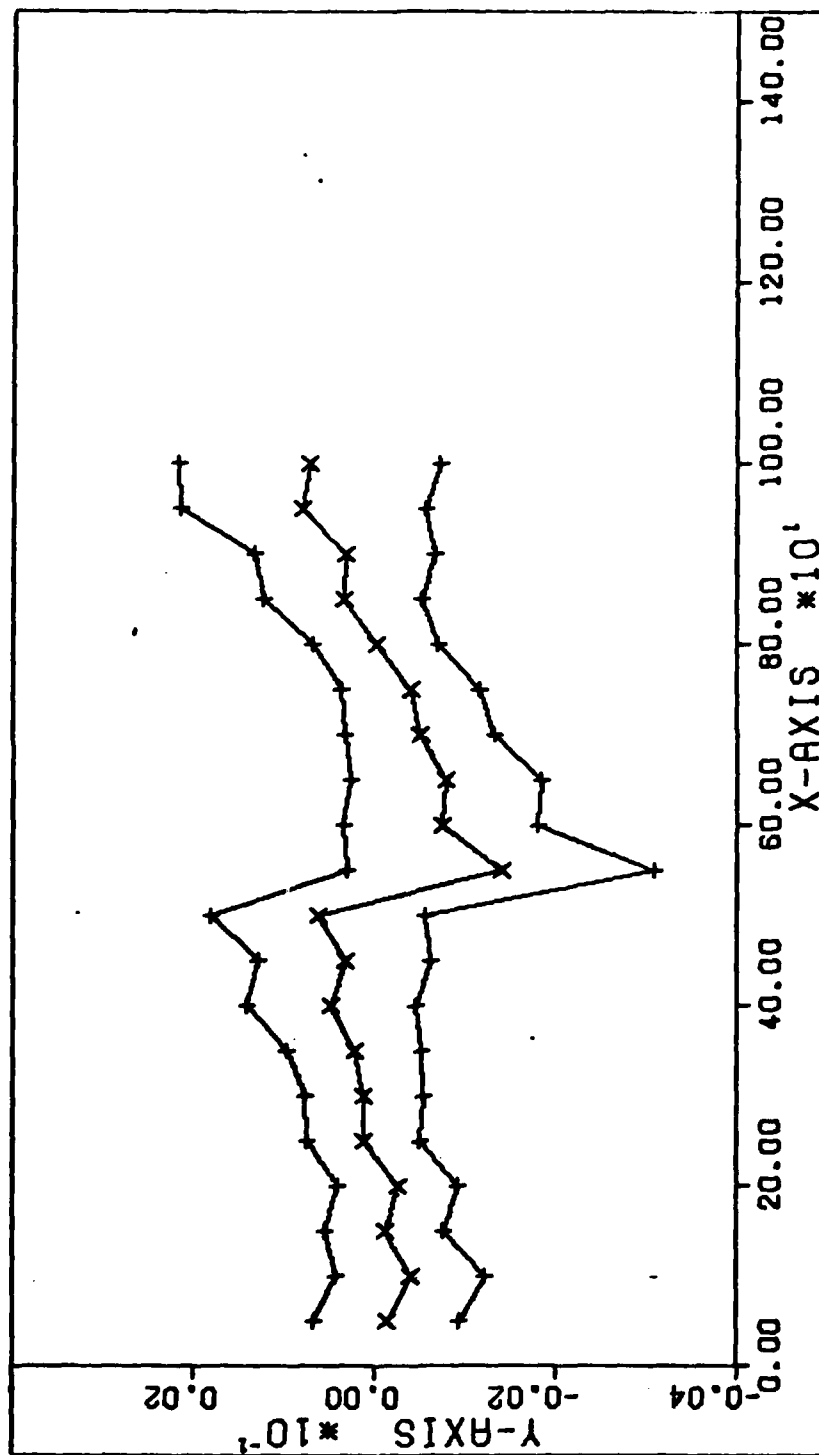Fig 48. $e_\Omega \pm \sigma_\omega$ vs t, Kalman Filter - Case I

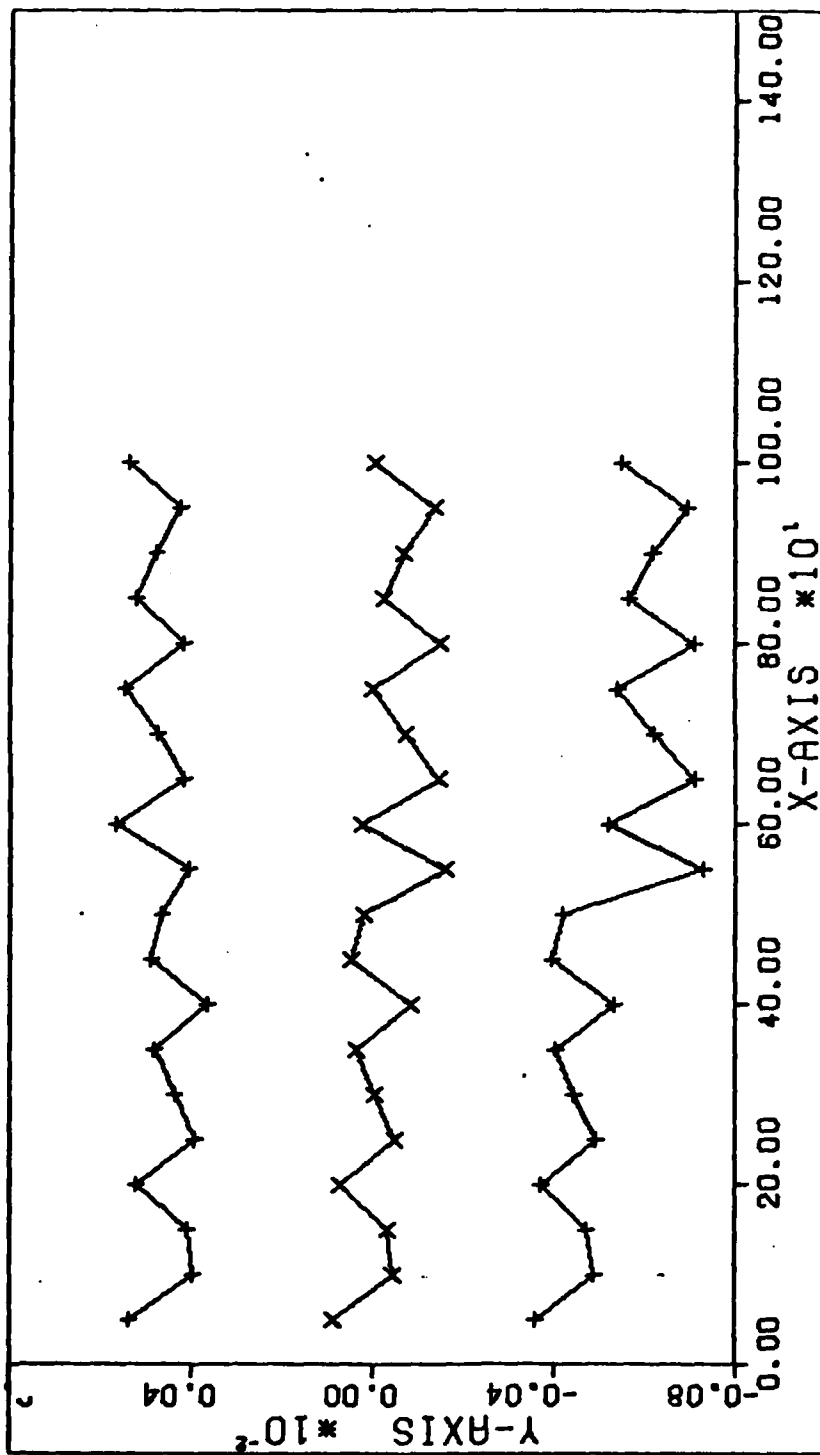Fig 49. $e_e \pm \sigma_e$ vs t, Least Squares Filter - Case II

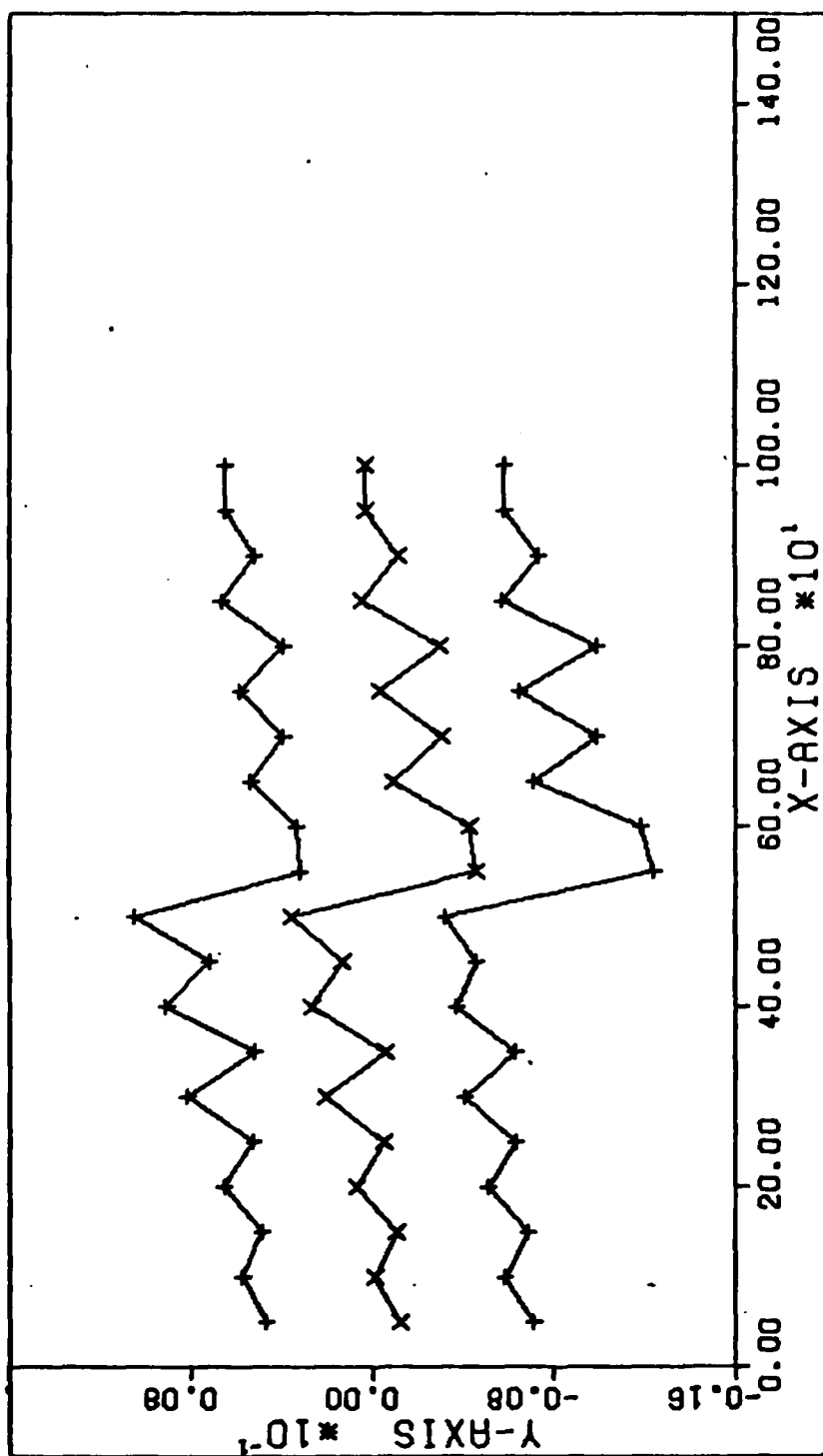Fig 50. $e_i \pm \sigma_i$ vs t, Least Squares Filter – Case II

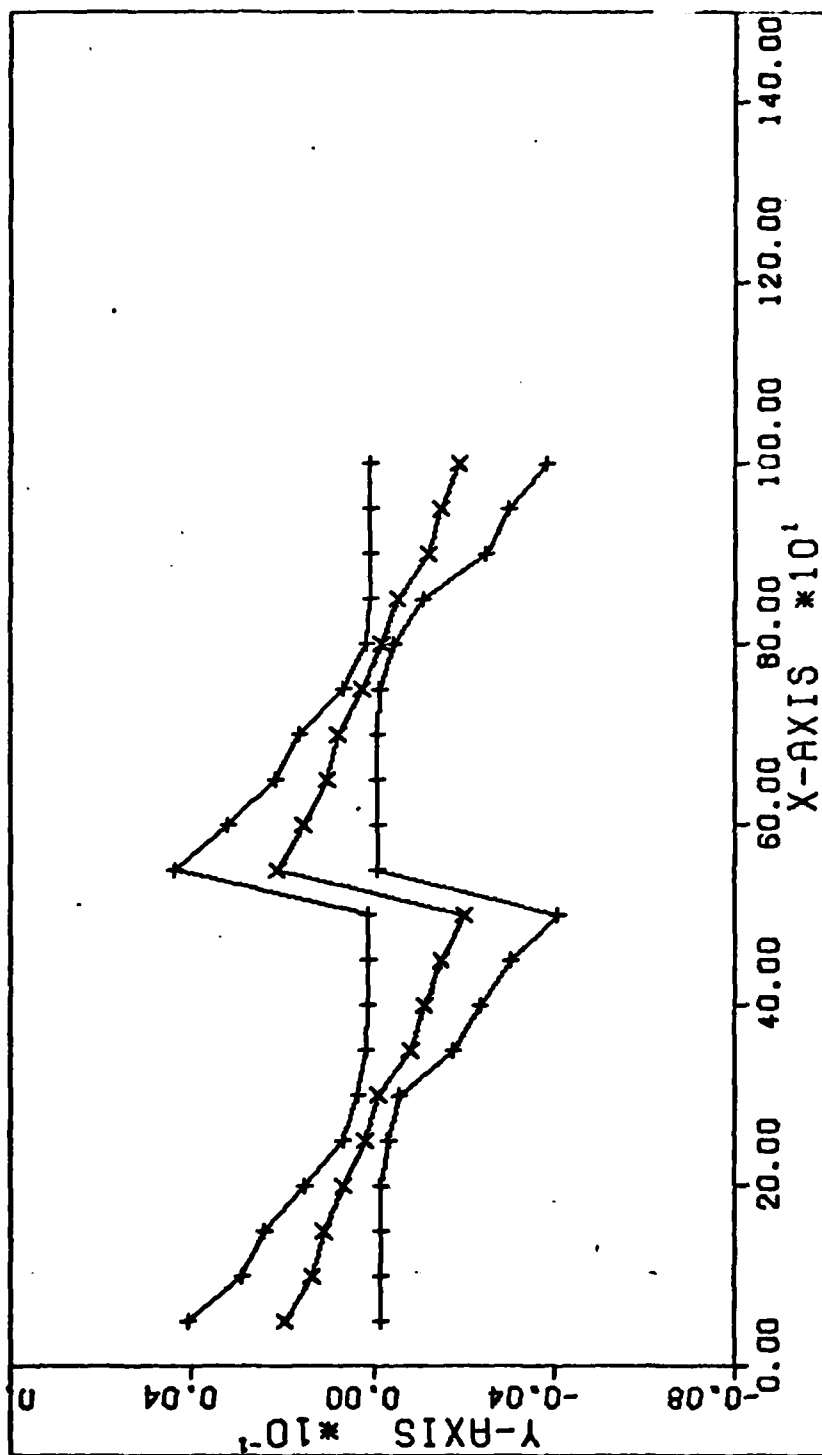Fig 51. $e_\omega \pm \sigma_\omega$ vs t, Least Squares Filter - Case II

103

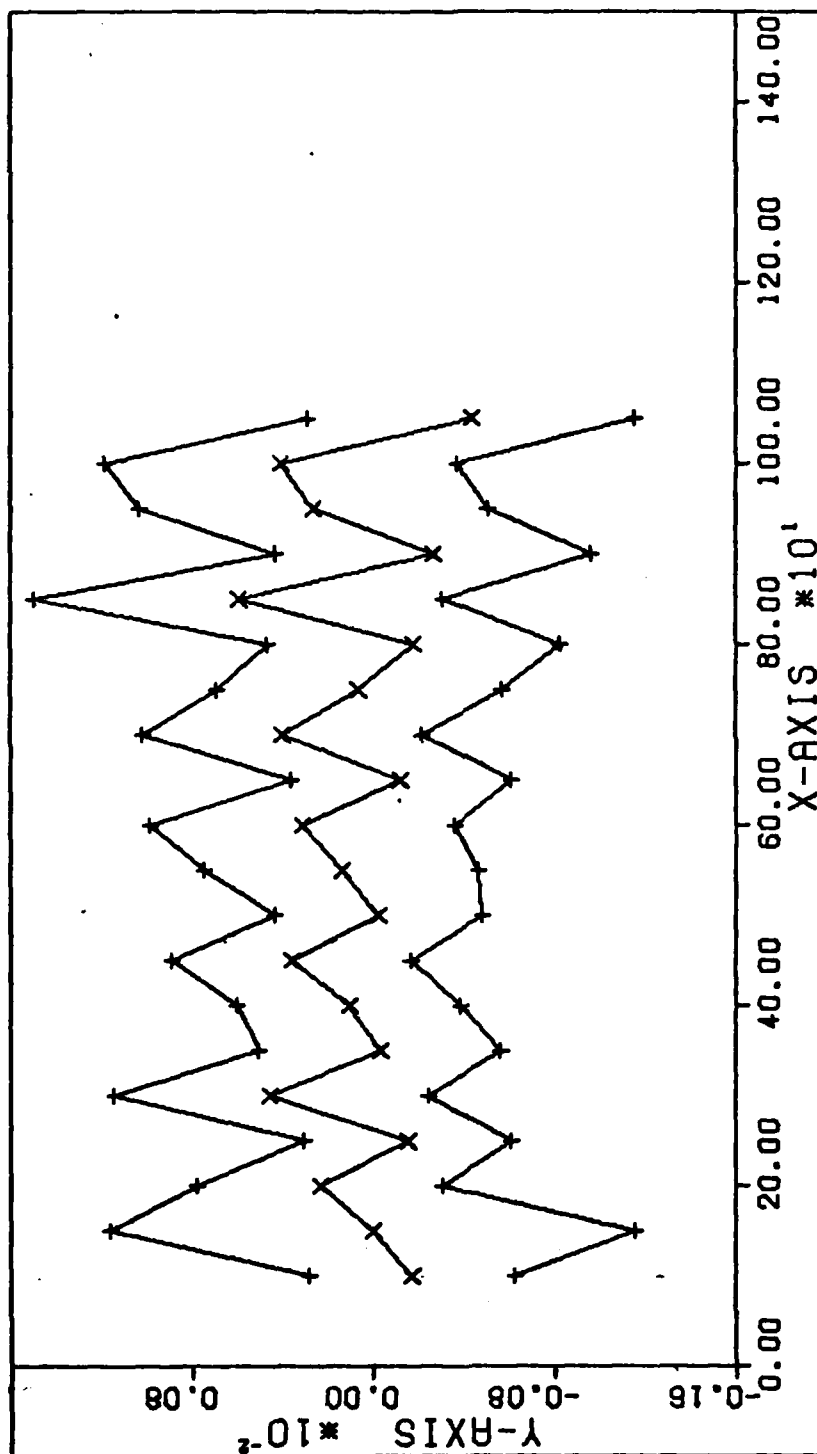Fig 52. $e_\Omega \pm \sigma_\Omega$ vs t, Least Squares Filter - Case II

104

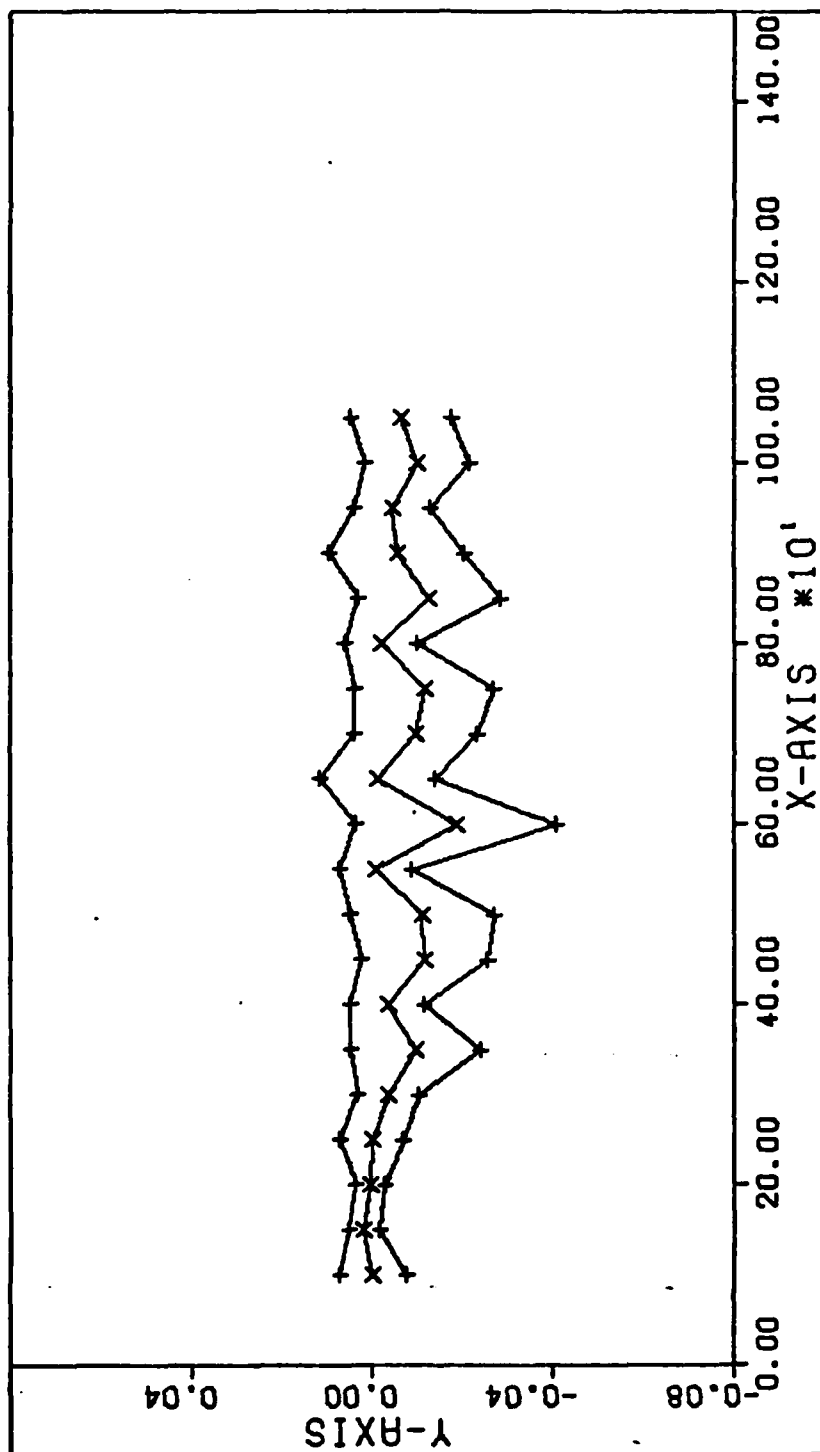Fig 53. $e_e \pm \sigma_e$ vs t, Bayes Filter, Case II

105

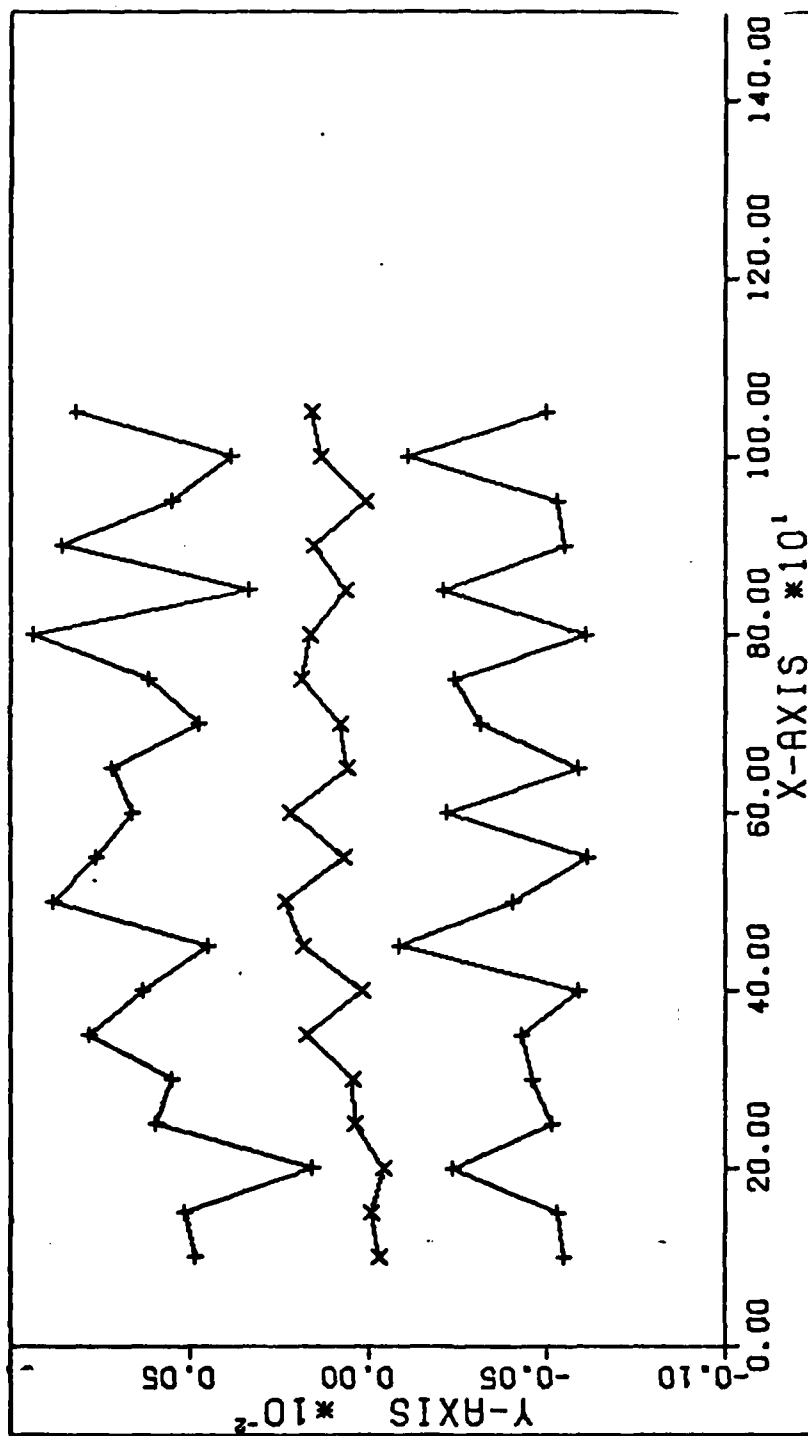Fig 54. $e_\omega \pm \sigma_\omega$ vs t, Bayes Filter - Case II

Fig 55. $e_\Omega \pm \sigma_\omega$ vs t, Bayes Filter - Case II

Vita

Daryl G. Boden was born on 20 May 1949 in Boulder, Colorado. He graduated from Fairview High School in Boulder in May 1967 and entered the University of Colorado in Boulder that fall. He received a Bachelor of Science degree in Aerospace Engineering from the University of Colorado in May 1972. Upon graduation he received a commission in the USAF via ROTC. He entered active duty in the Air Force in January 1973, as a Space Surveillance Officer at Ft Fisher AFS, North Carolina. He continued his work as a Space Surveillance Officer with one year tour of duty at Shemya AFB, Alaska in October 1975. Following this tour of duty in Alaska, he began work as a Ballistic Missile Systems Engineer with the Foreign Technology Division at Wright-Patterson AFB, Ohio. Captain Boden entered the School of Engineering, Air Force Institute of Technology in June 1978.

<div style="text-align: right">

Permanent address: 850 37th Street
Boulder, CO 80302

</div>

This thesis was typed by Mrs Anna L. Lloyd.

SECURITY CLASSIFICATION OF THIS PAGE *(When Data Entered)*

REPORT DOCUMENTATION PAGE		READ INSTRUCTIONS BEFORE COMPLETING FORM
1. REPORT NUMBER AFIT/GA/AA/79D-3	2. GOVT ACCESSION NO.	3. RECIPIENT'S CATALOG NUMBER
4. TITLE *(and Subtitle)* ORBITAL ESTIMATION USING TWO-BODY CLASSICAL ORBITAL ELEMENTS AS MEASUREMENT UPDATES		5. TYPE OF REPORT & PERIOD COVERED MS Thesis
		6. PERFORMING ORG. REPORT NUMBER
7. AUTHOR(s) Daryl G. Boden Capt, USAF		8. CONTRACT OR GRANT NUMBER(s)
9. PERFORMING ORGANIZATION NAME AND ADDRESS Air Force Institute of Technology (AFIT-EN) Wright-Patterson AFB, Ohio 45433		10. PROGRAM ELEMENT, PROJECT, TASK AREA & WORK UNIT NUMBERS
11. CONTROLLING OFFICE NAME AND ADDRESS		12. REPORT DATE December 1979
		13. NUMBER OF PAGES 121
14. MONITORING AGENCY NAME & ADDRESS*(if different from Controlling Office)*		15. SECURITY CLASS. *(of this report)* UNCLASSIFIED
		15a. DECLASSIFICATION/DOWNGRADING SCHEDULE

16. DISTRIBUTION STATEMENT *(of this Report)*

Approved for public release; distribution unlimited

17. DISTRIBUTION STATEMENT *(of the abstract entered in Block 20, if different from Report)*

18. SUPPLEMENTARY NOTES

Approved for public release; IAW AFR 190-17

JOSEPH P. HIPPS, Major, USAF
Director of Public Affairs, AFIT

19. KEY WORDS *(Continue on reverse side if necessary and identify by block number)*

Orbit Calculations	Satellite Tracking
Orbital Elements	Earth Orbits
Orbit Perturbation	Orbits
Orbital Position Estimation	Kalman Filtering
Satellite Drag	Least Squares Method

20. ABSTRACT *(Continue on reverse side if necessary and identify by block number)*

Currently, the Space Defense Center (SDC) uses the position and velocity data of a satellite track to update the orbital elements of the satellite. An alternate approach would be to process the radar data at the tracking site and transmit two-body orbital elements to SDC as measurement updates. This would significantly reduce the data load at SDC. The truth model used in this study to evaluate filter performance and provide measurement updates to the filters includes the first four zonal harmonics and the first sectoral harmonic of the geopotential and the air drag. The estimator models include two-body dynamics (contd)

DD $_{1\ JAN\ 73}^{FORM}$ 1473   EDITION OF 1 NOV 65 IS OBSOLETE   UNCLASSIFIED

SECURITY CLASSIFICATION OF THIS PAGE *(When Data Entered)*

Item 20 (contd)
and J_2 perturbations. In addition, the derivative of the semi-major axis is used to estimate the effects due to air drag. Perfect dynamics with measurement noise are assumed for the filter models. Three filters are evaluated; Least Squares, Bayes, and Kalman. The performance of the three filters is similar. The Bayes and Kalman Filters are nearly the same and indistinguishable in this study. All three filters performed adequately with the following exceptions. The filters diverge when singularities are present in the classical orbital elements. All three filters underestimate the covariance of the estimates. Finally, the filters track noise in the estimate of the derivative of the semi-major axis, degrading the prediction capabilities of the filters.